DNA Nanotechnology

DOI: 10.1002/anie.201404652

# DNA Switches: From Principles to Applications

*Fuan Wang, Xiaoqing Liu, and Itamar Willner**

**Keywords:**
DNA machines · DNA switches · DNAzymes · electrochemistry · photochemistry

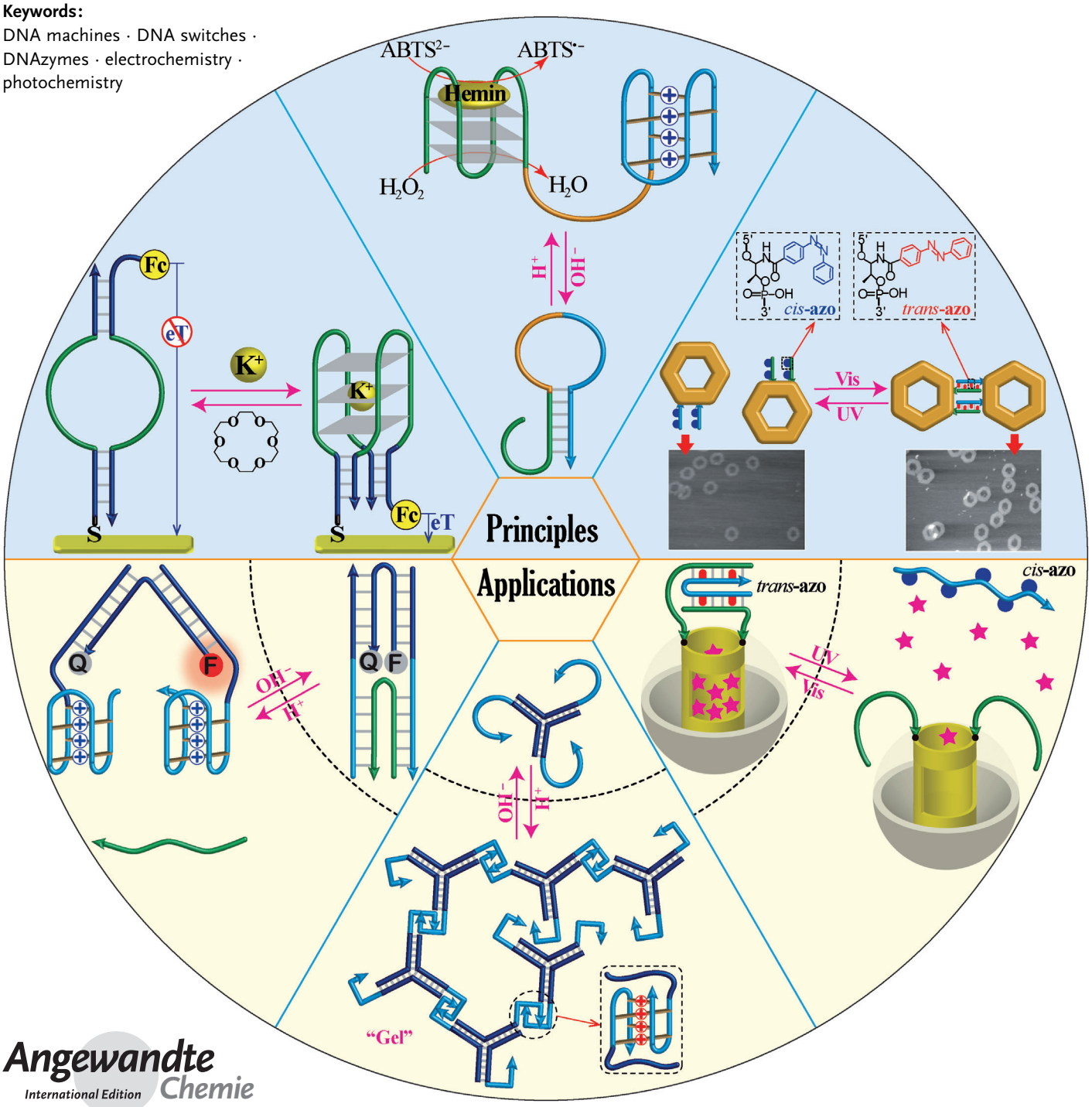

Angewandte International Edition Chemie

*The base sequence of nucleic acid encodes structural and functional properties into the biopolymer. Structural information includes the formation of duplexes, G-quadruplexes, i-motif, and cooperatively stabilized assemblies. Functional information encoded in the base sequence involves the strand-displacement process, the recognition properties by aptamers, and the catalytic functions of DNAzymes. This Review addresses the implementation of the information encoded in nucleic acids to develop DNA switches. A DNA switch is a supramolecular nucleic acid assembly that undergoes cyclic, switchable, transitions between two distinct states in the presence of appropriate triggers and counter triggers, such as pH value, metal ions/ligands, photonic and electrical stimuli. Applications of switchable DNA systems to tailor switchable DNA hydrogels, for the controlled drug-release and for the activation of switchable enzyme cascades, are described, and future perspectives of the systems are addressed.*

**From the Contents**



## 1. Introduction

The base sequence of nucleic acids encodes structural and functional information into the biopolymer. For example, the base-pair-stabilized formation of duplex DNA, the $H^+$-stimulated formation of i-motif structures,[1] the $K^+$- or $Pb^{2+}$-induced formation of G-quadruplexes,[2] the cooperative metal-ion-induced formation of duplex DNAs (e.g., by T-$Hg^{2+}$-T[3] or C-$Ag^+$-C[4] bridges), and the cooperative stabilization of double-stranded DNA by photoisomerizable units (e.g., *trans*-azobenzene)[5] represent structural motives dictated by the base sequences of the nucleic acids. Also, the reactivity of nucleic acids is controlled by the base sequence of the biopolymers. Sequence-specific nucleotides exhibit specific recognition sites for binding of low-molecular-weight substrates, biopolymers and even cells (e.g., aptamers).[6] Similarly, sequence-specific nucleic acids reveal catalytic functions (e.g., DNAzymes or ribozymes).[7] Also, sequence-specific domains in DNA dictate the selective binding of proteins,[8] and specific duplex domains are being specifically cleaved by enzymes (e.g., endonucleases or nicking enzymes).[9]

The stabilities of DNA structures are controlled by different parameters, such as the number of base-pairs, nature of bases, ionic-strength, cooperative effects of bridging duplexes, by ions, i-motif or G-quadruplex structures, and the intercalation of molecular substrates. The transition of one nucleic acid structure to another configuration requires the design of an energetically downhill process ($\Delta G < 0$). The energy control of the reconfiguration of DNA structures is exemplified in Figure 1, which details the strand-displacement process, and shows the effect of the encoded base sequence on the process.[10] The strand-displacement reaction is presented in Figure 1 A, where a duplex structure "**I**" composed of strands **1** and **2** interacts with the input strand **3**. As the input strand includes the domain $\mathbf{a_t}^*$ complementary to domain $\mathbf{a_t}$ of the complex **I**, its hybridization with the duplex **I** proceeds to yield the hybrid structure **1**/**2**/**3**. Since the input strand includes a protruding single-strand tether consisting of

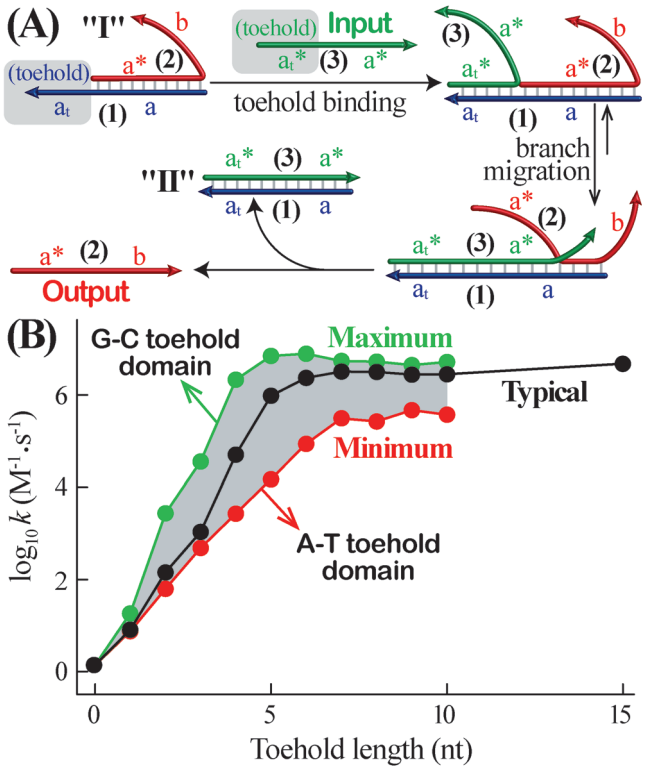


***Figure 1.*** A) The strand-displacement mechanism involving the input-guided exchange of a duplex structure consisting of a toehold domain. B) Theoretical modeling of the kinetics of strand displacement as a function of the length and base-composition of the toehold domains. Adapted with permission from Ref. [10a]. Copyright 2009 American Chemical Society.

[*] Dr. F. Wang,[+] Dr. X. Liu,[+] Prof. I. Willner
Institute of Chemistry
The Hebrew University of Jerusalem
Jerusalem 91904 (Israel)
E-mail: willnea@vms.huji.ac.il
Homepage: http://chem.ch.huji.ac.il/willner/
[+] These authors contributed equally to this work.

  

domain **a*** that is complementary to the sequence **a** of **1**, branch migration and strand displacement occur to form the energetically stabilized duplex **II**, accompanied by the release of output strand **2**. Figure 1B displays the kinetics of the strand-displacement process as a function of the nature and number of bases comprising the toehold region. The strand-displacement process is enhanced as the number of complementary bases in the toehold region increases, and the formation of energetically stabilized base-pairs in the toehold region accelerates the strand-displacement process.

The cyclic reconfiguration of DNA from one structure to another by a mechanically driven transition is the basis for the development of various DNA switches. Figure 2A outlines the principle of a DNA switch. A DNA structure in state A is subjected to a stimulus, Input $I_A$, that induces a structural reconfiguration of state A into state B. The subsequent interaction of state B with a second trigger, Input $I_B$, restores state A, thus establishing a reversible switchable DNA device. The construction of DNA switches requires the development of means to transduce the operation of the DNA switch. Figure 2A depicts the fluorescence readout of the switch functions of a fluorophore/quencher pair, where the fluorophore quenching is controlled by the distance separating the fluorophore/quencher pair. Figure 2B exemplifies the stimuli-responsive reconfiguration of a DNA system from a random-coil structure (state C) into a catalytically active DNAzyme structure (state D) by a stimulus, Input $I_C$, and the reverse dissociation of the DNAzyme structure, using a second input-trigger, Input $I_D$. The DNAzyme-stimulated catalytic process provides the readout signal for the switchable catalytic functions of the molecular device. Mechanically driven DNA switches must meet several fundamental features and functional pre-requisites: 1) The operation of the DNA switch requires an energy input (fuel). The fuel might be a chemical trigger (a nucleic acid strand generating an energetically stabilized duplex, ions that yield cooperatively stabilized DNA duplexes or DNA complexes, and $H^+$-triggers generating i-motif structures), light signals, electrical signals and more. 2) For reversible operation of DNA switches, the introduction of "anti-fuels" triggers that compensate for the fuel stimuli is essential. The anti-fuels may be nucleic acids that displace the fuel strands from the device, ligands that remove the metal-ion fuels, or changes of pH values that oppose the pH-fuel. Alternatively, illumination at other wavelengths that counteracts the light input, or a counter-biasing electrical potential that compensates for the electrical input, may be used as anti-fuels that reverse the switch devices.

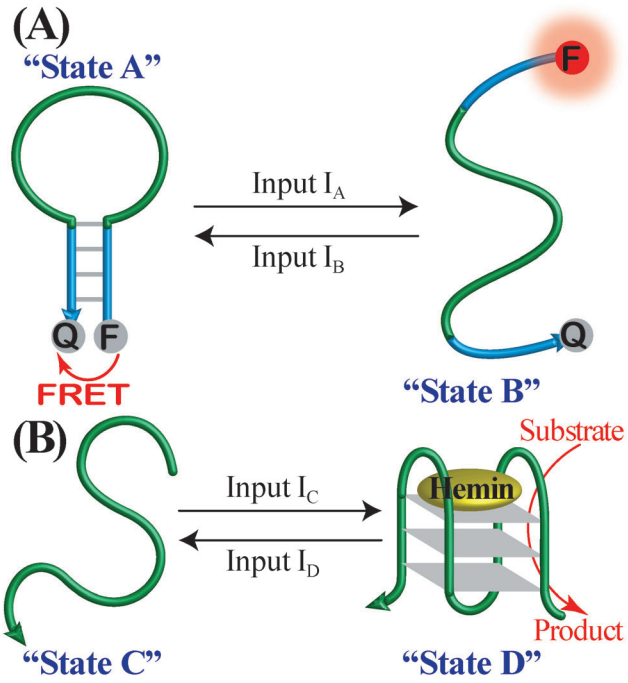


***Figure 2.*** A) Cyclic switchable reconfiguration of a DNA nanostructure using two different external triggers, $I_A$ and $I_B$. The reconfiguration is followed by the fluorescence intensities generated by a fluorophore/quencher reporting pair. B) Cyclic switchable transitions between a catalytically inactive random-coil nucleic acid, and a catalytically active hemin/G-quadruplex HRP-mimicking DNAzyme, using two external triggers, $I_C$ and $I_D$. The operation of the DNA switch is imaged by monitoring the DNAzyme-driven catalytic process.

Different applications of DNA switches may be envisaged. These include the design of switchable catalytic systems, for example, switchable DNAzymes, and the use of DNA switches as mechanical scaffolds that carry nano-objects, such as enzymes or nanoparticles. The switchable reconfiguration of such objects may be used to control enzyme cascades, or to regulate plasmonic functions. Also, switchable DNA systems may find important applications in materials science. For

*Itamar Willner completed his Ph.D. studies at The Hebrew University of Jerusalem in 1978. After postdoctoral research (1978–1981) at U.C. Berkeley, he joined the Institute of Chemistry at The Hebrew University of Jerusalem, where he was appointed as Professor in 1986. His research interests include bioelectronics, nanobiotechnology, functional monolayers, light-induced electron-transfer processes, artificial photosynthesis, and "smart" materials. He is a member of the Israel Academy of Sciences and the German National Academy of Sciences, Leopoldina.*

*Dr. Fuan Wang is currently a postdoc in the laboratory of Prof. Itamar Willner, Institute of Chemistry, The Hebrew University of Jerusalem. He received his B.S. degree from Zhengzhou University, China (2003) and completed his Ph.D. at Changchun Institute of Applied Chemistry, Chinese Academy of Sciences (2008). His research interests focus on DNA nanotechnology, including the development of DNA sensing, DNA computing, and DNA machines.*

example, switchable DNA hydrogels or the use of DNA switches as gates of mesoporous materials or nanopores may provide versatile principles for drug delivery and controlled release.

In this Review we present the methods to construct DNA switches, and we discuss their potential applications. It should be noted that DNA switches represent a subclass of DNA machines, a rapidly developing topic in DNA nanotechnology.[11] While extensive Review articles discussed the area of DNA machines, the area of DNA switches and their impact on DNA nanotechnology was underestimated to date. We thus believe that the present Review will provide new insights and principles to the field of "mechano-DNA".

## 2. Types of DNA Switches

### 2.1. Metal-Ion-Stimulated DNA Switches

G-rich nucleic acid sequences undergo metal-ion-stimulated random-coil to G-quadruplex transitions.[12] By the triggered interaction of the random-coil nucleic acids with the respective ions, the self-assembly of the G-quadruplex nanostructures occurred. The ligand-induced elimination of the stabilizing metal ions, separated the G-quadruplexes into the random-coil strand, thus allowing the cyclic switchable reconfiguration of G-quadruplex structures. Such an ion-induced DNA switch is exemplified in Figure 3A, in which $Pb^{2+}$ ions are used to stabilize the parallel G-quadruplex structure.[13] The duplex structure (**4**/**5**) includes in **4** the G-quadruplex sequence in a caged (that is, blocked) configuration. Treatment of the duplex structure with $Pb^{2+}$ ions led to the dissociation of strand **5**, and to the assembly of the energetically stabilized $Pb^{2+}$-functionalized parallel G-quadruplex. The association of $Zn^{II}$ protoporphyrin IX (ZnPPIX) to the G-quadruplex structure resulted in high fluorescence of the intercalated dye (Figure 3B, curve a). The subsequent treatment of the $Pb^{2+}$-functionalized G-quadruplex with 1,4,7,10-tetraazacyclododecane-1,4,7,10-tetraacetic acid (DOTA) ligand eliminated the $Pb^{2+}$ ions from the G-quadruplex, resulting in the separation of the G-quadruplex nanostructure, the recombination of the strands **4** and **5** to the duplex structure **4**/**5** and to the release of the $Zn^{II}$ protoporphyrin IX dye (ZnPPIX), exhibiting low fluorescence intensity (Figure 3B, curve b). By the cyclic treatment of the DNA duplex **4**/**5** with $Pb^{2+}$ ions, and the subsequent elimination of the $Pb^{2+}$ ions from the G-quadruplex nanostructure by means of DOTA, the fluorescence of the system was reversibly switched between high and low values. The $Pb^{2+}$-triggered switching of the duplex structure **4**/**5**, to the fluorescent $Pb^{2+}$-modified G-quadruplex/ZnPPIX complexes, was applied for the quantitative detection of $Pb^{2+}$ ions (detection limit 20 nM). Similarly, the treatment of the G-rich single-stranded nucleic acid **6** with $K^+$ ions resulted in the triggered assembly of the anti-parallel $K^+$-stabilized G-quadruplex structures,[14] Figure 3C. The association of hemin to the G-quadruplex resulted in the formation of a catalytically active hemin/G-quadruplex horseradish perox-

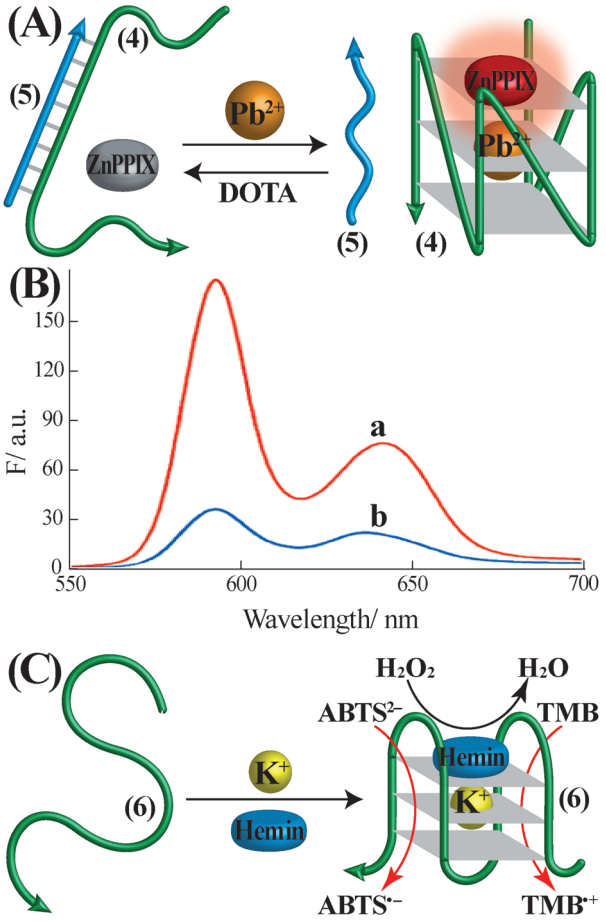


***Figure 3.*** A) Switchable $Pb^{2+}$-stimulated reconfiguration of a duplex DNA structure into the $Pb^{2+}$-stabilized G-quadruplex structure, and the reverse separation of the G-quadruplex by the elimination of the $Pb^{2+}$ ions with the DOTA ligand. The formation and dissociation of the G-quadruplex are followed by the binding of $Zn^{II}$ protoporphyrin IX (ZnPPIX) to the G-quadruplex (high fluorescence) and by the depletion of the fluorescence of ZnPPIX upon dissociation of the G-quadruplex. B) Fluorescence spectra corresponding to: a) The ZnPPIX bound to the $Pb^{2+}$-ion-stabilized G-quadruplex. b) The free ZnPPIX formed upon the DOTA-stimulated separation of the G-quadruplex, and the formation of the **4**/**5** duplex structure. Adapted with permission from Ref. [13]. Copyright 2010 American Chemical Society. C) $K^+$-ion-stimulated transition of a random-coil DNA strand into the catalytically active hemin/G-quadruplex horseradish peroxidase (HRP)-mimicking DNAzyme nanostructure.

*Dr. Xiaoqing Liu is a postdoc in the laboratory of Prof. Itamar Willner, Institute of Chemistry, The Hebrew University of Jerusalem. She received her B.S. degree from Shandong Normal University, China (2003) and her Ph.D. from Changchun Institute of Applied Chemistry, Chinese Academy of Sciences (2008). After working as a postdoctoral fellow with Prof. K. V. Gothelf at Aarhus University, Denmark, she joined Prof. Willner's group in 2010. Her research interests focus on the development of optical and electrical DNA-based sensors, and DNA machines.*

  

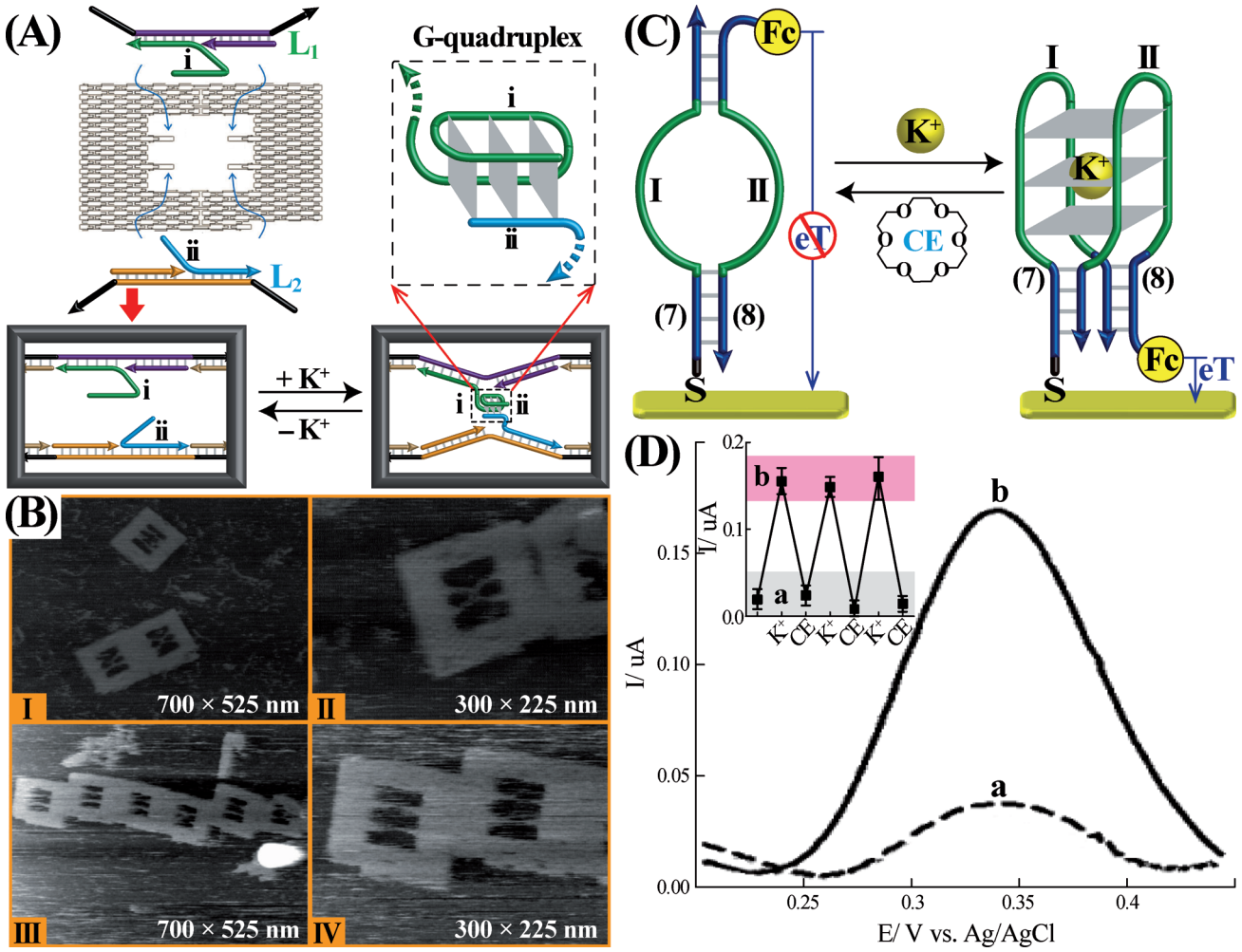


***Figure 4.*** A) Schematic representation of the formation of a DNA origami frame that includes protruding nucleic acids capable of undergoing $K^+$-ion-stimulated switchable G-quadruplex to random-coil structural transitions. B) AFM images corresponding to: Panels I and II, the $K^+$-stabilized G-quadruplex in the frame. Panels III and IV, the random-coil strand in the frame after elimination of the $K^+$ ions and the separation of the G-quadruplex. Adapted with permission from Ref. [15]. Copyright 2010 American Chemical Society. C) Electrochemical transduction of a loop-containing DNA duplex structure transformed into a G-quadruplex nanostructure associated with a Au electrode. The transition of the loop structure to the G-quadruplex is stimulated by the addition of $K^+$ ions, and the separation of the G-quadruplex is induced through the elimination of the $K^+$ ions from the nanostructure by adding 18-crown-ether (CE). D) Voltammetric responses of: a) The ferrocene-labeled loop structure. b) The ferrocene-labeled $K^+$-ion-stabilized G-quadruplex structure. Inset: Cyclic voltammetric responses upon the switchable transitions between the loop-containing duplex structure (a) and the G-quadruplex structure (b), in the presence of 18-crown-ether and $K^+$ ions, respectively. Adapted with permission from Ref. [16]. Copyright 2010 Wiley-VCH.

idase (HRP)-mimicking DNAzyme, that switched-on the catalyzed $H_2O_2$-stimulated oxidation of 2,2′-azino bis(3-ethylbenzothiazoline-6-sulphonic acid) ($ABTS^{2-}$), to the colored product $ABTS^{\bullet-}$, or catalyzed the oxidation of 3,3′,5,5′-tetramethylbenzidine (TMB) by $H_2O_2$, to the colored product 3,3′,5,5′-tetramethylbenzidine diimine ($TMB^{\bullet+}$). These systems were applied for the quantitative analysis of $K^+$ ions.

The $K^+$-stimulated formation of G-quadruplexes and the dissociation of the G-quartet were imaged at the single-molecule level using fast atomic force microscopy (AFM) measurements.[15] Duplex DNA structures, $L_1$ and $L_2$, that each included a middle-positioned protruding single-stranded nucleic acids (domains i and ii) composed of $^3/_4$ and $^1/_4$ of the G-quadruplex sequences, respectively, were integrated in a DNA origami frame (Figure 4A). In the presence of $K^+$ ions, the resulting G-quadruplex bridged the duplexes $L_1$ and $L_2$, yielding an X-shaped structure. This structure was then opened by the removal of the $K^+$ ions from the system. Figure 4B depicts the resulting X-shaped G-quadruplex-bridged structure (panels I and II), and the parallel duplexes structure (panels III and IV), formed upon the elimination of the $K^+$ ions.

The reversible switchable programmed transition between random-coil G-rich nucleic acids and G-quadruplex nanostructures was used to control interfacial electron-transfer reactions,[16] Figure 4C. The partial complementary duplex nucleic acid structure (**7**/**8**) was deposited on Au electrodes, and the redox-label ferrocene (Fc) was tethered to the 5′-end of strand **8**. The loop domains I and II of the duplex are composed of the G-rich sequences. In the presence of $K^+$ ions,

the G-containing DNA strands reconfigured into the G-quadruplex structure, and the subsequent 18-crown-ether (CE)-stimulated elimination of $K^+$ from the quadruplex regenerated the linear hairpin structure. As the spatial separation between the redox-label (Fc) and the electrodes is controlled by the nucleic acid scaffolds, the interfacial electron-transfer rates, and the voltammetric responses of the redox label, are dictated by the DNA backbone. The spatial separation between the ferrocene redox label and the electrode, dictated by the linear hairpin scaffold, leads to a low voltammetric response (Figure 4D, curve a), while the G-quadruplex, forcing proximity between the redox label and the electrode, intensified the voltammetric response (Figure 4D, curve b). By the cyclic reconfiguration of the surface-modified electrode between the linear hairpin structure and the G-quadruplex configuration, the voltammetric responses of the redox label were switched between low and high values, respectively (Figure 4D, inset). In a related study, an electrode was functionalized with a ferrocene-labeled random-coil nucleic acid consisting of the G-rich sequence.[17] The spatial separation of the redox label from the electrode resulted in inefficient interfacial electron transfer, and a poor voltammetric response. Treatment of the modified surface with $K^+$ ions self-assembled the anti-parallel G-quadruplex, a process that brought the redox label into close proximity to the electrode. This structural transition resulted in effective interfacial electron transfer, and a high voltammetric response. The $K^+$-ion-triggered switching of the random-coil structure to the G-quadruplex was applied for the quantitative detection of $K^+$ ions (detection limit 100 μM).

Ligand and transition-metal complexes were found to reversibly switch G-quadruplex and random-coil transitions.[18] The ligand bis(methylquinoliniumpyridine) dicarboxamide (**9**) revealed a high binding affinity to the $K^+$-ion-stabilized G-quadruplex structure (**10**), Figure 5A. The binding of $Cu^{2+}$ ions to the ligand **9** resulted in the dissociation of the G-quadruplex and the stabilization of a helical DNA coil by the electrostatic binding of the $Cu^{2+}$ ligand complex ($Cu^{2+}$-**9**). The subsequent elimination of the $Cu^{2+}$ ions from the ligand by ethylenediaminetetraacetic acid (EDTA), regenerated the free dicarboxamide ligand **9** and the re-assembly of the G-quadruplex structure. The transitions between the G-quadruplex and the helical-coil structures were monitored by circular dichroism (CD), Figure 5B. The formation of the G-quadruplex was followed by a CD band at $\lambda = 295$ nm, and this band was depleted upon the dissociation of the G-quadruplex by $Cu^{2+}$ ions.

Nucleotide bases act as ligands for various metal ions. For example, thymine yields stable thymine-$Hg^{2+}$-thymine (T-$Hg^{2+}$-T) complexes and cytosine forms cytosine-$Ag^+$-cytosine (C-$Ag^+$-C) structures.[4] These complexes might cooperatively stabilize the formation of duplex DNA structures. Upon elimination of the metal ions from the metal-ion-bridged hybrids, the duplexes separated, leading to metal-ion switchable structures. Different methods to construct metal-ion switchable DNA structures were developed, and optical or electrochemical transductions of the switchable functions of the systems were applied to monitor the molecular DNA switches. For example, Figure 6A shows a hairpin structure

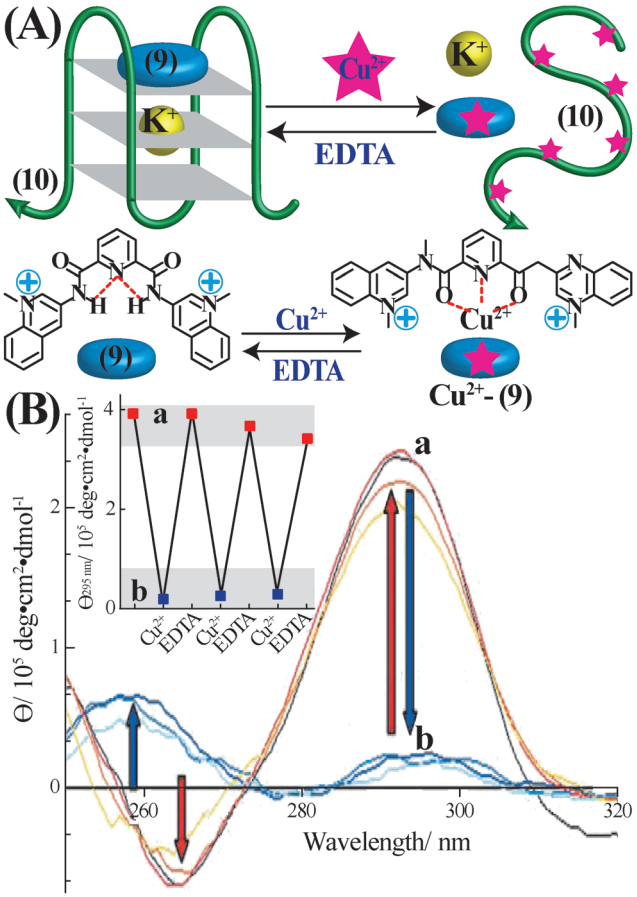


***Figure 5.*** A) Ligand-assisted switchable G-quadruplex/random-coil transitions. The ligand **9** and $K^+$ ions co-stabilize the G-quadruplex structure. Elimination of the ligand **9** from the G-quadruplex leads to the formation of the $Cu^{2+}$-**9** complex, leading to the separation of the G-quadruplex and to the random-coil structure. The addition of EDTA causes the $Cu^{2+}$-**9** complex to separate as a result of the binding of the $Cu^{2+}$ ions. The release of the ligand **9** restores, in the presence of $K^+$ ions, the G-quadruplex structure. B) Circular dichroism (CD) spectra corresponding to: a) The ligand **9** and $K^+$ ions cooperatively stabilized the G-quadruplex. b) The random-coil state formed upon elimination of ligand **9** through the formation of the $Cu^{2+}$-**9** complex. Inset: Cyclic CD spectral changes upon forming the $K^+$-ion/**9**-stabilized G-quadruplex (a), and upon elimination of the stabilizer units **9**, through the formation of the $Cu^{2+}$-**9** complexes (b). Adapted with permission from Ref. [18]. Copyright 2008 Wiley-VCH

(**11**) functionalized at its 3′- and 5′-ends with a fluorophore/quencher pair (F/Q). In this hairpin configuration the fluorophore is effectively quenched, leading to an "OFF" fluorescence readout signal. In the presence of a helper nucleic acid (**12**), partially complementary to the loop domain of the hairpin, and added $Hg^{2+}$ ions, the hairpin is opened leading to the duplex structure **11**/**12**, that includes complementary base pairs and T-$Hg^{2+}$-T bridges that cooperatively stabilize the duplex structure. The spatial separation of the fluorophore (6-carboxyfluorescein, FAM) from the quencher (Black Hole Quencher-1, BHQ-1) units leads to inefficient quenching of FAM and to an enhanced fluorescence of the fluorophore. Addition of $I^-$ ions removes the $Hg^{2+}$ ions from the duplex structure **11**/**12**, causing it to separate leading to

  

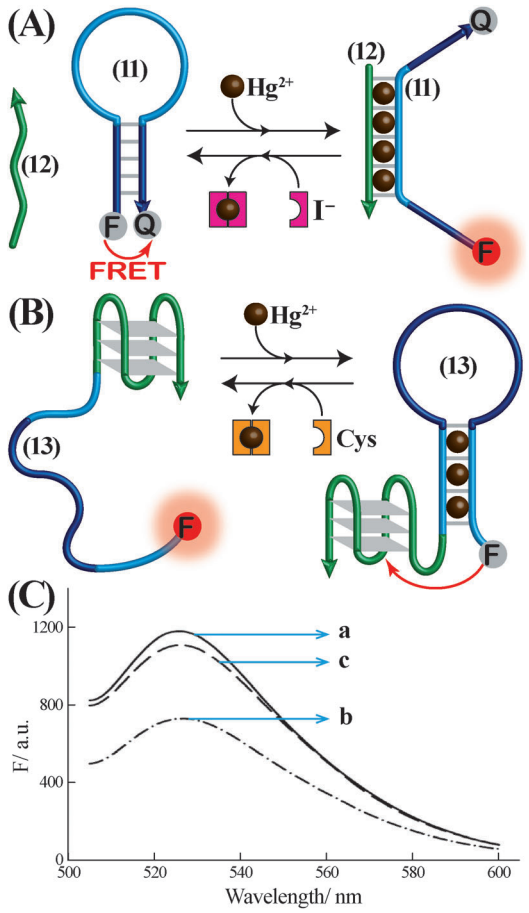


***Figure 6.*** A) Switchable and reversible transitions of a DNA hairpin structure to a duplex assembly, and back, using $Hg^{2+}$ and $I^-$ ions as triggers. B) $Hg^{2+}$/cysteine-stimulated switchable transitions between a random-coil and a $Hg^{2+}$-ion-bridged hairpin nanostructure. The G-quadruplex acts as internal quencher of the fluorophore (F). C) Fluorescence spectra corresponding to: a) The G-quadruplex-labeled random-coil DNA structure. b) The G-quadruplex-labeled $Hg^{2+}$-ion-bridged hairpin structure. c) The G-quadruplex-labeled random-coil structure generated upon the elimination of $Hg^{2+}$ ions, and the separation of the hairpin structure. Adapted with permission from Ref. [20]. Copyright 2012 Royal Society of Chemistry.

the reconfiguration of the strand **11** into the hairpin structure, whereby the fluorescence of FAM is quenched.[19] Figure 6B depicts a different approach to construct a fluorescence DNA switch based on the T-$Hg^{2+}$-T bridging units.[20] The system makes use of the fact that the G-quadruplex acts as quencher of fluorophores. Accordingly, the nucleic acid **13** consisting of the G-quadruplex tethered to the T-rich single-stranded domain, functionalized at its 5′-end with the FAM fluorophore (F) was used as the functional DNA switch. The spatial separation between the FAM fluorophore and the G-quadruplex led to inefficient quenching of the fluorophore and to the switched "ON" fluorescence state (Figure 6C, curve a). In the presence of $Hg^{2+}$ ions, intramolecular folding of the single-stranded DNA **13** proceeds by the formation of T-$Hg^{2+}$-T bridges, leading to intimate distances between the FAM fluorophore and the G-quadruplex structure and to the efficient quenching of the fluorophore (Figure 6C, curve b). The subsequent treatment of the switched "OFF" state with cysteine (Cys) eliminated the $Hg^{2+}$ ions from the folded structure, leading to the regeneration of random coil structure, exhibiting high fluorescence (Figure 6C, curve c).

A DNA-based electrochemical switch was assembled on an electrode surface, using T-$Hg^{2+}$-T bridging units,[21] Figure 7A. A 3′-thiolated nucleic acid (**14**) that includes two T-rich domains I and II was assembled on an electrode surface. The 5′-end of strand **14** was functionalized with a ferrocene

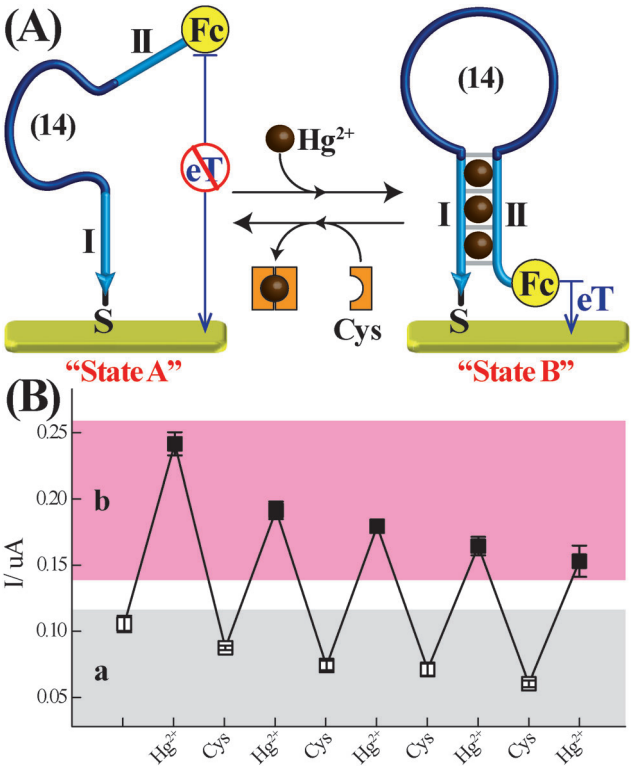


***Figure 7.*** A) Electrochemical transduction of switchable $Hg^{2+}$-ion/cysteine-stimulated transitions between a random-coil and $Hg^{2+}$-bridged hairpin structures, associated with an electrode. The spatial separation between the ferrocene (Fc) redox label of the different DNA structures and the electrode controls the voltammetric responses of the redox label. B) Cyclic voltammetric responses of the modified electrode in the presence of the random-coil structure (a), and in the $Hg^{2+}$-ion-bridged hairpin structure (b). Adapted with permission from Ref. [21]. Copyright 2009 Royal Society of Chemistry.

(Fc) redox-active label. In the single-stranded, random-coil configuration, the redox label is spatially separated from the electrode, giving rise to an inefficient electron-transfer communication, and to a low voltammetric response, state A. In the presence of $Hg^{2+}$ ions, the domains I and II are folded into a T-$Hg^{2+}$-T bridged structure, where the redox label (Fc) is in close proximity to the electrode. This change results in efficient electron-transfer, and a high voltammetric response, state B. The cysteine (Cys)-mediated elimination of the $Hg^{2+}$ ions regenerated the random-coil configuration (state A), exhibiting a low voltammetric response. By the cyclic treatment of the DNA-monolayer-modified electrode with $Hg^{2+}$ ions and Cys, the voltammetric responses of the

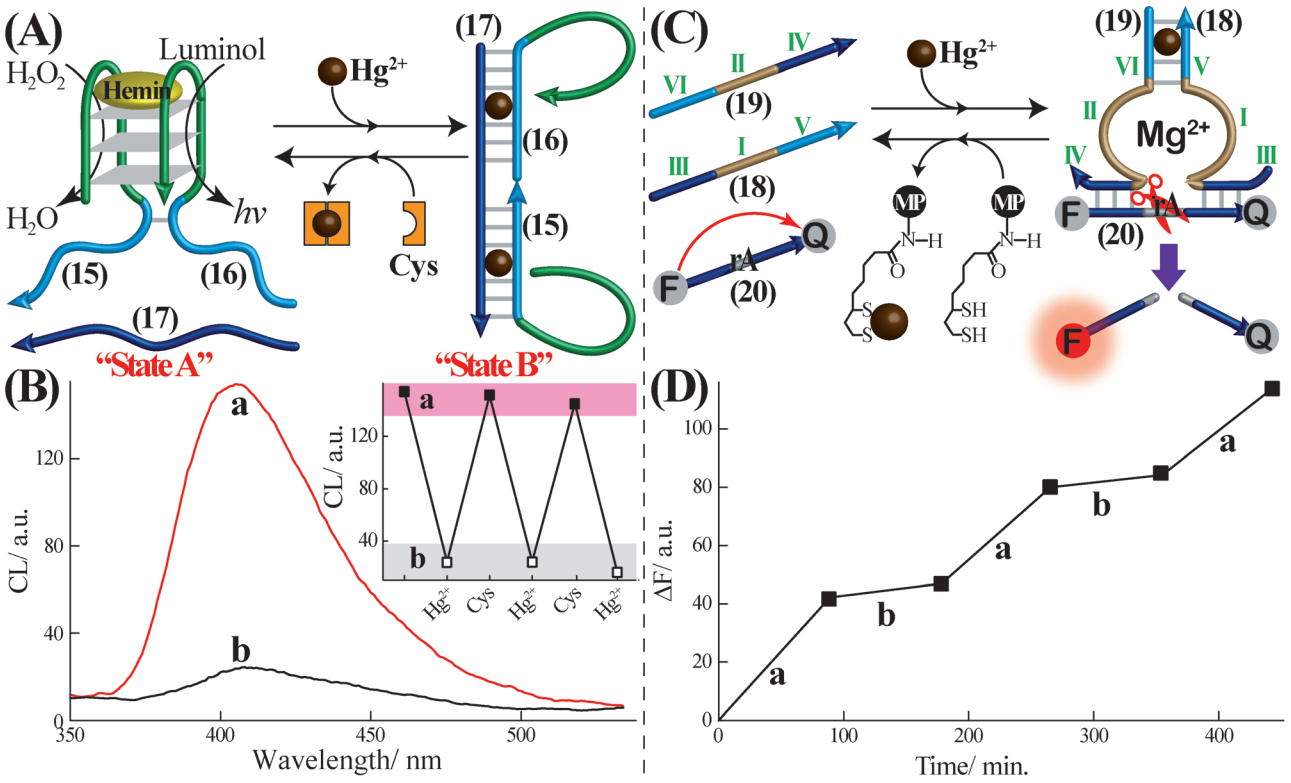


***Figure 8.*** A) $Hg^{2+}$-ion/cysteine-triggered cyclic switchable reconfiguration of a hemin/G-quadruplex HRP-mimicking DNAzyme structure, consisting of DNAzyme subunits **15** and **16**, and a catalytically inactive $Hg^{2+}$-stabilized duplex structure of the subunits. B) Probing the hemin/G-quadruplex DNAzyme to duplex transitions through the hemin/G-quadruplex DNAzyme-catalyzed oxidation of luminol by $H_2O_2$, and the generation of chemiluminescence: a) Chemiluminescence spectrum generated by the hemin/G-quadruplex DNAzyme. b) Chemiluminescence spectrum generated by the $Hg^{2+}$-ion-stabilized duplex structure. Inset: Cyclic chemiluminescence intensities in the presence of the hemin/G-quadruplex DNAzyme (a), and the $Hg^{2+}$-ion-stabilized duplex structure (b), generated in the presence of cysteine and $Hg^{2+}$ ions, respectively. Adapted with permission from Ref. [22]. Copyright 2013 American Chemical Society. C) $Hg^{2+}$-ion-driven formation and catalytic activation of the $Mg^{2+}$-dependent DNAzyme, and the switching "OFF" of the catalytic functions of the system by the elimination of the $Hg^{2+}$ ions with lipoic acid-functionalized magnetic particles (MP). D) Switchable "ON-OFF" activation of the $Mg^{2+}$-dependent DNAzyme: a) In the presence of added $Hg^{2+}$ ions. b) Upon the elimination of $Hg^{2+}$ ions with lipoic acid-modified MPs. Adapted with permission from Ref. [23]. Copyright 2010 Royal Society of Chemistry.

electrode were switched between high (ON) and low (OFF) values, respectively (Figure 7B). The T-$Hg^{2+}$-T cooperative stabilization of duplex DNA structures and the Cys-mediated separation of the duplexes by the elimination of the $Hg^{2+}$ ions was used to develop a switchable DNAzyme system,[22] Figure 8A. The system consists of the strands **15**, **16**, and **17**. The strands **15** and **16** are composed of subunits corresponding to the hemin/G-quadruplex HRP-mimicking DNAzyme sequence. Each of these sequences is elongated with T-containing domains that are partially complementary to strand **17**. In the absence of $Hg^{2+}$ ions the hemin/G-quadruplex DNAzyme structure was stabilized, resulting in the catalyzed generation of chemiluminescence through the DNAzyme-mediated oxidation of luminol by $H_2O_2$, state A. In the presence of $Hg^{2+}$ ions, the duplex generated by the cooperative formation of T-$Hg^{2+}$-T bridges between strand **17** and the tethers of strands **15** and **16** resulted in the separation of the DNAzyme structure and the formation of the catalytically inactive complex structure **15/16/17**, state B (Figure 8A). In this configuration, the generation of chemiluminescence was prohibited. Addition of cysteine (Cys) eliminated the $Hg^{2+}$ ions from the complex structure **15/16/17** causing the structure to separate and the regeneration of the catalytically active hemin/G-quadruplex DNAzyme. By the cyclic addition of $Hg^{2+}$ ions to the system in state A to yield state B, and the Cys-mediated transition of state B to state A, the chemiluminescence generated by the system was switched between "ON" and "OFF" states, respectively (Figure 8B).

Similarly, the $Mg^{2+}$-dependent DNAzyme was switched "ON" and "OFF" by the formation or dissociation of T-$Hg^{2+}$-T complexes,[23] Figure 8C. The strands **18** and **19** include in domains I and II the sequences corresponding to the DNAzyme subunits and the domains III and IV that can hybridize with the ribonucleobase-containing substrate **20**. The domains V and VI in strands **18** and **19** include partial base complementarity and T-base mismatches. While in the absence of $Hg^{2+}$ ions the formation of stable $Mg^{2+}$-dependent DNAzyme structures is prohibited, subjecting the system to $Hg^{2+}$ ions resulted in the cooperative stabilization of the $Mg^{2+}$-dependent DNAzyme structure that hybridized with the substrate strand **20**. The resulting DNAzyme/substrate structure catalyzed the hydrolytic cleavage of the substrate. As the substrate was labeled with a fluorophore/quencher pair (F/Q), cleavage of the substrate led to a fluorophore-

  

labeled fragmented product that enabled the fluorescence probing of the $Hg^{2+}$-ion-stimulated switched-on DNAzyme. Treating the system with magnetic particles (MP), functionalized with lipoic acid, resulted in the elimination of the $Hg^{2+}$ ions from the DNAzyme nanostructures, and the magnetic removal of the $Hg^{2+}$ ions from the system. This resulted in the separation of the DNAzyme subunits and the formation of a catalytically inactive system. Re-addition of $Hg^{2+}$ ions to the system regenerated the catalytically active DNAzyme structure. By the cyclic treatment of the system consisting of strands **18**, **19**, and **20** with $Hg^{2+}$ ions, and lipoic-acid-functionalized magnetic particles, the $Mg^{2+}$-dependent DNAzyme was switched between "ON" and "OFF" states, respectively (Figure 8D).

In analogy to T-$Hg^{2+}$-T bridges, that cooperatively stabilize duplex DNA structures, cytosine-$Ag^{+}$-cytosine (C-$Ag^{+}$-C) bridging complexes found similar applications. For example, the switchable and cyclic "ON" and "OFF" operation of the hemin/G-quadruplex HRP-mimicking DNAzyme was reported using $Ag^{+}$ ions and cysteine (Cys) as triggers.[24] It should be noted that many ion-triggered switches provide the basis for the development of ion sensors and sensor-regeneration systems.[25]

### 2.2. pH Value Triggered DNA Switches

The self-assembly of cytosine-rich i-motif structures at acidic pH values (ca. 5.0) was implemented as a general method to design switchable DNA structures. This approach is exemplified in Figure 9A with a system consisting of the C-rich sequence **21** and a partially complementary sequence **22**.[26] The 5′- and 3′-ends of strand **21** were functionalized with a fluorophore (F = Rhodamine green, RhG) and a quencher (Q = Dabcyl, Dab), respectively. At acidic pH values, (in this case pH 5.0) the i-motif structure of strand **21** is stabilized, resulting in the fluorophore/quencher pair being in close proximity, leading to the effective fluorescence quenching of the fluorophore. Neutralization of the system separated the i-motif structure, and this stimulated the formation of the duplex between nucleic acids **21** and **22**. The spatial separation between the fluorophore and quencher intensified the fluorescence of the fluorophore. Subjecting the system to the reversible pH cycles of pH 5.0 and pH 8.0, resulted in the cyclic switchable generation of the i-motif and duplex DNA structures, and the process was probed by the fluorescence intensities of the fluorophore (Figure 9B).

The pH-stimulated transition of a duplex nucleic acid structure to the i-motif structure has been implemented to design a switchable nanospring, Figure 10A.[27] The DNA ring α was separately cross-linked by the nucleic acids **23** and **24**, to form the two-ring subunits I and II, respectively. Subsequently, the strand **25**, modified at its two ends with a fluorophore/quencher pair, was used to bridge the subunits I and II, through two complementary hybridization domains with ring α, leading to oligomeric chains consisting of alternate subunits I and II, bridged by strand **25**. All the bridging strands **23**, **24**, and **25**, were composed of G-rich sequences, capable of forming the G-quadruplex nanostructures at

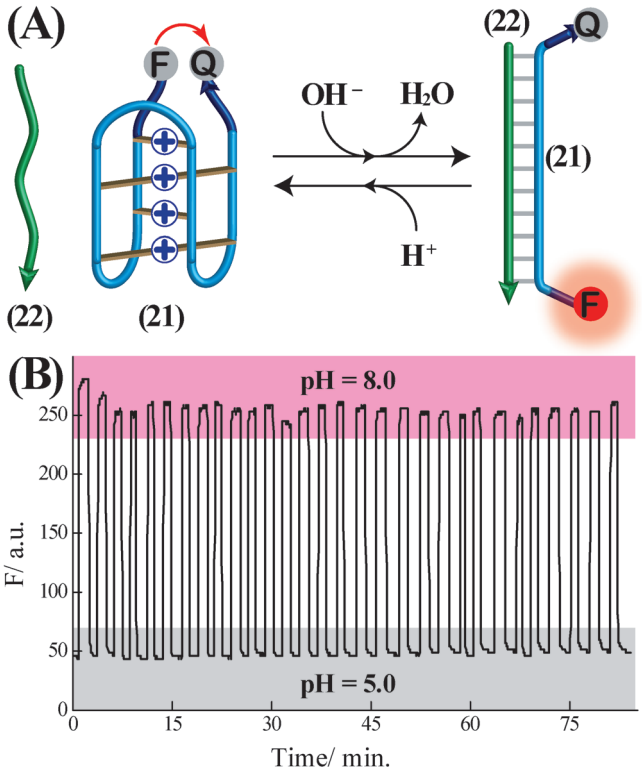


***Figure 9.*** A) pH-value-stimulated transitions between i-motif and duplex structures. Structural transitions are probed by the fluorescence intensities of a fluorophore label in the presence of a quencher unit. B) Cyclic fluorescence intensity changes of the fluorophore generated by the i-motif structure (pH 5.0, low intensity), and the reconfigured duplex structure (pH 8.0, high intensity). Adapted with permission from Ref. [26]. Copyright 2003 Wiley-VCH.

pH 6.0. The bridging strands were hybridized with the C-rich complementary strand **26** to yield the rigidified extended "spring" structure, state I. At pH 6.0 the C-rich strand **26** was released from the duplex structures and stabilized in the form of the i-motif structure, while leaving the bridging units in the compressed G-quadruplex structures, yielding the compressed "spring" structure, state II. By subjecting the system to cyclic acidic (pH 6.0) and basic (pH 8.0) environments, the system was reversibly switched between compressed and extended spring structures. These transitions were monitored by atomic force microscopy (AFM) and fluorescence measurements. Figure 10B shows the cyclic fluorescence intensity changes upon the pH-stimulated transitions of the system between the extended (state I) and compressed (state II) "spring" structures. The cyclic, pH-induced transitions of the nanospring system between the extended and compressed states were further used to control the aggregation/de-aggregation of Au nanoparticles (NPs) chains (Figure 10C). Au NPs were functionalized with a single nucleic acid (**26**), that was complementary to the bridging strands **23**, **24**, and **25**. The hybridization of the **26**-modified Au NPs with the two-ring subunits, and their interconnection, led at pH 8.0, to the extended Au NPs-functionalized spring structure, state III (Figure 10D, panel a). The TEM analysis of the resulting Au NPs chains revealed an inter-particle distance of approxi-

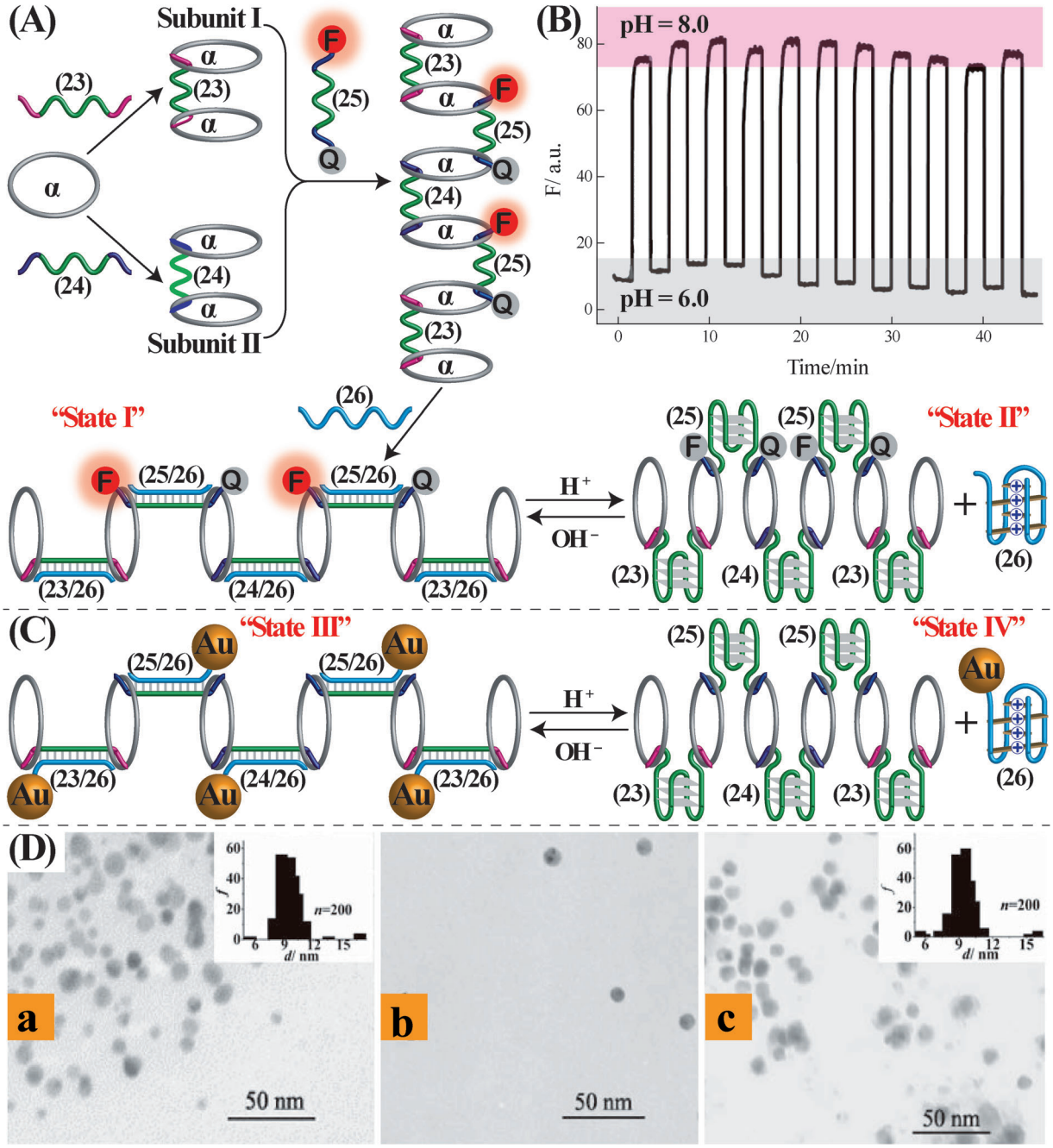


***Figure 10.*** A) Synthesis of a pH-value-driven DNA nanospring, and the cyclic pH-value-stimulated switchable transitions of the spring between the extended configuration, state I (pH 8.0) and the compressed configuration, state II (pH 6.0). The spring transitions are monitored by labeling the spring units with a fluorophore/quencher pair. The extended configuration, state I, reveals high fluorescence intensities, whereas the compressed configuration, state II, shows low fluorescence intensities. B) Fluorescence changes upon the pH-value-triggered cyclic switching of the DNA nanospring between the state I (pH 8.0, high fluorescence) and state II (pH 6.0, low fluorescence). C) Functionalization of the DNA nanospring with Au NPs by using nucleic acid-functionalized Au NPs as duplex-bridging units of the extended nanospring configuration. Subjecting the Au NPs-functionalized extended nanospring to acidic pH values yields the G-quadruplex-compressed nanospring and the separated individual i-motif-functionalized Au NPs. D) TEM images, and the respective histograms, of interparticle distances corresponding to: a) The Au NPs-modified extended nanospring at pH 8.0, b) The Au NPs generated upon treatment of the system in (a) at pH 6.0. c) The Au NPs assemblies formed upon treatment of the system in (b) at pH 8.0, and the regeneration of the extended Au NPs-modified nanospring. Adapted with permission from Ref. [27]. Copyright 2010 Wiley-VCH.

mately 10 nm, consistent with the inter-ring separation distances. The acidification of the system, pH 6.0, resulted in the separation of the **26**-modified Au NPs and the formation of the compressed nanospring structure, state IV. This transition was evident by the TEM image that revealed individual Au NPs (Figure 10 D, panel b). The subsequent neutralization of the system, pH 8.0, restored the extended nanospring structures that were functionalized by Au NPs to

  

form chains exhibiting inter-particle distances of approximately 10 nm (Figure 10D, panel c).

The pH-stimulated DNA duplex to i-motif structure transitions were further applied to generate switchable DNAzyme systems.[28,29] The C-rich sequence forming at acidic pH values the i-motif structure can hybridize, at neutral pH, with a G-rich sequence capable of forming a G-quadruplex structure. Such G-quadruplex structures may bind hemin to form a hemin/G-quadruplex horseradish peroxidase (HRP)-mimicking DNAzyme.[30] Accordingly, the hairpin structure **27** was designed to include in domain **a** the C-rich sequence and in domain **b** the partially complementary G-rich sequence (Figure 11A).[28] The hybridization between domains **a** and **b** yielded, at neutral pH, the energetically stabilized hairpin structure, in which the G-rich sequence was caged (blocked) in a structure that could not fold into a G-quadruplex configuration, state I. At pH 5.2 the C-rich sequence was stabilized in the form of the i-motif structure, leading to the uncaging (unblocking) of the G-rich sequence and to its folding into the catalytically active hemin/G-quadruplex DNAzyme structure, state II. The resulting DNAzyme catalyzed the $H_2O_2$-mediated oxidation of $ABTS^{2-}$, to the colored product $ABTS^{\bullet-}$ ($\lambda_{max} = 415$ nm), which provided the readout signal for the catalytic process. By subjecting state II to pH 7.0 the i-motif structure was dissociated, resulting in the re-assembly of the energetically stabilized hairpin structure state I, that lacked catalytic functions. The cyclic opening of the hairpin structure state I, at pH 5.2, and the reverse re-closure of the hairpin structure by subjecting state II to neutral conditions, at pH 7.0, resulted in the reversible switching "ON" and "OFF" of the catalytic functions of the hemin/G-quadruplex HRP-mimicking DNAzyme (Figure 11B).

The pH-stimulated formation and dissociation of the i-motif structure was further implemented to reversibly switch "ON" and "OFF" the catalytic functions of the $Mg^{2+}$-dependent DNAzyme,[29] Figure 11C. The nucleic acids **28** and **29** were used as functional subunits to control the activity of the DNAzyme by environmental pH value. The domains I and II of **28** and **29**, respectively, include the base sequences of the $Mg^{2+}$-dependent DNAzyme subunits, and the domains III and IV include the sequences complementary to the ribonu-

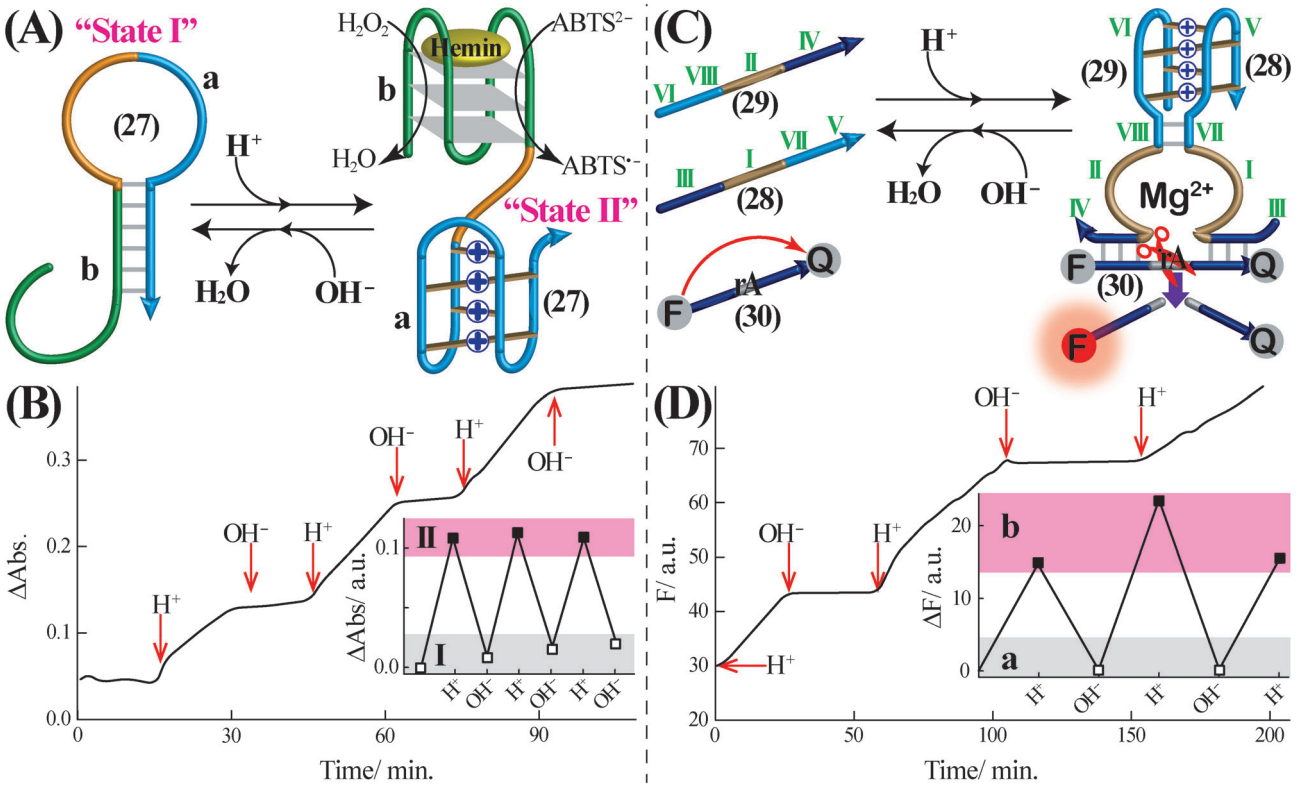


***Figure 11.*** A) Cyclic pH-value-triggered switchable transitions of a functional hairpin structure, state I, into an i-motif-hemin/G-quadruplex conjugate, state II, and the reverse process. The transitions are followed by the "ON" and "OFF" activities of the hemin/G-quadruplex DNAzyme in states II and I, respectively. B) Absorbance changes upon the $H^+$-triggered formation of the i-motif-hemin/G-quadruplex DNAzyme conjugate, state II, that catalyzes the $H_2O_2$-mediated oxidation of $ABTS^{2-}$ to $ABTS^{\bullet-}$, switched "ON", and the $OH^-$-induced switched "OFF" system, state I. Inset: Cyclic absorbance changes upon switching the system between states I and II. Adapted with permission from Ref. [28]. Copyright 2011 Royal Society of Chemistry. C) Cyclic pH-value-induced switchable assembly and separation of the $Mg^{2+}$-dependent DNAzyme using an i-motif bridging unit. The i-motif unit cooperatively stabilizes the DNAzyme subunits **28** and **29** into the catalytically active DNAzyme structure. The activity of the DNAzyme is monitored by the fragmentation of the fluorophore/quencher-modified substrate, and the generation of fluorescence. D) Fluorescence changes upon the switchable activation ($H^+$) and separation ($OH^-$) of the $Mg^{2+}$-dependent DNAzyme. Inset: Switchable fluorescence changes upon the pH-stimulated "ON/OFF" activation of the DNAzyme. Adapted with permission from Ref. [29]. Copyright 2010 Royal Society of Chemistry.

cleobase-containing substrate **30**. The respective regions V and VI in **28** and **29** consist of C-rich domains that are subunits of the i-motif structure. The sequences comprising domains VII and VIII in **28** and **29** include only three complementary base-pairs. At neutral pH, the DNAzyme subunits, **28** and **29**, and the DNAzyme substrate **30** are separate. At pH 5.8, the i-motif structure between domains V and VI is formed, and the DNAzyme catalytic core-loop structure is stabilized by the cooperative hybridization of domains VII/VIII and the i-motif nanostructures. This arrangement allows the binding of the substrate **30** to the supramolecular DNAzyme nanostructure. In the presence of $Mg^{2+}$ ions the DNAzyme is activated towards the cleavage of DNAzyme substrate. As the substrate is functionalized with a fluorophore/quencher (F/Q) pair, its catalytic cleavage leads to a fragmented fluorophore-functionalized nucleic acid, and the resulting fluorescence provides a readout signal for the DNAzyme activity. Neutralization of the system results in the separation of the i-motif complex, the dissociation of the supramolecular DNAzyme complex into the separated DNAzyme subunits **28** and **29**, and to the switching off of the DNAzyme functions of the system. By the cyclic changing the pH values of the system between 5.8 and 7.2 the catalytic functions of the DNAzyme system are reversibly switched between "ON" and "OFF" states, respectively (Figure 11 D).

The pH-value-induced transitions between i-motif structures and random-coil strands were further applied to control the aggregation of Au NPs.[31] While individual Au NPs exhibit a localized plasmonic excitation band (ca. $\lambda =$ 530 nm), the aggregation of Au NPs leads to a broad interparticle plasmonic coupling excitation ($\lambda > 560$ nm) and to a color change from purple (individual NPs) to blue (aggregated NPs). Such Au NPs aggregation phenomena were extensively used to develop different sensor or biosensing platforms.[32] Figure 12 A depicts schematically the pH-value-stimulated aggregation of Au NPs. Two types of Au NPs, I and II, were prepared where type-I particles were functionalized with the C-rich nucleic acid **31**, and type-II particles were modified with the nucleic acid **32**, complementary to strand **31**. At neutral pH, the hybridization between **31** and **32** leads to the aggregated Au NPs. In turn, at pH 5.0 the strand **31** forms the stable i-motif structure that prohibits the formation of the aggregated Au NPs. Subjecting the aggregated Au NPs to an environment with an acidic pH value (pH 5.0) results in the separation of the aggregates through the stabilization of the i-motif DNA-protected individual NPs. By the cyclic neutralization and acidification of the system, the aggregation of Au NPs is reversibly switched between "ON" and "OFF" states respectively (Figure 12 B).

The pH-stimulated reconfiguration of DNA structures between two states was extended to systems mimicking mechanical machines. For example, Figure 13 A depicts the pH-value-induced opening and closure of DNA tweezers.[33] The molecular device consists of two "arms", **33** and **34**, bridged by the strands **35** and **36**. The sequences I and II in the "arms" **33** and **34** include C-rich domains capable of forming i-motif structures at pH 5.2. The bridging strand **35** was modified at its 3′- and 5′-ends with the fluorophore/quencher

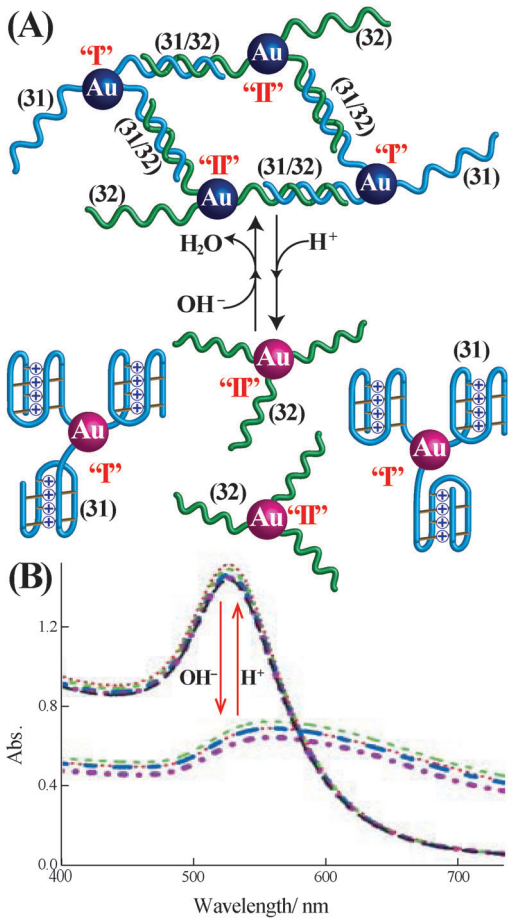


***Figure 12.*** A) Cyclic pH-value-stimulated switchable aggregation and de-aggregation of Au NPs. B) Absorption spectra corresponding to the separated Au NPs, generated under acidic conditions, and of the aggregated Au NPs formed under basic conditions. Adapted with permission from Ref. [31]. Copyright 2007 Royal Society of Chemistry.

(F/Q) pair, and these acted as labels for the mechanical operation of the DNA device. At pH 7.2, the linker strands **35** and **36** bridge the "arms" **33** and **34** to form the closed structure of the tweezers, state A. The close proximity between the fluorophore (F) and quencher (Q) units lead to an effective quenching of the fluorophore (Figure 13 B, curve a). Acidification of the system leads to the reconfiguration of the domains I and II of the "arms" into the i-motif structures. This change results in the release of the bridging unit **36**, and the opening of the tweezers to give state B. The greater spatial separation between the fluorophore and quencher units in the open-tweezers state leads to less effective quenching and to a higher fluorescence of the fluorophore (Figure 13 B, curve b). Neutralization of the system dissociated the i-motif structure, resulting in the rebinding of bridging strand **36** to the "arms" **33** and **34**, and to the closure of the tweezers. By alternating the molecular DNA system between pH 5.2 and pH 7.2, the tweezers were cycled between open and closed states, respectively (Figure 13 B, inset). A similar concept was applied for the pH-value-stimulated reconfiguration of a triangular DNA nanostructure, Figure 13 C.[34] The system consisted of a two-arm

  

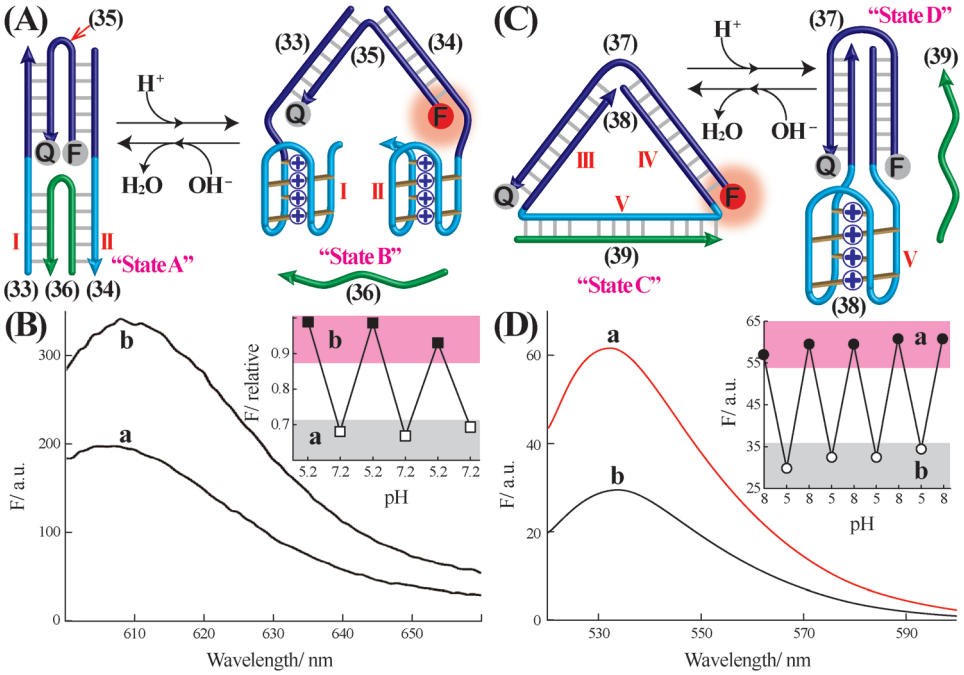


***Figure 13.*** A) pH-value-stimulated cyclic switchable opening and closure of a DNA tweezers device. The mechanical functions of the device are monitored by the labeling of the bridging unit of the tweezers with a fluorophore/quencher pair (open tweezers: high fluorescence intensity. Closed tweezers: low fluorescence intensity). B) Fluorescence spectra corresponding to: a) The closed tweezers, and b) the open tweezers. Inset: Cyclic changes in fluorescence intensity upon switching the tweezers between the closed (a) and open (b) states of the device. Adapted with permission from Ref. [33]. Copyright 2009 American Chemical Society. C) pH-stimulated cyclic switchable reconfiguration of a DNA triangle nanostructure. The system undergoes switchable transitions between an extended structure and an i-motif-assisted compressed structure. The transitions are probed by monitoring the fluorescence features of the system labeled with a fluorophore/quencher pair. D) Fluorescence spectra corresponding to: a) the extended structure, and b) the compressed structure. Inset: Switchable changes in fluorescence intensity upon the reversible pH-value-stimulated conversion of the extended structure (high fluorescence) into the compressed, i-motif-driven structure (low fluorescence), and back. Adapted with permission from Ref. [34]. Copyright 2009 Royal Society of Chemistry.

nucleic acid frame **37**, a closed loop template **38**, which includes domains III and IV complementary to the frame, and a third C-rich domain V, complementary to the auxiliary strand **39**. Under neutral conditions; the DNA composite is stretched into a DNA triangle, state C. The 3′- and 5′-ends of the frame strand **37** were labeled by a fluorophore/quencher (F/Q) pair, and the spatial separation of the pair, by the triangular structure, resulted in inefficient quenching of the fluorophore and a high fluorescence signal. As the domain V of the template **38** is composed of C-rich bases, acidification of the system resulted in the stabilization of the i-motif structure, the release of the strand **39**, and the construction of the DNA nanostructure to state D. The close proximity between the fluorophore and quencher units in state D resulted in effective quenching of the fluorophore. The neutralization of the system dissociated the i-motif structure, and this led to the re-binding of auxiliary strand **39** to domain V of strand **38**, and the formation of the extended DNA triangular nanostructure, state C. By the reversible acidification and neutralization of the system; the DNA scaffold was cycled between states D and C, respectively, and the mechanical operations of the device were monitored by the low and high fluorescence readout signals (Figure 13D). Also, interlocked DNA rings (catenanes) were reversibly reconfigured by the pH-stimuli-driven formation/dissociation of an i-motif structure.[35] By applying an oscillatory pH system that leads to pH values changing between 5.2 and 6.9, the autonomous oscillation of the interlocked catenane between the two states (a "DNA pendulum") was demonstrated.[35] Also, reversible pH-triggered walkers on DNA scaffolds were reported using the formation or dissociation of i-motif structures.[36]

The pH-value-stimulated transitions between random-coil and i-motif structures were further examined on surfaces, and particularly, on conductive surfaces (electrodes). The structural transitions led to the establishment of electrical or photoelectrochemical DNA-based switches, and to the control of the electron-transfer properties at electrode surfaces. Figure 14A shows schematically the operation of a pH-stimulated electrochemical switch.[37] The thiolated nucleic acid **40** was assembled on an electrode surface, and the ferrocene-labeled nucleic acid **41**, exhibiting partial complementarity to **40**, was hybridized with strand **40**. The two strands include non-complementary C-rich domains I and II. The resulting rigidified hybrid duplex **40**/**41** formed at pH 8.0 leads to the spatial separation of the ferrocene redox label from the electrode surface, resulting in poor electron transfer with the electrode and a weak voltammetric response (Figure 14B, curve a). Acidification of the electrolyte solution, pH 5.8, reconfigures the duplex structure into the i-motif assembly, where the ferrocene redox label is in close proximity to the electrode surface. This change results in effective electrical contact between the redox label and the electrode, which is reflected by a high voltammetric response (Figure 14B, curve b). By the cyclic control of the pH value of the electrolyte solution between pH 8.0 and pH 5.8, the voltammetric responses of the system were switched between low and high values, respectively (Figure 14B, inset). The pH-stimulated control of the voltammetric responses of a ferrocene-labeled DNA associated with an electrode, that undergoes switchable random-coil to i-motif structures, was further applied to develop electrochemical pH-value-sensing platforms.[38]

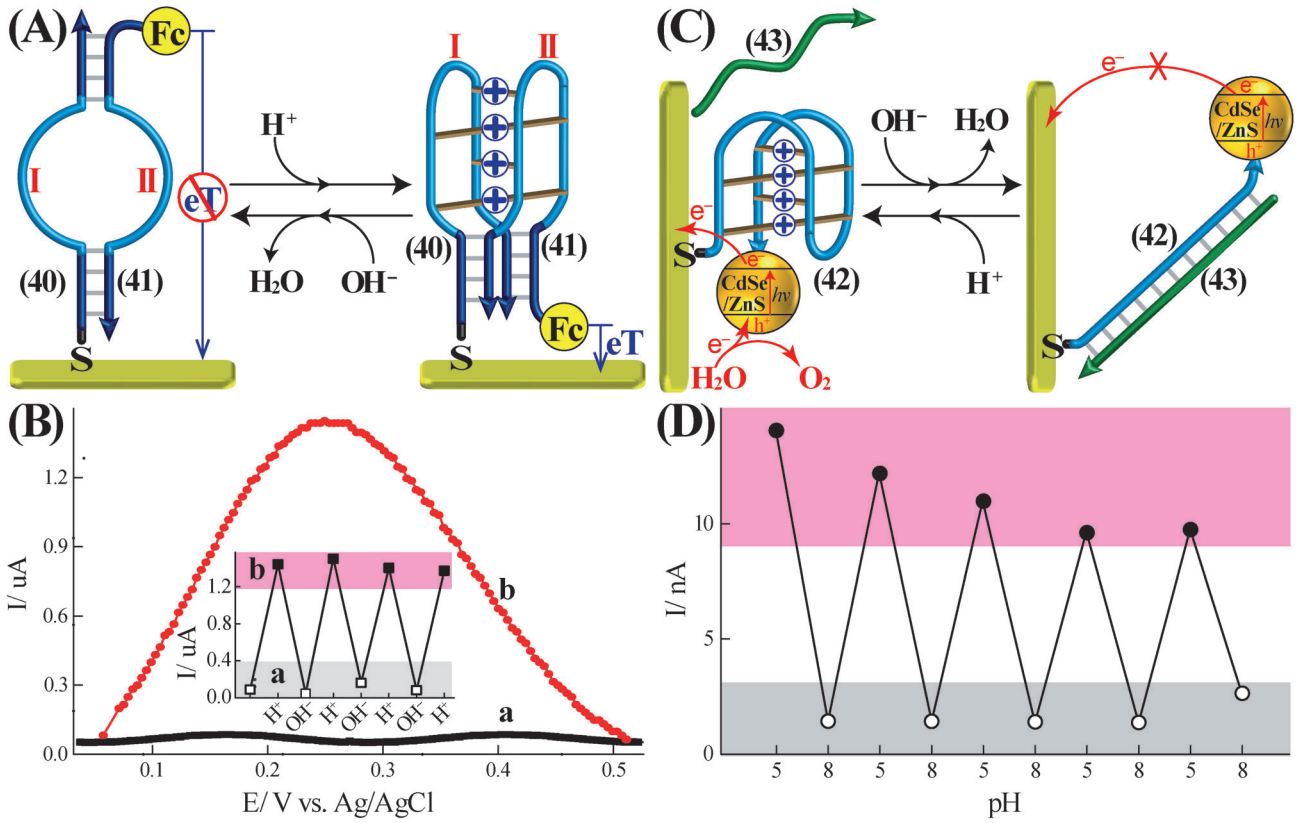


***Figure 14.*** A) Electrochemical transductions of the pH-value-induced cyclically switchable reconfiguration of a redox-labeled DNA structure on an electrode surface. Reconfiguration proceeds between a ferrocene-labeled loop-containing duplex structure (pH 8.0) and a ferrocene-labeled i-motif structure (pH 5.8). B) Voltammetric responses of the ferrocene-labeled DNA nanostructures: a) In the loop-duplex configuration, b) In the i-motif configuration. Inset: Cyclic voltammetric responses upon switching the pH value of the modified electrode between a) the loop-duplex structure, and b) the i-motif structure. Adapted with permission from Ref. [37] Copyright 2012, Elsevier. C) Photoelectrochemical transductions of the pH-stimulated transitions between i-motif-functionalized CdS NPs and duplex-DNA-modified CdS NPs. The i-motif-functionalized CdS NPs modifying the electrode (pH 5.0) leads to a high photocurrent, owing to the close proximity between the NPs and the electrode. Dissociation of the i-motif structure (pH 8.0), and rigidification of the separated strands by means of the **42**/**43** duplex, spatially separates the CdS NPs from the electrode, thus prohibiting the photocurrent. D) Cyclically changing photocurrents upon reversible changes in pH values which cause the transformation between the i-motif-CdS NPs (pH 5.0) and the duplex DNA-CdS NPs (pH 8.0) structures. Adapted with permission from Ref. [39]. Copyright 2009 Royal Society of Chemistry.

A related approach has been utilized to design a DNA-based photoelectrochemical switching device, Figure 14C.[39] A 5′-thiolated nucleic acid **42**, consisting of a C-rich sequence, was assembled on an Au electrode, and the nucleic acid was modified at its 3′-end with CdSe/ZnS quantum dots (QDs). At acidic pH values (pH 5.0), the nucleic acid **42** folded into an i-motif structure, leading to close proximity between the QDs and the electrode surface. This change led to a high photocurrent. The photocurrent was attributed to the injection of the photoexcited conduction-band electrons to the electrode, followed by the oxidation of water to $O_2$ by the valence-band holes. The neutralization of the system, and in the presence of the added auxiliary strand **43**, complementary to **42**, the i-motif structure dissociated, while forming the rigidified QDs-functionalized duplex. This change led to the spatial separation of the QDs and the electrode support, resulting in inefficient electron ejection of the conduction-band electrons to the electrode, and to the blocking of the photocurrent. Subjecting the modified electrodes to cyclic changes in pH values between 5.0 and 8.0 led to switchable "ON" and "OFF" photocurrents, respectively (Figure 14D).

The interfacial electron-transfer properties of C-rich DNA-monolayer-modified electrodes were switched by the pH-value-stimulated transitions between random-coil and i-motif configurations, Figure 15A.[40] A thiolated nucleic acid **44**, consisting of a C-rich sequence, was assembled on a Au electrode. The negative charge associated with the random-coil DNA monolayer repelled the negatively charged redox labels solubilized in the electrolyte solution (e.g., $[Fe(CN)_6]^{3-/4-}$), thus increasing the interfacial electron-transfer resistance (Figure 15B, curve a). The pH-value-stimulated formation of the protonated inter-cytosine i-motif structure reduced the negative charge associated with the electrode, thus decreasing the interfacial electron-transfer resistance (Figure 15B, curve b). The respective interfacial electron-transfer resistances were probed by Faradaic impedance spectroscopy. The random-coil monolayer-modified electrode revealed a high interfacial electron-transfer resistance, $R_{et} =$ 500 Ω, while the i-motif monolayer-functionalized electrode showed a lower interfacial electron-transfer resistance, $R_{et} =$ 300 Ω. By the cyclic switching of the pH values of the electrolyte solution between 5.8 and 7.0, the interfacial

  

electron-transfer resistances were reversibly switched between low and high values, respectively (Figure 15C).

The pH-value-stimulated switchable control of the fluorescence properties of a fluorophore-modified i-motif monolayer associated with the electrode was demonstrated by reversible pH-value-induced i-motif to duplex DNA structures,[41] Figure 15D. In the fluorophore-modified i-motif monolayer **45**, the fluorophore is effectively quenched by the close proximity of the fluorophore and the metallic surface. Neutralization of the system, and in the presence of the auxiliary strand **46** that is complementary to **45**, led to the dissociation of the i-motif structure, and the hybridization between nucleic acids **45** and **46**. The rigidification of the fluorophore-tethered strand, through the formation of the **45**/**46** duplex structure, and the spatial separation of the fluorophore from the surface, result in inefficient quenching of the fluorophore and trigger the fluorescence of the fluorophore. By the application of cyclic changes in pH values between pH 5.2 and pH 7.2, the system was switched between i-motif (low fluorescence) and duplex structures (high fluorescence). The autonomous oscillatory transitions between a random-coil and i-motif structures on surfaces, using an oscillatory pH-value system, were also monitored by fluorescence spectroscopy,[42] Figure 15E. An Au surface was modified with a 5′-thiolated nucleic acid **47** functionalized at its 3′-end with a fluorophore (F = Rhodamine green) unit. In the random-coil configuration at pH 7.0 the fluorophore is spatially separated from the Au surface, leading to inefficient

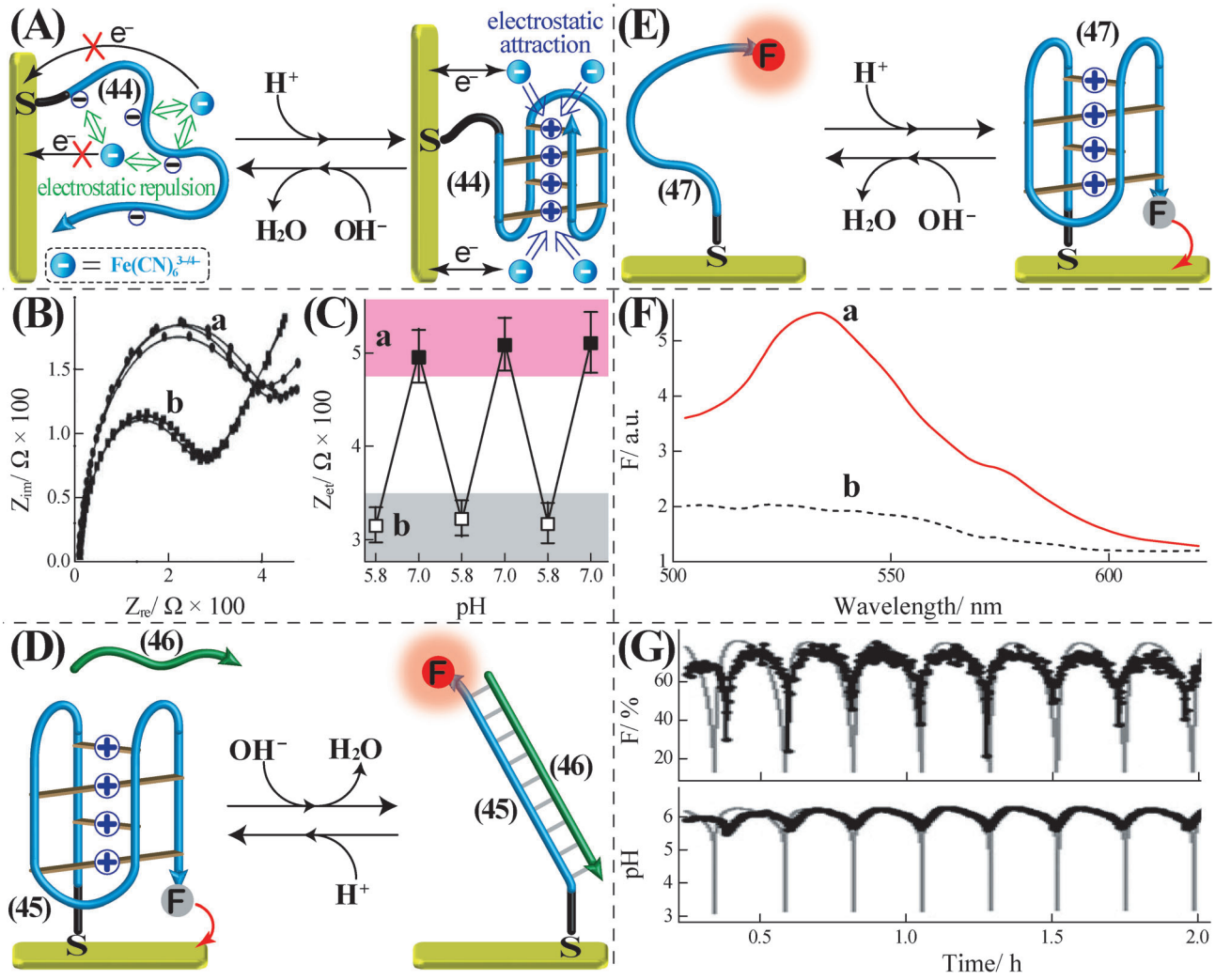


***Figure 15.*** A) Controlling the interfacial electron-transfer resistances at a Au electrode upon the pH-value-stimulated transitions between a random-coil nucleic acid (pH 7.0) and an i-motif structure (pH 5.8). Interfacial electron-transfer resistances are probed by Faradaic impedance spectroscopy using $[Fe(CN)_6]^{3-/4-}$ as a redox probe. B) Faradaic impedance spectra corresponding to: a) The random-coil DNA-modified electrode (pH 7.0). b) The i-motif-modified electrode (pH 5.8). C) Cyclic interfacial electron-transfer resistances upon reversible switching of the DNA monolayer-modified electrode between a) the random-coil and b) i-motif nanostructures. Adapted with permission from Ref. [40]. Copyright 2013 Royal Society of Chemistry. D) Fluorescence probing of the cyclic switchable transitions between an i-motif DNA structure and a rigidified duplex structure associated with a Au surface. E) Fluorescence probing of the random-coil-to-i-motif transitions, using a fluorophore-modified DNA monolayer associated with a Au surface. F) Fluorescence spectra corresponding to: a) The random-coil configuration, b) The i-motif configuration. G) Autonomous fluorescence changes upon subjecting the system shown in (E) to a system with oscillating pH values. Adapted with permission from Ref. [42]. Copyright 2006 Wiley-VCH.

quenching of the fluorophore (Figure 15F, curve a). In turn, at pH 5.5, the **47**-monolayer folded into the i-motif structure, in which the fluorophore was in intimate contact with the Au surface. This transformation results in an effective fluorescence quenching of the fluorophore (Figure 15F, curve b). The fluorophore-labeled DNA-monolayer-modified Au surface was subjected to a chemical system with oscillating pH values, consisting of $NaIO_3/Na_2SO_3/Na_2S_2O_3/H_2SO_4$. The resulting oscillations of pH values between 5.5 and 6.2 resulted in the cyclic transition of the **47**-monolayer between the i-motif and random-coil configurations, leading to overlapping oscillatory fluorescence responses between low (pH 5.5) and high (pH 6.2) values (Figure 15G). Analogous pH-value driven oscillatory transitions between an i-motif structure and a random-coil configuration were imaged by fluorescence spectroscopy in solution.[43]

### 2.3. Light-Stimulated DNA Switches

The interaction of photoisomerizable compounds with duplex DNA might allow the stability of the resulting double-stranded DNA structures to be controlled by light. Specifically, azobenzene photoisomerizable compounds were found to interact with DNA. Azobenzene compounds undergo *trans*-to-*cis* photoisomerization (upon UV irradiation) and reverse *cis*-to-*trans* photoisomerization (upon visible-light irradiation). It was found that *trans*-azobenzene units intercalate into duplex DNA structures through π–π interactions. This process leads to cooperative stabilization of the duplex structures. In turn, *cis*-azobenzene lacks affinity for duplex DNA, and hence, does not stabilize the duplex nucleic acid structures.[44,45] These fundamental interactions between the photoisomerizable azobenzene compounds and double-stranded nucleic acids were used to develop cyclic photostimulated DNA switches undergoing duplex to random-coil reversible transitions, Figure 16A.[46] The nucleic acid **48** is stabilized in the form of a hairpin structure by cooperative interactions consisting of base-pairing and the intercalated *trans*-azobenzene chromophores. As the hairpin structure is modified at its 5′- and 3′-ends with a fluorophore/quencher (F/Q) pair effective, quenching of the fluorophore occurs, resulting in low fluorescence, state I. UV-stimulated photoisomerization of the *trans*-azobenzene to *cis*-azobenzene results in chromophores lacking affinity for the stem region of the hairpin. This results in the separation of the hairpin into a random-coil structure, exhibiting high fluorescence of the fluorophore, state II. The reverse visible-light-induced photoisomerization of the *cis*-azobenzene units to *trans*-azobenzene components reconfigured the *trans*-azobenzene-stabilized hairpin structure, exhibiting low fluorescence of the fluorophore, state I. By the cyclic photoisomerization of the azobenzene units between the *trans* and *cis* states, the nucleic acid was reversibly reconfigured between the hairpin structure, state I, exhibiting low fluorescence and the random-coil configuration, state II, revealing high fluorescence (Figure 16B). The effect of photoisomerizable azobenzene units on the stabilities of duplex DNA structures were addressed in several studies by probing the melting temperatures and circular dichroism (CD) spectra of the DNA structures in the presence of the different photoisomers.[45]

Programmed photoisomerizable azobenzene molecules may interact with sequence-specific domains of duplex DNA structures, thereby controlling the stability of the resulting duplexes.[47] For example, two strands including the 5′-CGG-3′/3′-GGC-5′- mismatched sequences were found to bind selectively the *cis*-bis(naphthyridine carbamate) azobenzene, *cis*-NADA, **49a**, by the formation of hydrogen bonds between mismatched guanosine (G) units, positioned on opposing sites of the two nucleic acid strands, Figure 16C.[48] Accordingly, the two DNA strands **50** and **51** included the pyrene chromophore (X) as an internal modifier, and the sequence-specific domains for binding the *cis*-NADA (**49a**). In the presence of **49a**, the cooperative stabilization of the DNA duplex **50/51** occurred, resulting in the inter-chain formation of the pyrene excimer ($\lambda_{em} = 520$ nm), state III. Visible-light-triggered photoisomerization of *cis*-NADA (**49a**) to the *trans*-isomer, *trans*-NADA (**49b**) decreased the affinity interactions between **49b** and the nucleic acid strands, leading to their separation, state IV. The separated DNA strands **50** and **51** revealed the characteristic fluorescence of monomer pyrene ($\lambda_{em} = 430$) (Figure 16D). By the cyclic photoisomerization between **49a** and **49b** states, the reversible switchable formation of the duplex **50/51** structure (state III) and the separated strands **50** and **51** (state IV), respectively, was demonstrated (Figure 16D inset).

The photo-stimulated transitions of DNA nanostructures by means of photoisomerizable azobenzene units were further used to switch telomere G-rich chains between G-quadruplex and random-coil configurations. The bis(piperidinium) *trans*-azobenzene (**52a**) exhibited high binding affinity towards the telomeric G-rich sequence **53**, thereby stabilizing the G-quadruplex structure. The UV-light-induced photoisomerized *cis*-bis(piperdinium) photoisomer (**52b**) lacked binding affinity to the nucleic acid **53**, and its separation from the telomeric chains destabilized the G-quadruplex nanostructures, resulting in a single-stranded random-coil configuration,[49] Figure 17A. By the cyclic photoisomerization of the azobenzene compound between the *trans*- and *cis*-isomer states, the telomeric chain **53** was reversibly cycled between the G-quadruplex and random-coil configurations. The structural transitions of the nucleic acid were monitored by CD spectra, in which the formation of the G-quadruplex was evident by a positive band at $\lambda = 265$ nm that disappeared upon transition to the random-coil structure (Figure 17B).

Furthermore, the visible-light-stimulated stabilization of duplex DNA by *trans*-azobenzene compounds, and the subsequent separation of the duplex by the UV-stimulated photoisomerization of *trans*-azobenzene to *cis*-azobenzene, was implemented to photo-regulate the aggregation of Au NPs, Figure 18A.[50] Two kinds of nucleic acid-functionalized Au NPs (type I and II) were prepared, where type-I Au NPs were modified with nucleic acid **54**, that included *trans*-azobenzene photoisomerizable tethers, and type-II Au NPs were functionalized with nucleic acid **55**, exhibiting partial complementarities to strand **54**. Mixing the two types of the NPs resulted in the *trans*-azobenzene cooperative stabiliza-

  

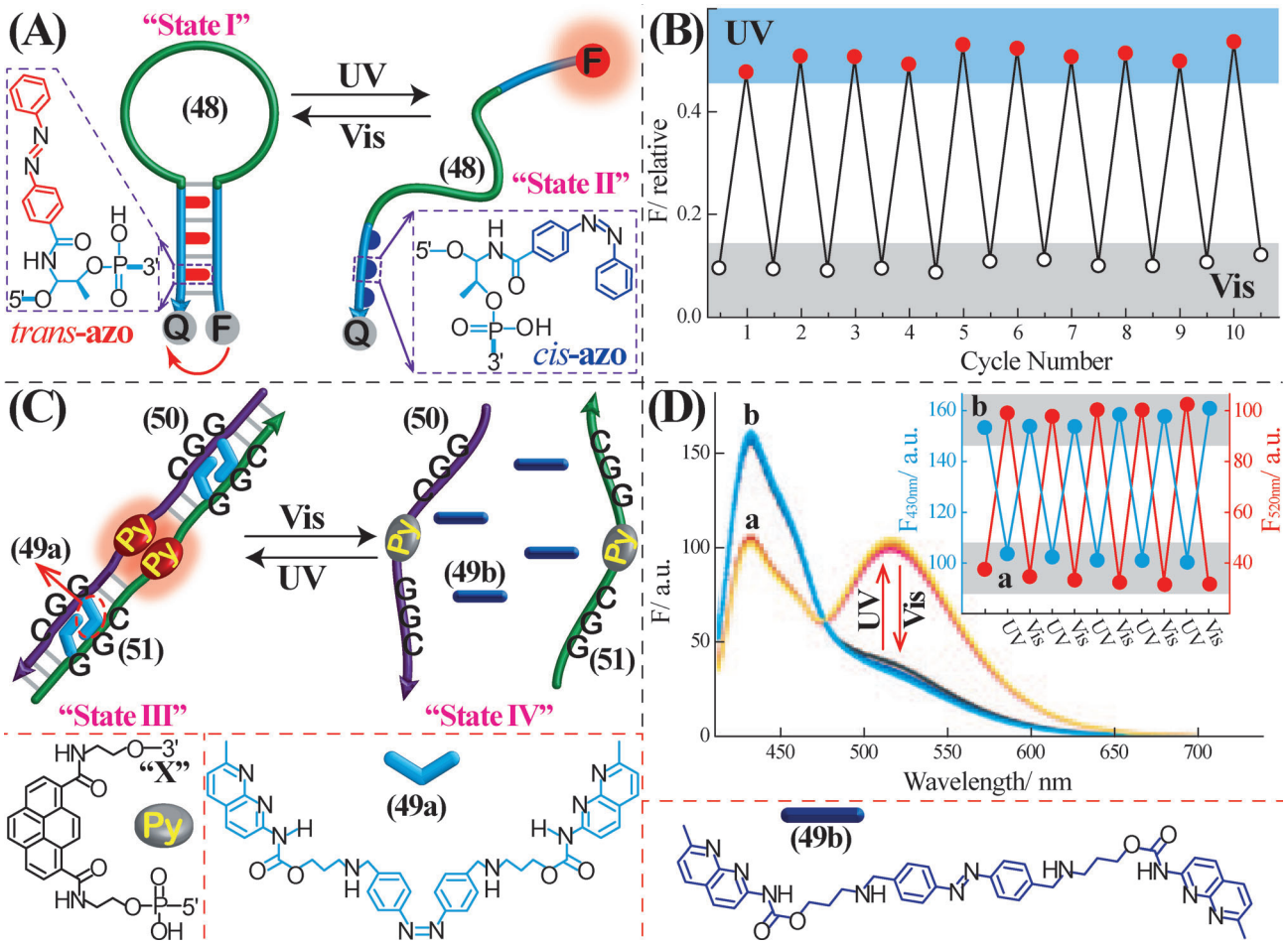


***Figure 16.*** A) Photo-stimulated cyclic switchable transitions between a hairpin structure, state I, and a random-coil configuration, state II, using azobenzene photoisomerizable units. B) Fluorescence changes upon the cyclically switchable transitions between states I and II. Adapted with permission from Ref. [46]. Copyright 2009 American Chemical Society. C) Photo-stimulated duplex-to-single-strand transitions, using photoisomerizable azobenzene intercalator units **49**. The exciplex/monomer emissions of the pyrene labels associated with the strands follow the cyclic transitions between states III and IV. D) Emission spectra of the pyrene labels in: a) state III, and b) state IV. Inset: Cyclic changes in fluorescence at $\lambda = 430$ nm (blue) and $\lambda = 520$ nm (red) upon switching the system between states III and IV. Adapted with permission from Ref. [48]. Copyright 2009 Wiley-VCH.

tion of the duplexes **54**/**55**, leading to the aggregation of the NPs. UV-light-irradiation of the aggregated NPs photoisomerized the *trans*-azobenzene units to *cis*-azobenzene compounds, leading to the separation of the aggregates. The cyclic aggregation/de-aggregation of the NPs was monitored by absorption spectroscopy, and could also be visually imaged (Figure 18B).

The azobenzene-stimulated formation and dissociation of duplex DNA structures was implemented to monitor switchable DNA structures at the single molecular level.[51] A DNA origami frame that includes protruding anchoring tethers **a**, **b**, **c**, and **d** was prepared, and the anchoring tethers **a**, **b** and **c**, **d** were bridged by duplex DNA strands, $L_1$ and $L_2$, that included the appropriate toeholds **a**′, **b**′ and **c**′, **d**′, respectively. The duplex structures $L_1$ and $L_2$ included two scaffolds **x**′ and **y**′ with which the strands $\mathbf{x}_1$, $\mathbf{x}_2$ and $\mathbf{y}_1$ and $\mathbf{y}_2$ were hybridized. The sequences $\mathbf{x}_1$ and $\mathbf{y}_1$ included protruding chains **e** and **f** that consisted of partial complementarities, and included tethered azobenzene photoisomerizable chromophores. In the *cis*-azobenzene configuration, the duplex **e**/**f** is insufficiently energetically stable, and the duplex structures $L_1$ and $L_2$ did not interact with each another, giving rise to rigid duplexes, $L_1$ and $L_2$, bridging the sites **a**, **b** and **c**, **d** on the origami frame, respectively (Figure 19A). Visible-light-triggered photoisomerization of the *cis*-azobenzene units to the *trans*-azobenzene configuration resulted in the cooperative stabilization of the duplex **e**/**f**, connecting the $L_1$ and $L_2$ duplexes, giving rise to a nanostructure with cross-links between the duplexes. By the reversible UV-stimulated photoisomerization of the *trans*-azobenzene units to the *cis*-isomer compounds, the inter-duplex cross-linking site was separated, leading to the individual rigidified duplexes $L_1$ and $L_2$. The cyclic transitions of the separated duplexes to the cross-linked duplexes, and back, upon the cyclic photoisomerization of the *cis*-azobenzene-modified duplexes to the *trans*-azobenzene state, were imaged by fast AFM (Figure 19B). Also, hexagon-shaped origami frames that are modified at programmed edges with protruding nucleic acids **56** or **57**,

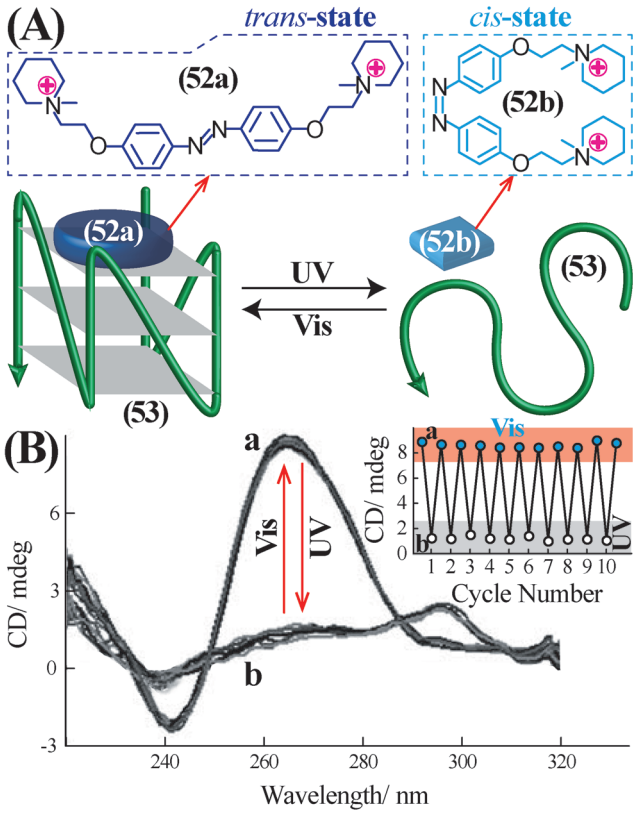


***Figure 17.*** A) Photo-stimulated G-quadruplex to random-coil transitions using a photoisomerizable azobenzene intercalator **52a** that stabilizes the G-quadruplex structure. B) Circular dichroism (CD) spectra corresponding to: a) The G-quadruplex structure stabilized in the presence of **52a**. b) The random-coil structure in the presence of **52b**. Inset: Cyclic CD intensity changes at $\lambda = 265$ nm upon the photo-stimulated switching of the system between the G-quadruplex and random-coil structures, respectively. Adapted with permission from Ref. [49]. Copyright 2010 Wiley-VCH.

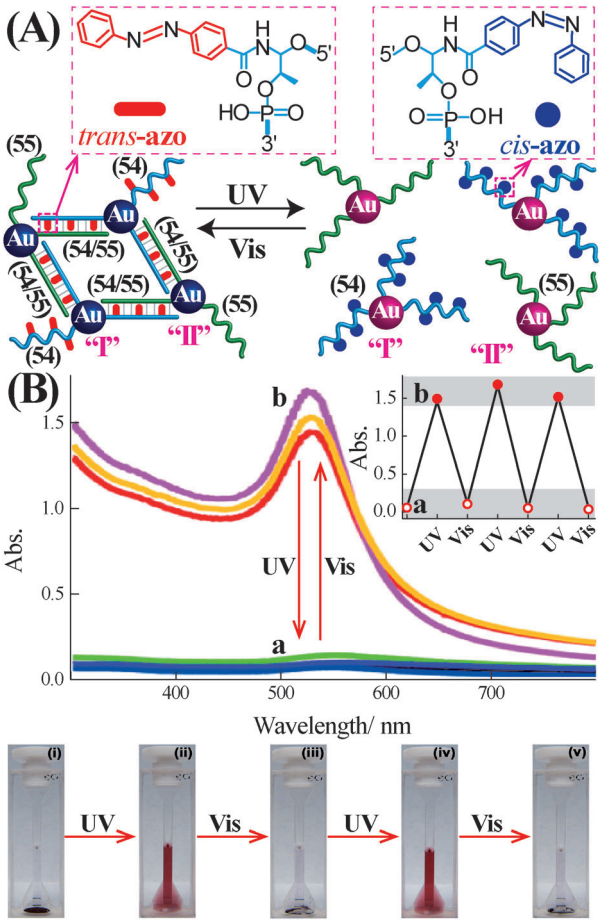


***Figure 18.*** A) Photo-stimulated aggregation/de-aggregation of nucleic acid-functionalized Au NPs that include azobenzene photoisomerizable components. B) Absorption spectra corresponding to: a) The aggregated Au NPs in the presence of the *trans*-azobenzene intercalator units. b) The de-aggregated Au NPs in the presence of the *cis*-azobenzene units. Inset: Cyclic changes in absorbance upon the cyclic, light-induced aggregation and de-aggregation of the NPs. Below: photographs corresponding to the light-induced aggregates of the Au NPs (i, iii, and v) and the de-aggregated Au NPs (ii and iv). Adapted with permission from Ref. [50]. Copyright 2012 American Chemical Society.

exhibiting partial complementarities and modified with azobenzene photoisomerizable units, were synthesized, Figure 19C.[52] In the *cis*-azobenzene configuration of the tethered nucleic acids, the hexagon-shaped DNA origami units are separated, since the base-pairing between strands **56** and **57** is insufficient to stabilize duplex structures. In turn, visible-light-stimulated photoisomerization of the *cis*-azobenzene units to *trans*-azobenzene isomers results in the cooperative stabilization of the duplexes **56**/**57** at the edges of the hexagons, yielding dimers of the hexagon-shaped origami structures. By the cyclic photoisomerization of the system between the *cis*- and *trans*-azobenzene states, the switchable transitions between monomer and dimer hexagon structures were demonstrated (Figure 19D). Furthermore, upon the functionalization of two different edges of one of the hexagons with protruding tethers containing the azobenzene photoisomerizable units, the light-induced programmed assembly of several hexagon-shaped structures was demonstrated. For example, the reaction of the hexagon-shaped origami $O_1$, functionalized at the opposite edges with the *cis*-azobenzene-functionalized nucleic acids **56**, with the hexagon-shaped origami $O_2$, that includes the *cis*-azobenzene-modified protruding sequences **57** only on one edge ($O_1$:$O_2$ ratio 1:2), resulted in, upon visible-light-stimulated photoisomerization of the *cis*-units to *trans*-azobenzene, the linear three-hexagon structure (Figure 19E). On the other hand, treatment of the *cis*-azobenzene-functionalized hexagon-shaped origami structure $O_2$, with a hexagon-shaped origami structure that includes the protruding *cis*-azobenzene nucleic acid units **56** on two edges separated by a single edge structure $O_3$ ($O_3$:$O_2$ ratio 1:2) yielded, upon visible-light-triggered photoisomerization of the *cis*-azobenzene units to the *trans*-azobenzene groups, the cooperatively stabilized concave three-hexagon structure (Figure 19F).

The reversible transitions of duplex to single-stranded DNA by means of the photoisomerization of *trans*-azobenzene chromophores to *cis*-azobenzene isomers were implemented to control protein–protein interactions,[53] to construct switchable nanoscale devices,[54–57] and to design photo-

  

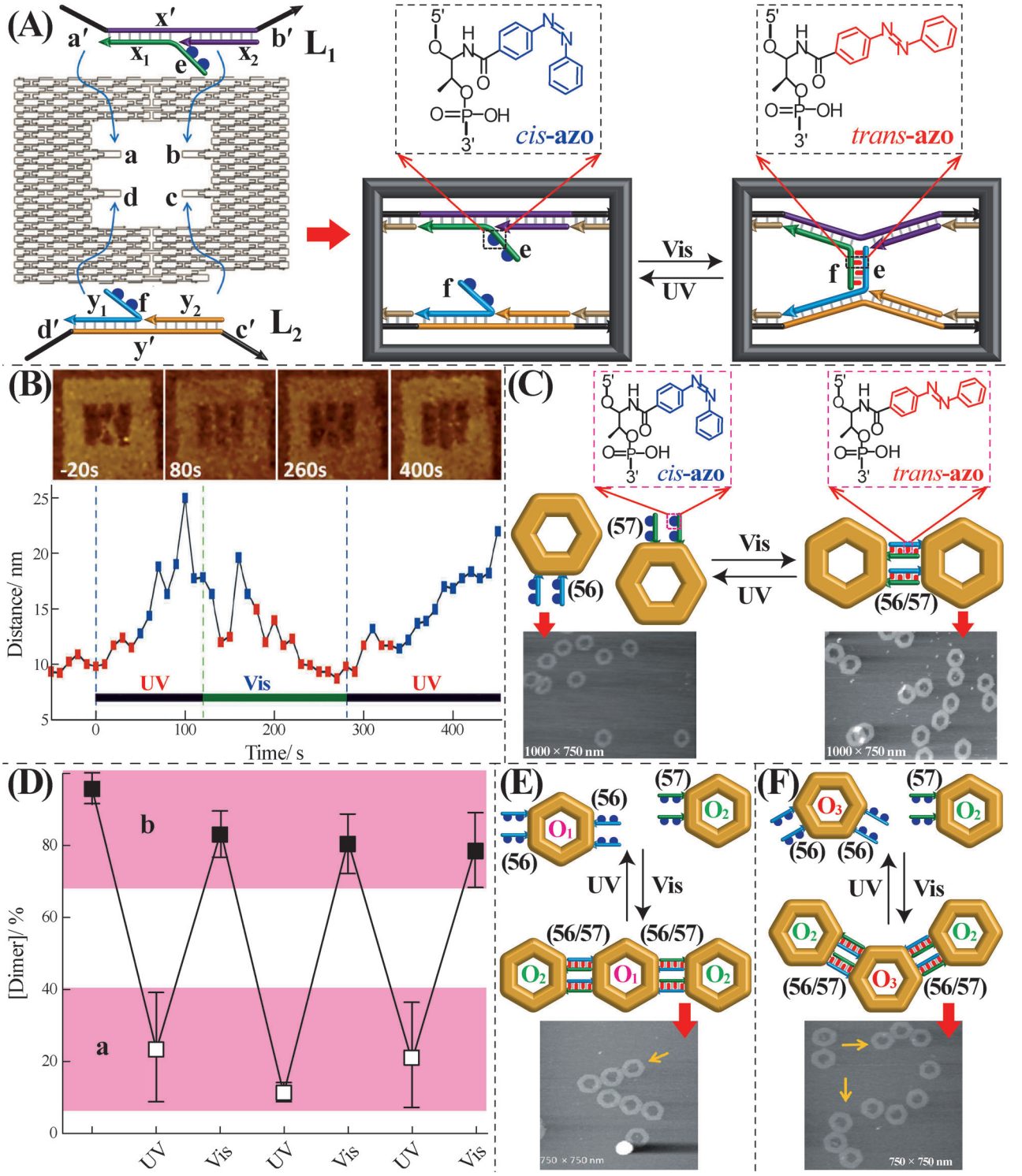


***Figure 19.*** A) Schematic representation of the photo-stimulated cyclic, switchable, transitions of two single-stranded tethers (**e** and **f**) into a duplex structure (**e**/**f**), and back, at the single-molecular level, using a DNA origami frame as a template, and photoisomerizable azobenzene units as the switching triggers. The *trans*-azobenzene stimulates the duplex formation, while the *cis*-azobenzene separates the duplex. B) Kinetic probing of the photo-stimulated transitions between the duplex DNA and the single-stranded DNAs by rapid AFM measurements showing the distances between the duplex strands ($L_1$ and $L_2$). Adapted with permission from Ref. [51]. Copyright 2012 Wiley-VCH. C) Switchable photo-stimulated assembly and separation of dimeric hexagonal DNA origami structures, in which each of the hexagons is functionalized with complementary strands consisting of azobenzene photoisomerizable units. AFM images show the dimers/monomers. D) Switchable populations changes of the dimer structure upon photoisomerization of the azobenzene units. E) Photo-stimulated formation of linear trimer DNA hexagonal structure generated upon mixing an origami DNA hexagon ($O_2$) modified at one edge with photoisomerizable azobenzene units and an origami DNA hexagon ($O_1$) modified at two opposing edges with photoisomerizable azobenzene units ($O_2$/$O_1$ ratio 2:1). F) Photo-stimulated assembly of concave trimer structures of DNA origami hexagons. One type of hexagon is modified at a single edge with the photoisomerizable azobenzene units ($O_2$), whereas the second hexagon ($O_3$) is asymmetrically modified at two edges by the photoisomerizable azobenzene units ($O_2$/$O_3$ ratio 2:1). Adapted with permission from Ref. [52]. Copyright 2012 American Chemical Society.

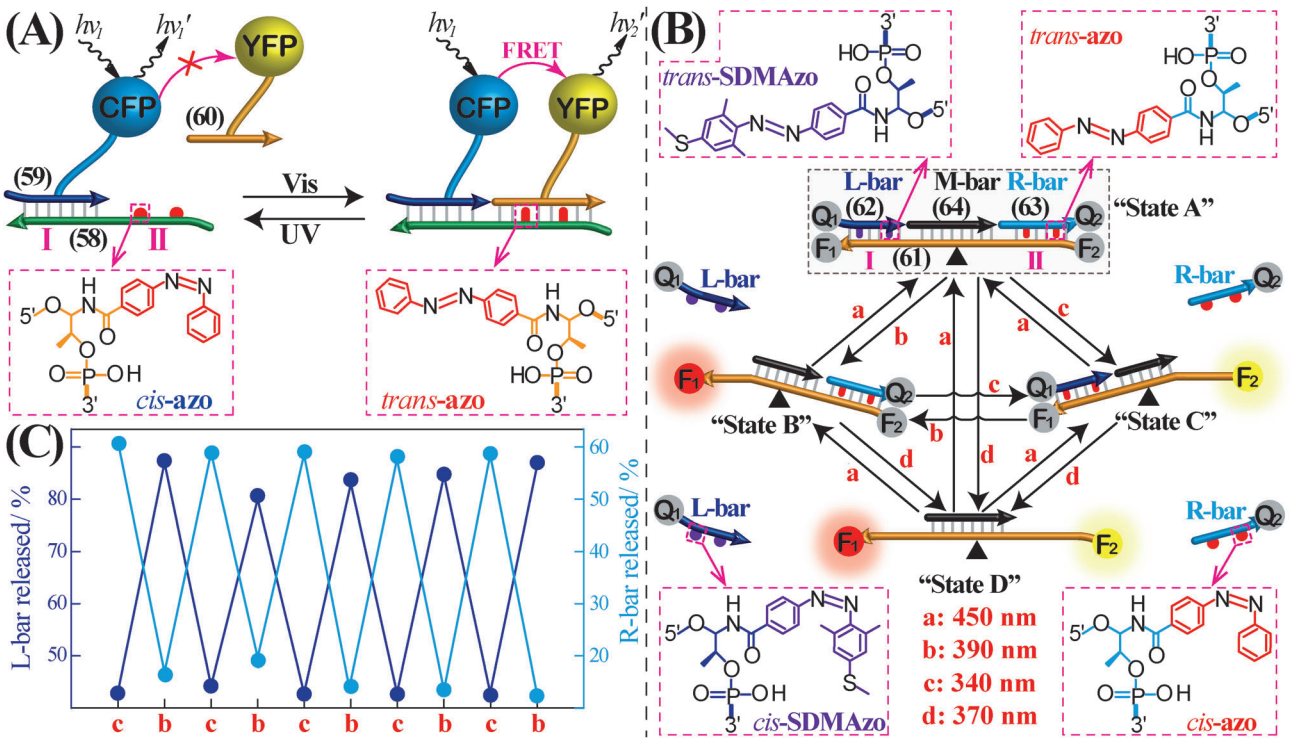


***Figure 20.*** A) Photo-stimulated control of the FRET process between two proteins in the presence of a nucleic acid scaffold functionalized with azobenzene photoisomerizable units. B) A photo-stimulated DNA "seesaw"-like device undergoing switchable light-induced transitions between states A, B, C, and D using photoisomerizable azobenzene units. The states of the device are probed by two fluorophore/quencher pairs $F_1/Q_1$ and $F_2/Q_2$. C) Fluorescence changes upon the cyclic transitions between states B and C. Adapted with permission from Ref. [54]. Copyright 2012 Wiley-VCH.

switchable DNAzymes.[58–61] Figure 20 A depicts the switchable control of the Förster resonance energy transfer (FRET) between the two fluorescent proteins, cyan fluorescent protein (CFP) and yellow fluorescent protein (YFP), using the photoisomerization of azobenzene units as switching motif.[53] A DNA scaffold (**58**) that includes two domains, I and II, acted as the template to organize the two proteins CFP and YFP, respectively. The domain II of scaffold **58** included bases tethered to *cis*-azobenzene units, and the protein CFP was functionalized with a nucleic acid **59** complementary to domain I, while the protein YFP was functionalized with nucleic acid **60** that had a limited number of complementary bases that could hybridize with domain II. Under these conditions only the CFP protein hybridizes with domain I. Visible-light-stimulated photoisomerization of the *cis*-azobenzene units to the *trans*-state, cooperatively stabilized the hybridization of the YFP protein with the domain II of scaffold **58**. The close proximity between the CFP and YFP proteins stimulated the effective FRET process between the CFP donor and YFP acceptor. By the cyclic photoisomerization of the system between the *trans*-azobenzene and *cis*-azobenzene states, the system could be switched between the FRET-generating configuration and the separated proteins configuration (lacking the FRET reaction), respectively. Figure 20 B depicts the assembly of a seesaw-like DNA device activated through the photoisomerizable azobenzene chromophores, composed of different substituents that allow the programmed and selective photoisomerization of the different chromophores.[54] The nucleic acid **61** acts as the base-scaffold of the device, and it is modified at its 3′- and 5′-ends with the pyrene (Py, $F_1$) and carboxyfluorescein (FAM, $F_2$) fluorophores. The nucleic acid **62** functionalized with the anthraquinone (An, $Q_1$) quencher and the nucleic acid **63** modified with the N-4-(4-dimethylamino)phenylazobenzoic acid (Dab, $Q_2$) quencher were used as left and right bars (L-bar and R-bar) that exhibit partial complementarities to domains I and II of the device. To the nucleic acid **62** were tethered dimethylthiomethyl substituents, SDMAzo, whereas to the nucleic acid **63** were tethered non-substituted azobenzene groups. The nucleic acid **64**, (middle bar; M-bar), was used to hybridize with the central domain of the device to rigidify the device. In the presence of the *trans*-azobenzene configurations of the fluorophore-tethered L- and R-bars, the cooperative stabilization of the duplexes between L-bar and R-bar with domains I and II of the scaffold proceeded to yield "state A" of the device. Under these conditions the Py fluorophore ($F_1$) and the FAM fluorophore ($F_2$) are quenched. Photo-irradiation of state A, $\lambda = 390$ nm, resulted in the selective photoisomerization *trans*-SDMAzo units of the L-bar to the *cis*-SDMAzo state, resulting in the formation of state B, in which the L-bar is separated, leading to the fluorescence of Py ($F_1$), and switched-off fluorescence of FAM ($F_2$). In turn, photo-irradiation of the system at $\lambda =$ 340 nm resulted in the selective photoisomerization of the non-substituted *trans*-azobenzene units to the *cis*-configuration, causing the selective separation of the R-bar from the

  

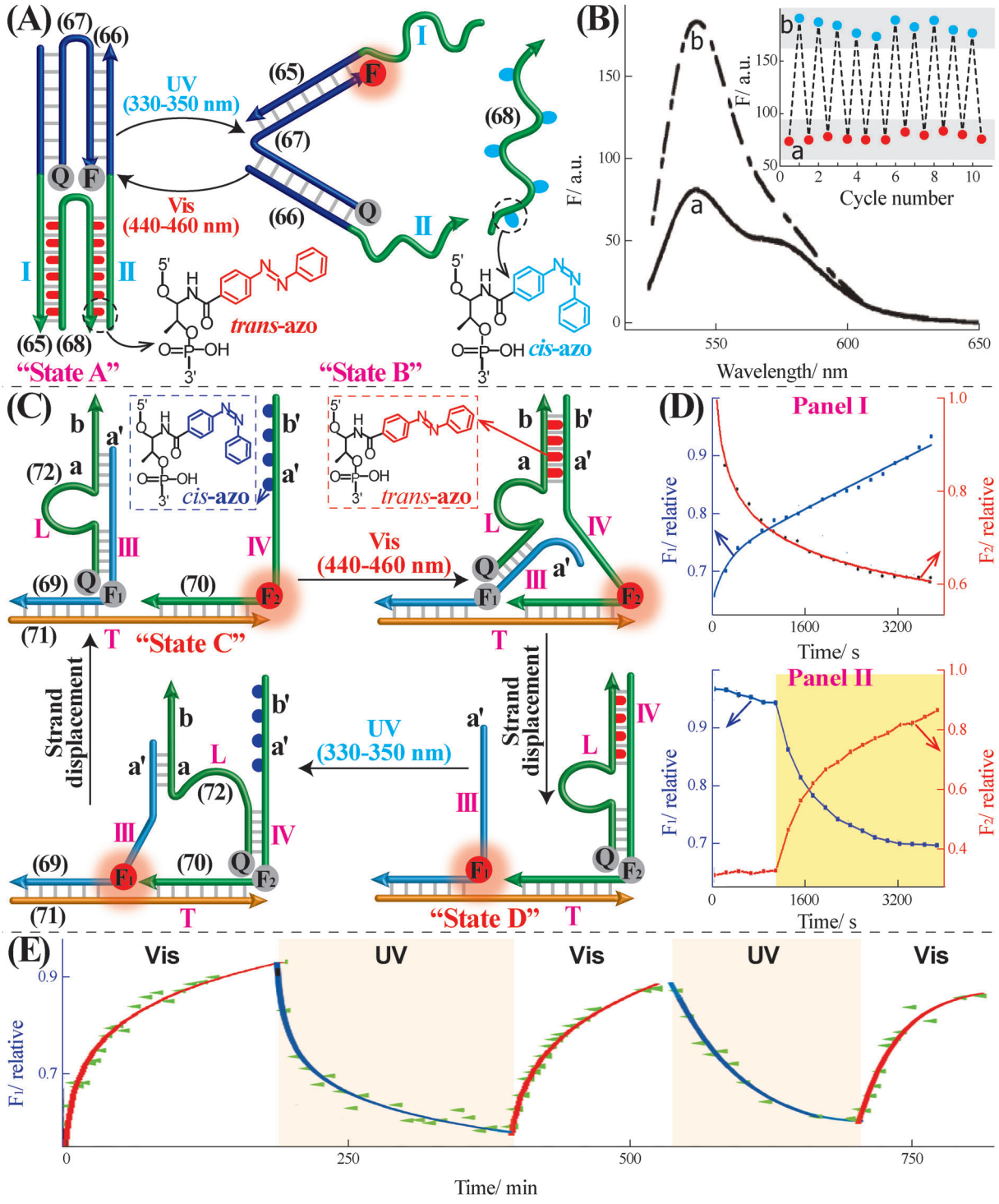


***Figure 21.*** A) A photo-stimulated DNA tweezers based on azobenzene photoisomerizable units. The opening and closure of the tweezers is probed by labeling the bridging "arm" with a fluorophore/quencher pair, and monitoring the FRET quenching efficiency of the fluorophore in the different states of the device. B) Fluorescence spectra corresponding to: a) The closed tweezers, state A, in the presence of *trans*-azobenzene units. b) The open tweezers, state B, in the presence of *cis*-azobenzene units. Inset: Cyclic, switchable fluorescence changes upon closure and opening of the tweezers. Adapted with permission from Ref. [55]. Copyright 2008 Wiley-VCH. C) A photo-stimulated DNA walker undergoing reversible light-induced transitions between two footholds associated with a DNA scaffold. Transitions are probed by labeling the footholds III and IV with the fluorophores $F_1$ and $F_2$, respectively, and by labeling the walker element with a quencher unit Q. D) Fluorescence changes corresponding to: Panel I: photo-stimulated transition of the walker from states C to D. Panel II: photo-stimulated transition of the walker from states D to C. E) Time-dependent fluorescence changes upon the photo-induced cyclic, switchable transitions between states C and D, and back. Adapted with permission from Ref. [56]. Copyright 2012 American Chemical Society.

device, state C. In this configuration, the Py ($F_1$) fluorophore is quenched, while the FAM ($F_2$) fluorescence is on. Finally, photo-irradiation of state A at $\lambda = 370$ nm photoisomerized the *trans*-azobenzene modified units associated with L-bar and R-bar, yielding state D. In this state the fluorescence of the Py ($F_1$) and the FAM ($F_2$) fluorophores is on. By the reverse photoisomerization of the *cis*-azobenzene separated units, $\lambda > 450$ nm, the original configuration of the device was restored. That is, by the photo-irradiation of the system at selected wavelengths the interconversion between all the states could be achieved. Figure 20 C exemplifies the switchable transitions between states B and C, using Py ($F_1$) and FAM ($F_2$) as fluorescence labels.

A two-state light-controlled machine was similarly constructed, using photoisomerizable azobenzene units as driving elements,[55] Figure 21 A. The closed state of the tweezers, state A, was composed of the nucleic acid arms **65** and **66** bridged by the nucleic acids **67** and **68**, where the hybridization of the bridging strand **68** with domains I and II, associated with the two arms, is cooperatively stabilized by the *trans*-azobenzene intercalator units. Photoisomerization of the *trans*-azobenzene units to the *cis*-state ($\lambda = 320$–380 nm) removes the intercalators from the duplex regions between strand **68** and the domains I and II associated with the two "arms" of the tweezers. Removal of the intercalator units weakens the duplexes, resulting in the separation of the bridging DNA **68**, and the opening of the tweezers, state B. Reverse photoisomerization of the *cis*-azobenzene to the *trans*-azobenzene units ($\lambda = 440$–460 nm) leads to the re-stabilization of the duplex structure between **68** and the domains I and II, associated with the two "arms" **65** and **66**, respectively, resulting in the re-closure of the tweezers, state A. As the linker strand **67** is modified at its 5′-and 3′-ends with a fluorophore/quencher (F/Q) pair, the opening and closure of the tweezers was probed by monitoring the fluorescence of the fluorophore label (closed tweezers: state A, low fluorescence. Open tweezers: state B, high fluorescence). By the cycling the photoisomerization of the azobenzene units between the *trans*- and *cis*-isomer states, the tweezers were reversibly switched between state A and state B (Figure 21 B). A further light-driven mechanical switch is depicted in Figure 21 C, in which a nucleic acid "walker" undergoes cyclic switchable transitions between two states on a DNA track.[56] The system consists of two footholds **69** and **70** hybridized with the track **71**. The footholds include protruding tethers III and IV, and these provide the binding positions. The foothold IV is modified with *cis*-azobenzene photoisomer units. Under these conditions, the walker element, L (**72**), is bound to foothold III, that provides the energetically favored hybridization site, state C. Photoisomerization of the *cis*-azobenzene units to the *trans*-azobenzene state results in the strand displacement of the walker L, and its transition to foothold IV, where the resulting duplex is stabilized by complementary base-pairing and cooperative binding of the *trans*-azobenzene to the resulting duplex, state D. Back photoisomerization of the *trans*-azobenzene to the *cis*-photoisomer weakens the duplex between the walker element L and foothold IV, resulting in the reverse strand displacement of the walker by foothold III, and the reverse transition of the walker L to foothold III, state C. By the labeling of the footholds III and IV with fluorophores $F_1$ and $F_2$, respectively, and the functionalization of the walker element L with a quencher unit, Q, the dynamics of the transition of the walker from foothold III to foothold IV, and the reverse process, could be monitored by the time-dependent fluorescence changes of the respective fluorophores (Figure 21 D panels I and II). By the cyclic photoisomerization of the azobenzene units between *cis* and *trans* states, the reversible switching of the walker between footholds III and IV was demonstrated (Figure 21 E).

The "mechanical" light-induced switching of DNA structures was, similarly, demonstrated by using azobenzene photoisomerizable units,[57] Figure 22 A. An extended tetrahedron structure, state A, was self-assembled using the strands **73**–**76**, and the co-added *trans*-azobenzene-function-

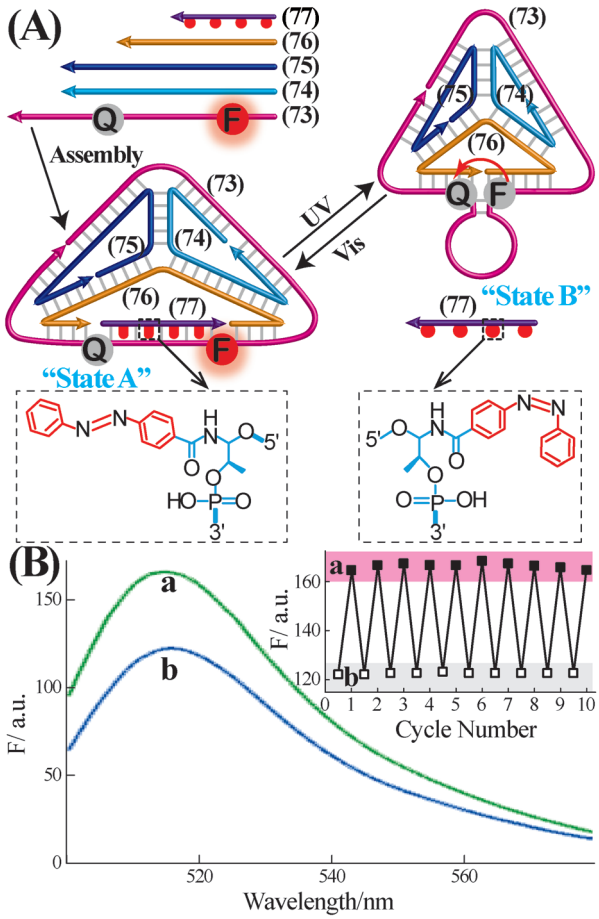


***Figure 22.*** A) Photo-induced cyclic reconfigurations of a DNA tetrahedron between an extended configuration, state A, and compressed configuration, state B, using photoisomerizable azobenzene units. By labeling one of the tetrahedron edges with a fluorophore/quencher pair, the transitions between states A and B are monitored by the efficiency of the respective FRET-quenching processes. B) Fluorescence spectra corresponding to: a) The tetrahedron in the extended configuration, state A. b) The tetrahedron in the compressed configuration, state B. Inset: Cyclic changes in fluorescence upon switching the tetrahedron between state A (high fluorescence) and state B (low fluorescence). Adapted with permission from Ref. [57]. Copyright 2011 Royal Society of Chemistry.

  

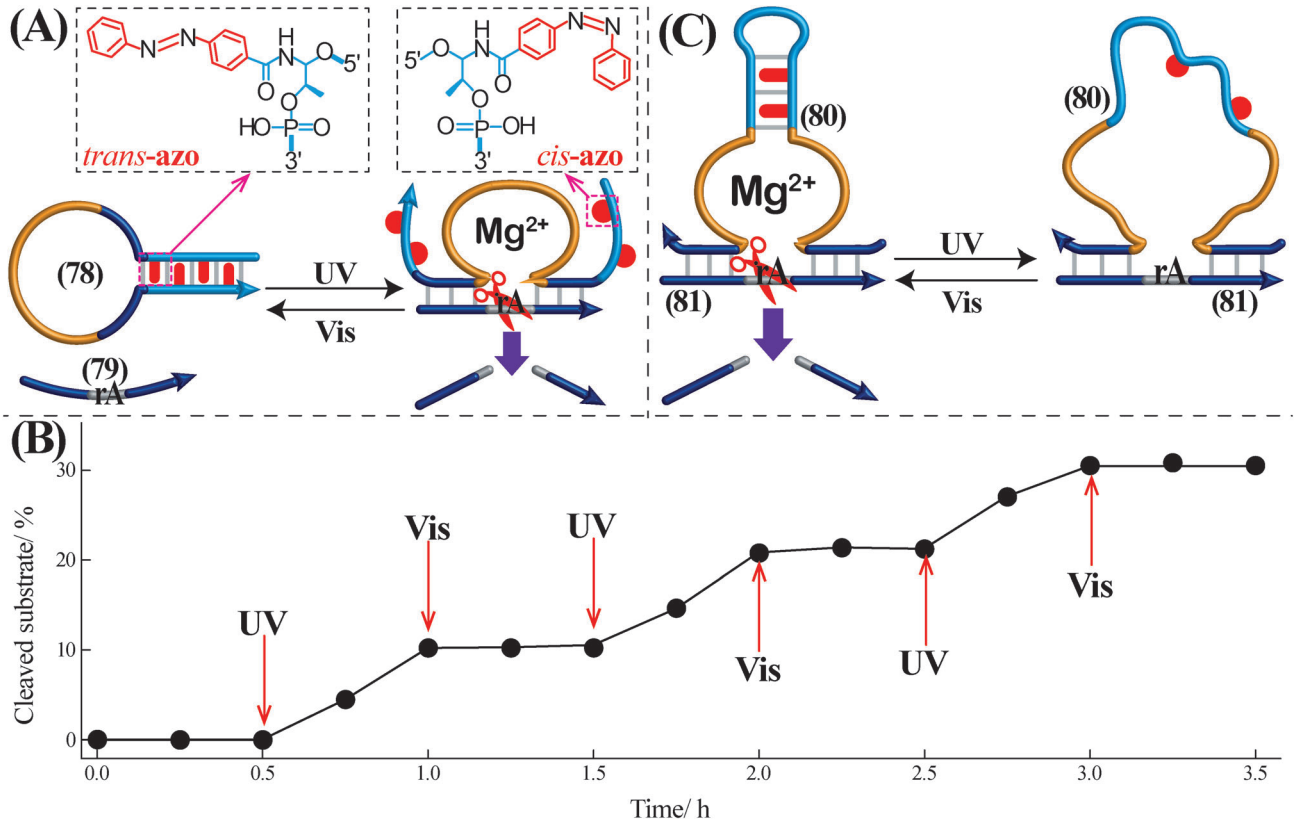


***Figure 23.*** A) Photo-stimulated transitions of a catalytically inactive hairpin DNA nanostructure into the active $Mg^{2+}$-dependent DNAzyme, and back, using azobenzene photoisomerizable units. B) Photo-induced switchable activation of the $Mg^{2+}$-dependent DNAzyme. In the *trans*-azobenzene state, the stabilized hairpin structure is in a catalytically inactive configuration. UV irradiation of the system yields *cis*-azobenzene generating the catalytically active $Mg^{2+}$-dependent DNAzyme. Further visible-light re-isomerization of *cis*-azobenzene to *trans*-azobenzene regenerates the catalytically inactive hairpin structure. The photo-induced "ON/OFF" activation and deactivation of the DNAzyme were monitored by the electrophoretic characterization of the fragmented products generated by the DNAzyme. C) Photo-stimulated "ON/OFF" activation and deactivation of the $Mg^{2+}$-dependent DNAzyme by the photo-induced rigidification of a tandem sequence inserted into the DNAzyme loop-sequence using photoisomerizable azobenzene units. Adapted with permission from Ref. [58]. Copyright 2010 Wiley-VCH.

alized strand **77** hybridized with **73**. The intercalation of the *trans*-isomer units in the complementary domains between strands **73** and **77** yielded the extended tetrahedron structure, state A. Photoisomerization of the *trans*-azobenzene units to the *cis*-azobenzene components (UV light) led to the separation of the duplex domain between strands **73** and **77,** and this contracted the tetrahedron structure, state B. By the reverse photoisomerization of the *cis*-azobenzene units to *trans*-azobenzene (visible light), the extended tetrahedron configuration, state A was restored. By the labeling of strand **73** with a fluorophore/quencher (F/Q) pair, the reversible, light-induced switching of the system between the extended and contracted configurations of the DNA tetrahedron was probed (Figure 22 B; State A: high fluorescence. State B: low fluorescence).

The photoinduced switchable "ON/OFF" activation of the 10–23 type $Mg^{2+}$-dependent DNAzyme, using azobenzene photoisomerizable groups as optical triggers, is shown in Figure 23 A.[58] The nucleic acid **78** included the catalytic DNAzyme sequence and extended tethers consisting of base-pairs of partial complementarities modified with the *trans*-azobenzene chromophores. In this configuration the *trans*-azobenzene units cooperatively stabilize the hairpin structure of strand **78** and the formation of the catalytic DNAzyme loop is prohibited. UV-stimulated photoisomerization of the *trans*-isomer units to the *cis*-azobenzene state destabilized the stem region of the hairpin, leading to the opening of the hairpin structure. This change enables the self-assembly of the catalytically active DNAzyme loop sequence, and the formation of the complex with the ribonucleobase-containing substrate **79**. In the presence of $Mg^{2+}$ ions the catalytic cleavage of the substrate proceeded. The subsequent visible-light-stimulated photoisomerization of the *cis*-azobenzene units to *trans*-isomer regenerated the catalytically inactive hairpin structure **78** (Figure 23 B). Also, the internal modification of the catalytic core-loop region of the 10–23-type $Mg^{2+}$-dependent DNAzyme with azobenzene photoisomerizable units led to switchable catalytic functions of the DNAzyme,[59] Figure 23 C. The *trans*-azobenzene configuration of the DNAzyme sequence **80** generated, in the presence of $Mg^{2+}$ ions, a catalytically active structure that catalyzed the hydrolytic cleavage of the ribonucleobase-containing substrate **81**. In turn, the UV-stimulated photoisomerization of the *trans*-azobenzene units to the *cis*-photoisomer ($\lambda =$ 366 nm) distorted the DNAzyme loop structure and perturbed the catalyzed cleavage of substrate **81**. The reverse

visible-light-triggered photoisomerization of the *cis*-azobenzene units to the *trans*-azobenzene configuration ($\lambda = 435$ nm) reactivated the catalytic functions of the DNAzyme.

### 2.4. Electrochemically Switchable DNA Systems

The stabilization of G-quadruplexes by metal ions enabled the electrochemical switchable transition between the $Pb^{2+}$-ion-stabilized G-quadruplex and the random-coil states, Figure 24 A.[62] In the presence of $Pb^{2+}$ ions the strand **82** assembles into the G-quadruplex. The electrochemical reduction of the $Pb^{2+}$ ions separated the G-quadruplex into the random-coil structure. The electrochemical oxidation of the electrode-deposited $Pb^0$ to $Pb^{2+}$ ions re-assembled the $Pb^{2+}$-stabilized G-quadruplex. The cyclic transitions between the $Pb^{2+}$-stabilized G-quadruplex and the random-coil states were probed by monitoring the enhanced fluorescence of crystal violet (CV) upon association to the random-coil structure (Figure 24 B).

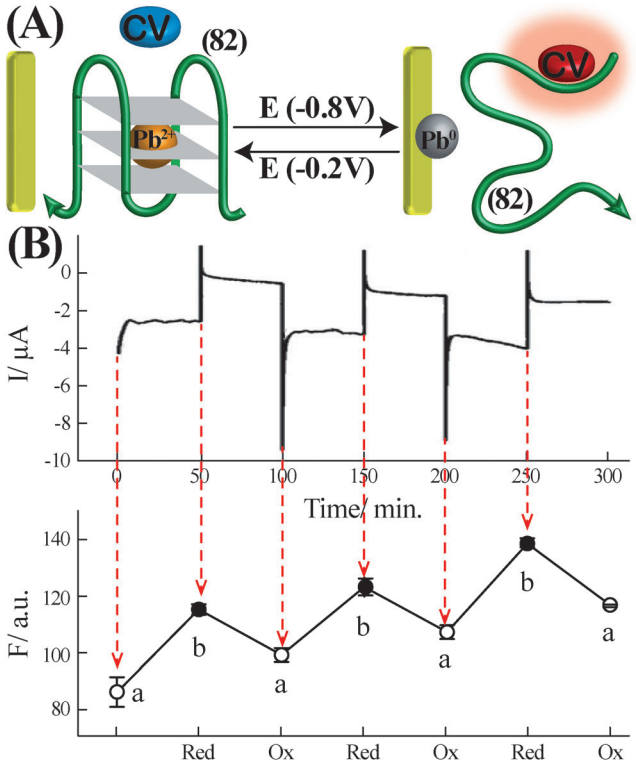


***Figure 24.*** A) Electrochemically induced cyclic switchable formation and dissociation of the $Pb^{2+}$-stabilized G-quadruplex. The voltammetric stripping of $Pb^{2+}$ and the deposition of $Pb^0$ on the electrode leads to separation of the G-quadruplex, while re-oxidation of the $Pb^0$ to $Pb^{2+}$ ions regenerated the $Pb^{2+}$-stabilized G-quadruplex. The fluorescence generated by Crystal Violet (CV) bound to single-stranded DNA provides the readout signal. B) Top: Cyclic voltammetric steps corresponding to the reduction of the $Pb^{2+}$ ions to $Pb^0$ and the reverse oxidation of $Pb^0$ to $Pb^{2+}$ ions. Bottom: Cyclical changes in the fluorescence intensity of CV in the presence of: a) The $Pb^{2+}$-stabilized G-quadruplex. b) The random-coil DNA. Adapted with permission from Ref. [62] Copyright 2013, Elsevier.

A different approach to electrochemically switch DNA systems has involved the use of electrodes to switch the pH of the electrolyte solution, and thereby to stimulate the DNA switchable systems. One approach to stimulate the pH values of the electrolyte solution involved the acidification of the electrolyte solution through the oxidation of $H_2O$ to oxygen, Equation (1), and the neutralization of the acidified aqueous solution by the electrochemical reduction of water, and the evolution of hydrogen ($H_2$),[63] Equation (2).

$$2\,H_2O - 4\,e^- \rightarrow 4\,H^+ + O_2 \quad (1)$$

$$2\,H_2O + 2\,e^- \rightarrow H_2 + 2\,OH^- \quad (2)$$

Accordingly, the C-rich strand **83**, labeled at its 5′- and 3′-ends with a fluorophore/quencher (F/Q) pair was subjected to the electrochemically driven changes in pH value (Figure 25 A). At acidic pH values, the i-motif structure of strand **83** was generated, leading to fluorescence quenching of the tethered fluorophore. The subsequent electrochemically driven reduction of water and evolution of $H_2$ yielded a basic solution, pH 8.0, resulting in the separation of the i-motif structure, and an intense fluorescence of the fluorophore. By the cyclic electrochemically driven changes of pH value in the electrolyte solution, the DNA strand **83** was switched between i-motif and random-coil configurations (Figure 25 B).

A different method to electrochemically control the pH value of the electrolyte solution, and thereby the subsequent "ON/OFF" triggering of the catalytic activity of the $Mg^{2+}$-dependent DNAzyme, has implemented a bis(aniline) cross-linked Au nanoparticle (NPs) matrix linked to the electrode,[64] Figure 25 C. Thioaniline-modified Au NPs (diameter $3.6 \pm 0.3$ nm) were electropolymerized on a roughened electrode to yield an Au NPs matrix cross-linked with bis(aniline). The bis(aniline) units exhibit quasi-reversible redox properties ($E = -0.05$ V vs. saturated calomel electrode (SCE)) and undergo oxidation to the quinoide state, resulting in the release of protons. The reverse process, in which the quinoide units are reduced to the bis(aniline) states, involves the uptake of protons from the solution. Indeed, it was found that the potential-biased oxidation of the electrode modified with the bis(aniline)-bridged Au NPs matrix ($E = 0.25$ V vs. SCE), in the presence of a neutral electrolyte solution resulted in the acidification of the solution to pH 5.8. The reverse biasing of the electrode potential to $-0.05$ V vs. SCE resulted in the reduction of the quinoide bridging units to the bis(aniline) state, while uptaking protons from the solution, a process that regenerated the neutral electrolyte solution, pH 7.2. Accordingly, the bis(aniline)-cross-linked Au-NPs-modified electrode was applied to switch the catalytic activities of the $Mg^{2+}$-dependent DNAzyme (Figure 25 D). The strands **28** and **29** included the functional domains to trigger "ON" and "OFF" the DNAzyme catalytic activity. The domains I and II include the sequences comprising the loop region of the DNAzyme and the domains III and IV provide the substrate binding sites. The domains V and VI of strands **28** and **29** include C-rich sequences that form an i-motif structure under acidic conditions (pH 5.8). The domains

  

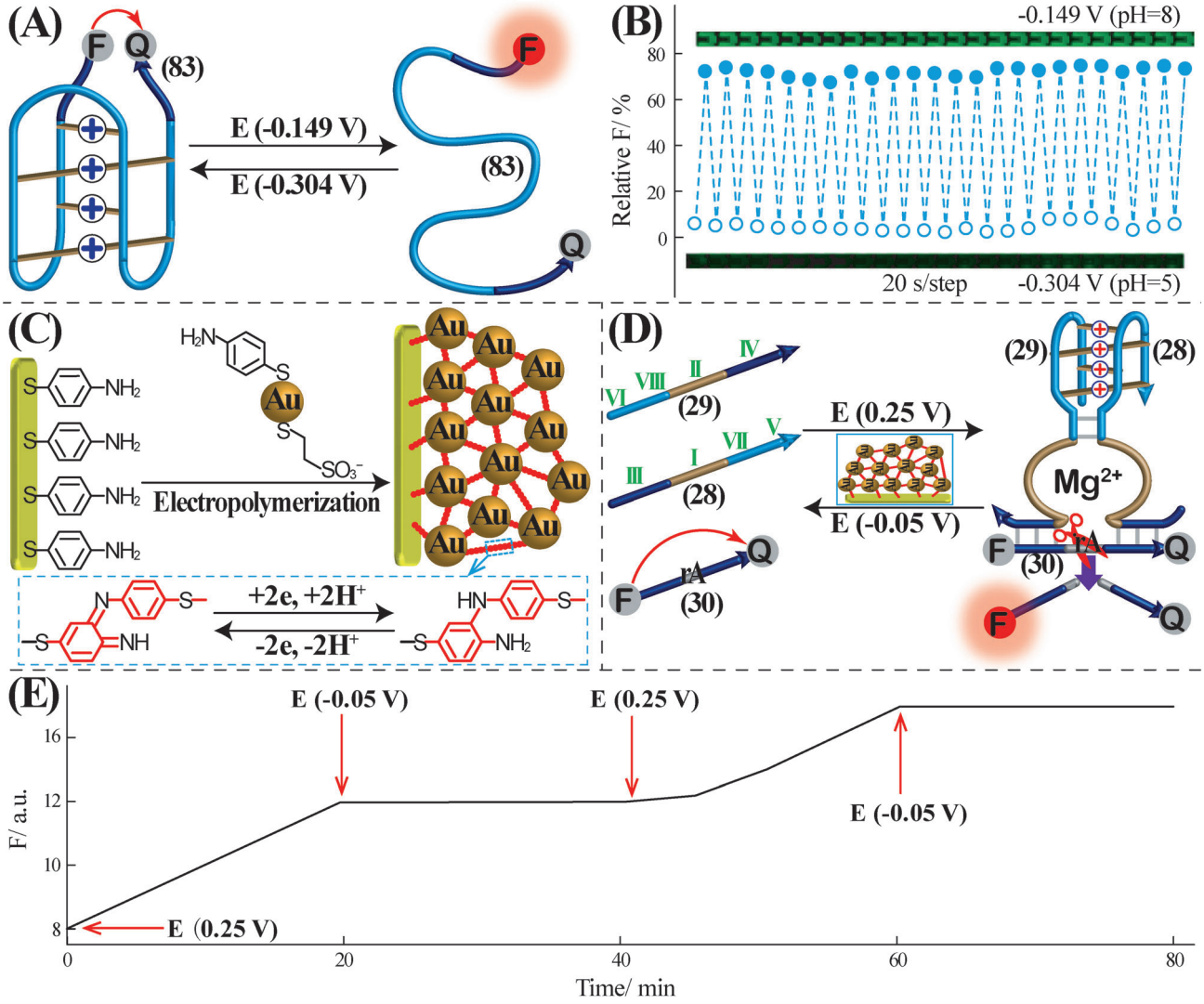


***Figure 25.*** A) Electrochemically induced i-motif-to-random-coil transitions through the cyclic electrochemical oxidation of water (pH 5.0) and electrochemical reduction of water to hydrogen (pH 8.0). The DNA structure is labeled with a fluorophore/quencher pair and the switchable i-motif-to-random-coil transitions are probed by monitoring the fluorescence changes of the fluorophore. B) Fluorescence changes upon cyclic, switchable transitions of the i-motif, pH 5.0 (low fluorescence), to the random-coil, pH 8.0 (high fluorescence), and back. Adapted with permission from Ref. [63]. Copyright 2010 American Chemical Society. C) Electrochemical synthesis of bis(aniline)-cross-linked Au NPs matrices on an electrode surface and the cyclic, electrochemically induced, acidification or neutralization of the electrolyte solution through the oxidation or reduction of the bis(aniline) cross-linking bridging units. D) Electro-stimulated activation and deactivation of the $Mg^{2+}$-dependent DNAzyme by the electrochemical switching of the pH value of the electrolyte solution by means of oxidation and reduction of the bis(aniline)-cross-linked Au NPs, associated with the electrode. E) Electrochemically induced "ON" and "OFF" activation of the $Mg^{2+}$-dependent DNAzyme, using the bis(aniline)-cross-linked NPs linked to the electrode as a functional matrix for electro-stimulated changes in pH value. The "ON" and "OFF" activation and deactivation of the DNAzyme are probed by the fluorescence generated upon the DNAzyme-catalyzed cleavage of the fluorophore/quencher-modified substrate. Adapted with permission from Ref. [64]. Copyright 2010 American Chemical Society.

VII and VIII exhibit three base-pairing complementarities, and these were included to favor, under acidic conditions, the self-assembly of the catalytically active DNAzyme unit through stabilization of the supramolecular structure between nucleic acids **28** and **29** by a cooperative i-motif structure and base-pairing of the duplex domain VII/VIII. The substrate of the $Mg^{2+}$-dependent DNAzyme, **30**, is functionalized at its 5′- and 3′-ends with a fluorophore/quencher (F/Q) pair. The electrochemically stimulated oxidation of the bis(aniline) units bridging the Au NPs ($E = 0.25$ V vs. SCE) resulted in an acidic electrolyte solution, pH 5.8, that yielded the catalytically active $Mg^{2+}$-dependent DNAzyme structure. This stimulated the hydrolytic cleavage of the substrate **30** and resulted in the generation of the fluorescence of the fluorophore-modified fragmented product. The subsequent electrochemical reduction of the quinoide bridges ($E = -0.05$ V vs. SCE) to the bis(aniline) state, turned the pH value of the electrolyte to 7.2, a process that dissociated the i-motif structure, which is part of the DNAzyme unit. This separated the subunits **28** and **29** into a catalytically inactive configuration. By the cyclic oxidation and reduction of the bridging units of the Au NPs matrix, the pH value of the electrolyte was switched between

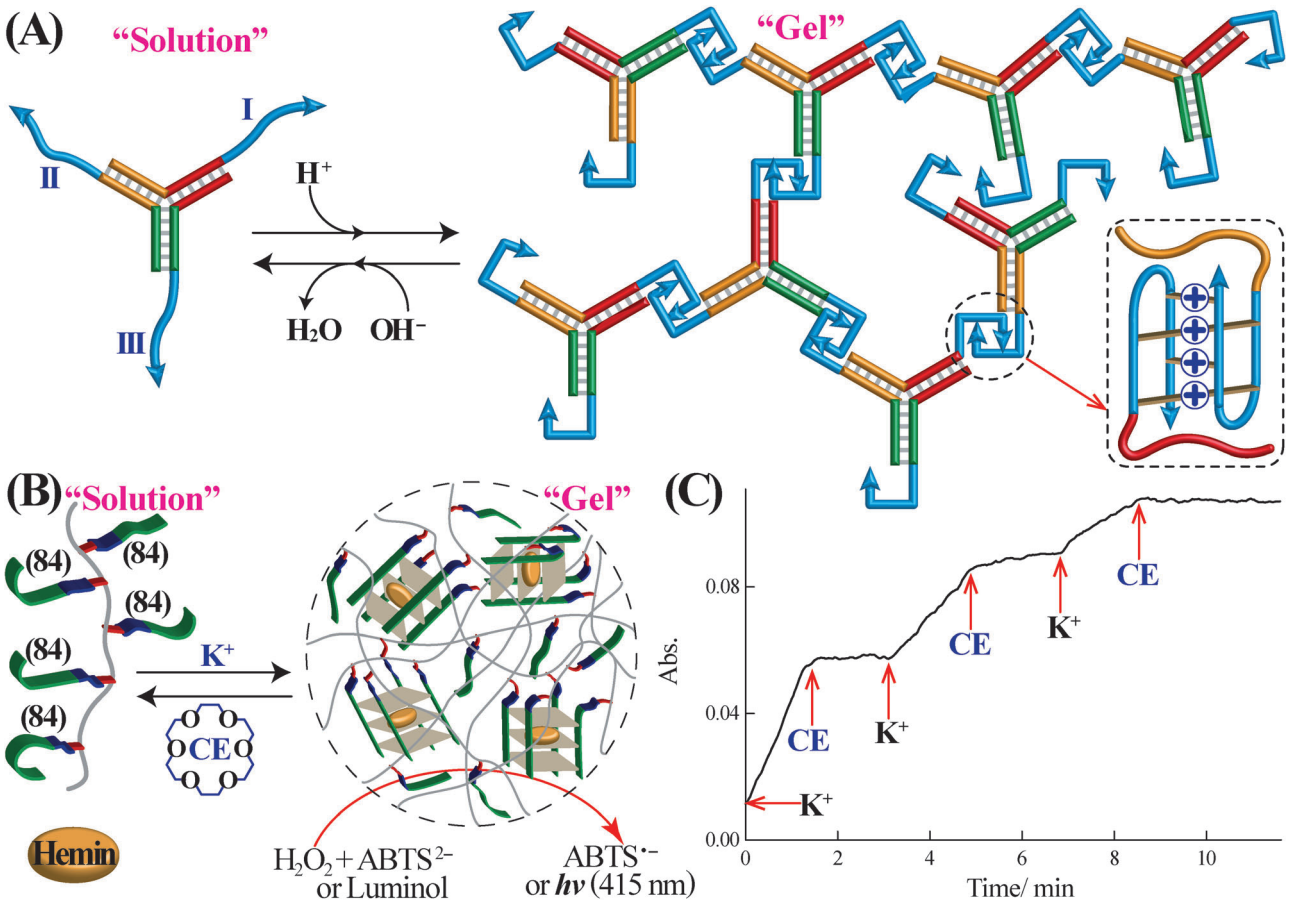


***Figure 26.*** A) pH-value-stimulated assembly of DNA hydrogels using the i-motif as cross-linking element. B) Cyclic, switchable transitions of a nucleic acid-modified acrylamide copolymer between copolymer solution and G-quadruplex-cross-linked hydrogel states. $K^+$ ions stabilize the G-quadruplex-cross-linked hydrogels while the crown-ether-induced binding of $K^+$ ions separates the G-quadruplex units, and leads to the copolymer solution. The binding of hemin to the G-quadruplex units leads to a horseradish peroxidase (HRP)-mimicking DNAzyme hydrogel that stimulates the catalyzed oxidation of $ABTS^{2-}$ by $H_2O_2$ to yield $ABTS^{\bullet-}$. C) Absorbance changes upon the cyclic activation of the DNAzyme hydrogel towards the oxidation of $ABTS^{2-}$: Switched ON by addition of $K^+$ ions. Switched OFF by addition of 18-crown-6-ether (CE). Adapted with permission from Ref. [70]. Copyright 2013 American Chemical Society.

5.8 and 7.2, leading to the cyclic "ON" and "OFF" triggering of the DNAzyme functions, respectively (Figure 25E).

## 3. Applications of Switchable DNA Systems

The development of DNA hydrogels has attracted substantial recent research interest.[65] The DNA hydrogels are formed by the cross-linking of DNA subunits or by the cross-linking of nucleic acid-functionalized hydrophilic polymer chains, such as nucleic acid-modified acrylamide copolymer chains. The possibility to link nucleic acid units by means of base-pairing,[66] ion-stabilized structures,[67] pH value changes,[68] or light irradiation[69] provides a rich platform of cross-linking motives. Particularly interesting are switchable DNA hydrogels that undergo stimuli-triggered gel-to-solution transitions. Different applications of DNA hydrogels for controlled drug delivery,[69] catalysis,[70] and the removal of pollutants[71] were suggested. The design of a pH-value-triggered DNA hydrogel is depicted in Figure 26A.[68] The building block of the gel consists of a tri-arm Y-shaped DNA structure that includes three single-stranded toeholds I, II, and III, that each form a subunit of the C-rich i-motif structure. At pH 5.2, the cross-linking of Y-shaped DNA units by the formation of i-motif linkages led to the formation of the hydrogel. The neutralization of the system at pH 7.0 dissociated the i-motif bridges, resulting in a solution of the monomer Y-shaped nucleic acid units. The gel-to-solution transitions stimulated by changes in pH value were characterized by rheology measurements. A different approach to design switchable catalytic DNA hydrogels has involved the synthesis of an acrylamide copolymer consisting of the acrydite nucleic acid **84** and acrylamide monomer.[70] The copolymer chains included the nucleic acid tethers **84**, consisting of 5′-AAGGG-3′ that provided subunits for the $K^+$-ion-stimulated assembly of the G-quadruplex-bridged hydrogel (Figure 26B). The elimination of the stabilizing $K^+$ ions from the G-quadruplex units, by the addition of 18-crown-6-ether (CE), separated the G-quadruplexes, and led to a solution of the separated acrylamide chains. By cycling the addition of $K^+$ ions and CE, the system was switched between hydrogel and solution phases, respectively. Rheology

  

measurements supported the hydrogel-to-solution transitions (storage modulus of the hydrogel $G' \approx 5$ Pa). The binding of hemin to the $K^+$-ion-stimulated cross-linking of the hydrogel by the G-quadruplex units resulted in the formation of the catalytically active hemin/G-quadruplex HRP-mimicking DNAzyme, that catalyzed the oxidation of $ABTS^{2-}$, by $H_2O_2$ to the colored product, $ABTS^{\bullet-}$ (Figure 26C). By the cyclic $K^+$-ion-induced formation of the catalytically active DNAzyme hydrogel and by the CE-triggered separation of the hydrogel, the catalytic functions of the system were switched between "ON" and "OFF" states, respectively. Also, $Ag^+$-ion-stimulated cross-linking of all DNA Y-shaped nucleic acid units, or of nucleic acid-functionalized acrylamide copolymers to form hydrogels was reported through the formation of cooperatively stabilized duplex nucleic acids using C-$Ag^+$-C bridges.[67] The switchable hydrogel-to-solution transitions were accomplished by the elimination of the $Ag^+$ ions from the bridging units, using cysteamine.

Mesoporous materials and particularly mesoporous $SiO_2$ nanoparticles (MP $SiO_2$ NPs) are interesting high-surface-area nano-containers that can incorporate molecular substrates in their pores, and act as drug-delivery systems.[72,73] Particularly interesting are MP $SiO_2$ NPs loaded with substrates and capped by "smart gates" that unlock the pores and release the drug in the presence of appropriate triggers. Indeed different triggers, such as light,[74,75] redox reactions,[75,76] catalytic processes,[77] pH value,[78] or thermal triggers[79] have been used to unlock the pores of the MP $SiO_2$ NPs. A major advance could be, however, anticipated, by designing switchable-triggered caps, since such gated pores may lead to dose-controlled release of drugs.

The photon-triggered switchable release of a Rhodamine 6G (Rh6G) substrate from DNA-gated MP $SiO_2$ NPs has been demonstrated,[80] Figure 27A. The MP $SiO_2$ NPs were modified with the nucleic acid **85** and their pores were loaded with Rh6G substrate. The internally functionalized *trans*-azobenzene nucleic acid **86a** was used to cap the pores by its hybridization with the surface-anchored nucleic acid units **85**. The resulting duplexes are stabilized by base-pairing and cooperative intercalation of the *trans*-azobenzene units. The UV-stimulated photoisomerization of the *trans*-azobenzene units, to the *cis*-photoisomer sate **86b**, destabilized the duplexes, resulting in the separation of the capping duplexes and the release of the pore-entrapped Rh6G substrate. The further visible-light photoisomerization of *cis*-azobenzene-labeled DNA **86b** to *trans*-azobenzene state **86a** restored the capping units and prohibited the release of Rh6G substrate. By the cyclic photoisomerization of the *trans*-azobenzene-functionalized duplex caps to the *cis*-state and back again, the switchable, gated "ON" and "OFF" release of Rh6G substrate was demonstrated (Figure 27B). By the trapping of doxorubicin chemotherapeutic drug by means of the *trans*-azobenzene caps, the UV-stimulated intracellular release of the drug was demonstrated.[80]

The release of a substrate entrapped in MP $SiO_2$ NPs, stimulated by changing the pH value, was demonstrated using the i-motif DNA structure as pH-value-responsive capping gate,[81] Figure 28A. The C-rich nucleic acid **87** was covalently linked to the surface of MP $SiO_2$ NPs, and the nanopores were

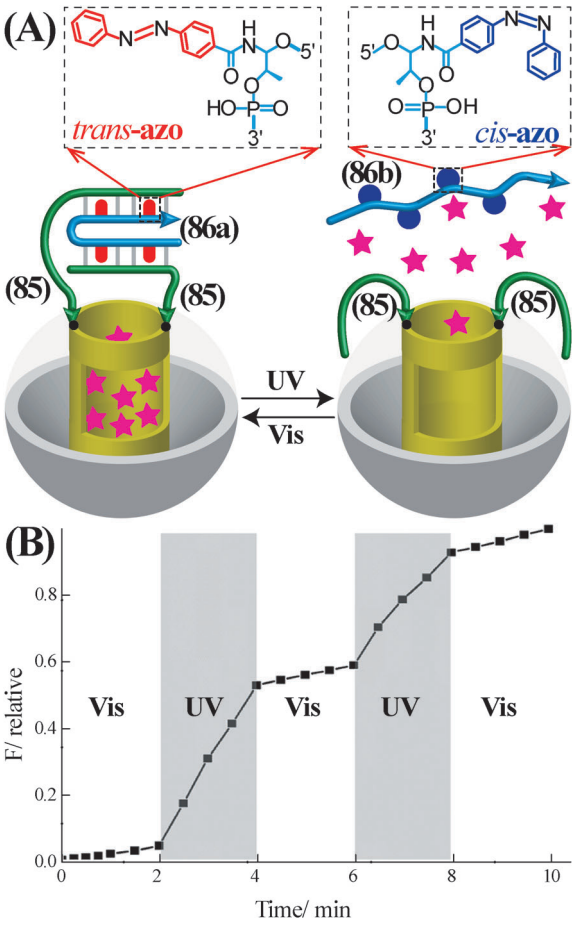


***Figure 27.*** A) Photo-stimulated locking and unlocking of mesoporous $SiO_2$ NPs using nucleic acid caps functionalized with photoisomerizable units. The *trans*-azobenzene modified nucleic acid **86a** hybridizes with the nucleic acid units **85**, to form duplex capping units. Photoisomerization of the *trans*-azobenzene units to *cis*-azobenzene dissociates the strand **86b**, leading to the unlocking of the pores, and to the release of the pore-loaded substrate (Rh6G). B) Fluorescence changes upon the photo-stimulated cyclical release of Rh6G and blocking of Rh6G release from the pores. Adapted with permission from Ref. [80]. Copyright 2012 American Chemical Society.

loaded with the substrate Rhodamine B (RhB), at pH 8.0. The acidification of the system, pH 5.0, led to the formation of the i-motif structure that trapped the substrate in the pores. Unlocking of the pores by subjecting the system to pH 8.0, and transforming the i-motif capping units into the random-coil structures, released the substrate. By the cyclic control of the pH value of the system between acidic (pH 5.0) and basic (pH 8.0) conditions, the switchable locking, "OFF"-state, and release, "ON"-state of RhB entrapped in the pores was demonstrated (Figure 28B). The photonic triggering of changes in the pH value of the solution was further implemented to unlock the MP $SiO_2$ NPs gating caps, and to release the pore-entrapped substrate,[82] Figure 28C. The system made use of the fact that malachite green carbinol (MGC; **88a**) undergoes photo-induced dissociation to the carbocation **88b** and $OH^-$ ions, while the resulting carbocation/$OH^-$ recombine in the dark to regenerate MGC (**88a**).[83] That is, the irradiation of the system releases $OH^-$ ions turning the

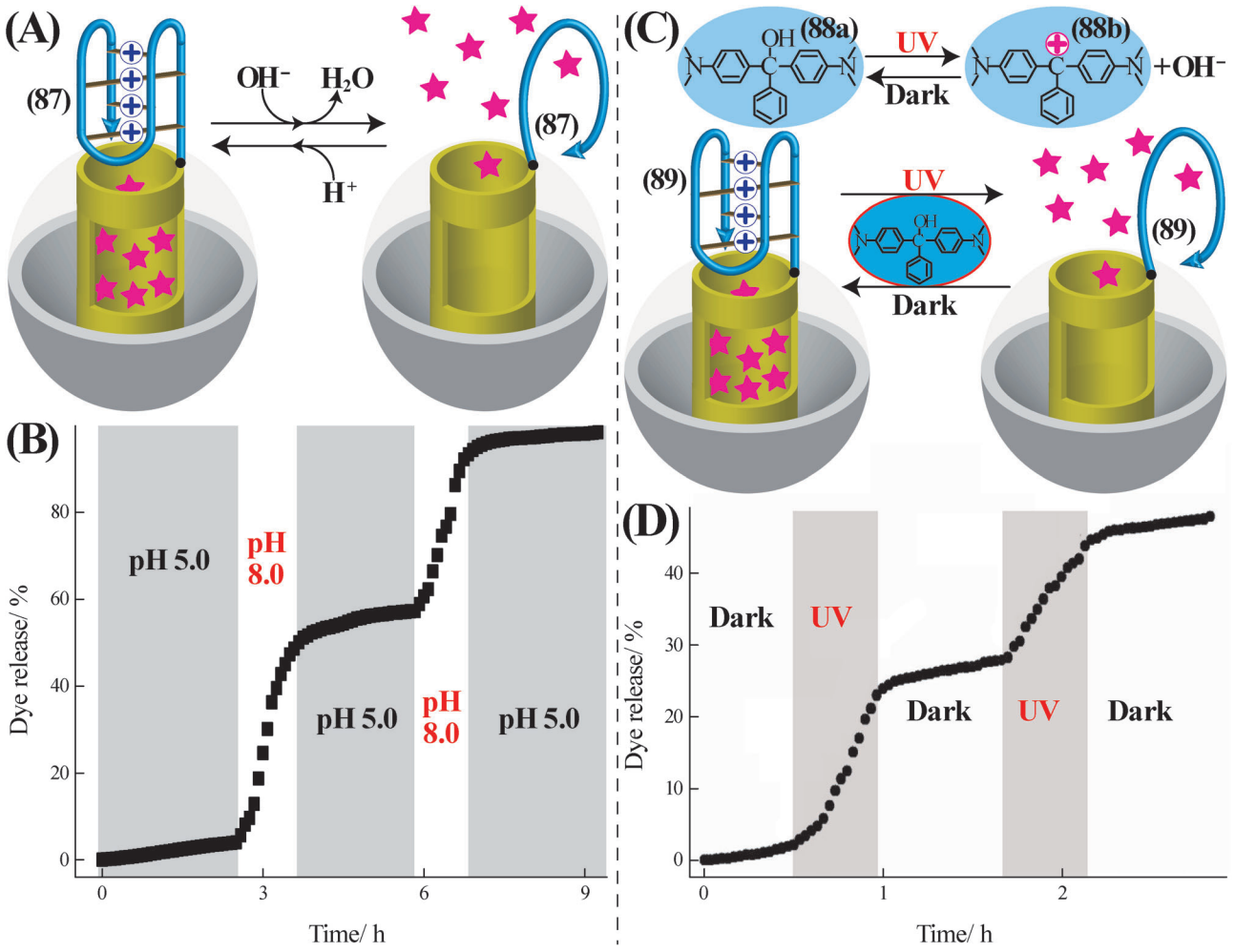


***Figure 28.*** A) pH-stimulated cyclic release and blockage of the release of a fluorescent dye (RhB) using the i-motif as locking/unlocking gating units. B) Time-dependent fluorescence changes upon the switchable release of RhB from the mesoporous $SiO_2$ NPs induced by changes in pH value: pH 5.0 switched OFF; pH 8.0 switched ON. Adapted with permission from Ref. [81]. Copyright 2011 Oxford University Press. C) Photo-stimulated Malachite Green (**88a**) induced changes in pH value in the solution caused by the switchable light-induced dissociation of the capping i-motif units and the release of the entrapped $[Ru(bpy)_3]^{2+}$ fluorescent substrate, and the reverse recapping of the pores by the recombination of the carbonium ion **88b** and $OH^-$ photoproducts in the dark. D) Cyclic fluorescence changes upon unlocking the i-motif capping units by the photo-induced dissociation of Malachite Green (**88a**) and the reversible re-blocking of the pores by the i-motif units, through recombination of the carbocation **88b** and $OH^-$ photoproducts. Adapted with permission from Ref. [82]. Copyright 2012 Wiley-VCH.

solution basic, while the recombination of the ionic products acidifies the solution by removing the $OH^-$ ions. Accordingly, the C-rich nucleic acid **89** was covalently linked to the surface of MP $SiO_2$ NPs. The $Ru^{II}$-tris(bipyridine) substrate, $[Ru(bpy)_3]^{2+}$, was loaded in the pores, while retaining the **89**-chains in the random-coil configuration. Acidification of the system transformed the nucleic acid strands **89** into the i-motif configuration that capped the pores. In the presence of added MGC (**88a**), the photonic and thermally triggered changes in pH value enabled the cyclic and switchable "ON/OFF" release of the substrate (Figure 28D). The system was subjected to acidic conditions that retained the DNA caps in the i-motif configuration. The UV-light-induced dissociation of MGC neutralized the system, resulting in the dissociation of the i-motif units and the release of substrate $[Ru(bpy)_3]^{2+}$. The dark thermal recombination of the carbocation **88b** with $OH^-$ ions re-acidified the solution, leading to the reconfiguration of the gating i-motif caps. By the cyclic "ON" and "OFF" irradiation of the system the switchable "ON" and "OFF" release of the substrate was achieved.

An interesting application of ion-triggered formation and dissociation of nucleic acid duplexes has involved the $Hg^{2+}$-gated ion-flow through single nanochannels.[84] Conical nanochannels were fabricated by an asymmetric track-etch technique, and the channels were sputtered with gold. The random-coil thymine-rich nucleic acid **90** was covalently linked to the gold surface coating the channels, and the pores were blocked,[84a] Figure 29A. In the presence of $Hg^{2+}$ ions, the nucleic acids **90** were rigidified and compressed into duplex hairpin structures, stabilized by T-$Hg^{2+}$-T bridges, resulting in the opening of pores. That is, the pores blocked by DNA strand **90** led to low ion current flow, whereas the $Hg^{2+}$-ion-stimulated opening of the pores led to a high ion current flow. By the cyclical treatment of the modified pores with

  

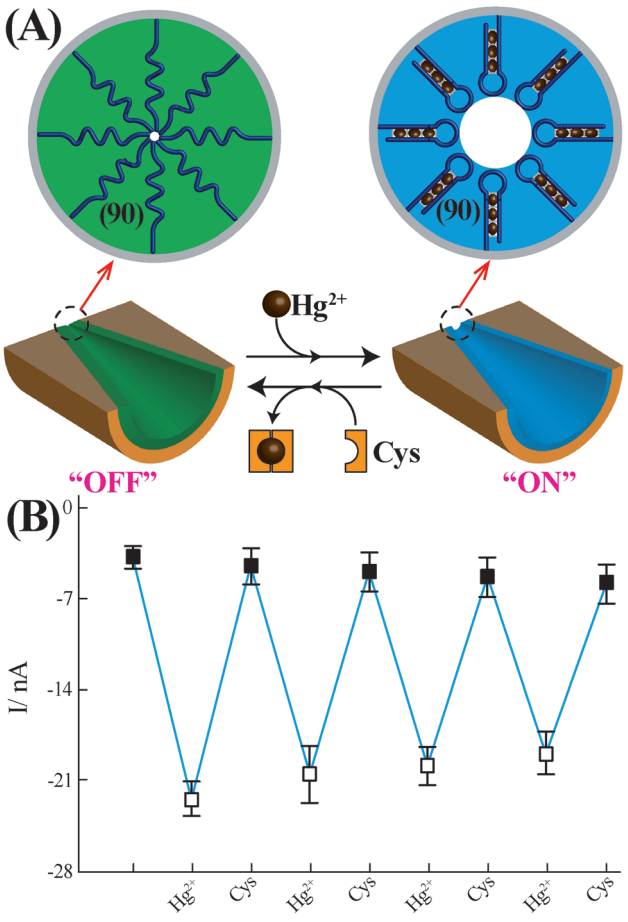


***Figure 29.*** A) $Hg^{2+}$ ions/cysteine-induced switchable opening and blocking of nanopores. B) Switchable ion currents stimulated in the presence of closed nanopores (low currents) or open nanopores, in the presence of $Hg^{2+}$ ions, (high currents). Adapted with permission from Ref. [84a]. Copyright 2013 Royal Society of Chemistry.

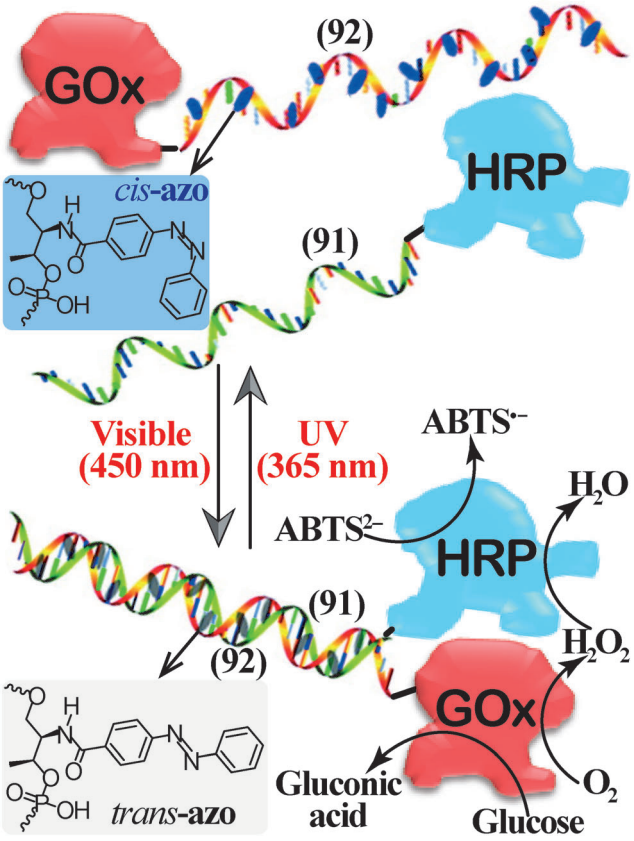


***Figure 30.*** A photo-stimulated bi-enzyme cascade using glucose oxidase (GOx) functionalized with a *trans*-azobenzene-modified nucleic acid **91** and the nucleic acid **92**-modified horseradish peroxidase (HRP). The *trans*-azobenzene-stabilized duplex **91**/**92** leads to the activation of the bi-enzyme cascade. Photoisomerization of the *trans*-azobenzene units to the *cis*-azobenzene state leads to the separation of the duplex, and to the blockage of the bi-enzyme cascade. Adapted permission from Ref. [86]. Copyright 2011 American Chemical Society.

$Hg^{2+}$-ion/cysteine, the ion current flow across the pore was switched between "ON" and "OFF" states, respectively (Figure 29 B).

The activation of enzyme cascades, or enzyme/DNAzyme cascades, finds growing interest in nanobiotechnology.[85] Specifically, the organization of enzymes on DNA scaffolds was reported as a general means to drive biocatalytic cascades. The photochemically stimulated formation or dissociation of duplex nucleic acids by means of photoisomerizable azobenzene units was used to switch biocatalytic cascades or enzyme/DNAzyme cascades,[86] Figure 30. Horseradish peroxidase (HRP), was modified with the nucleic acid **91**, and glucose oxidase, GOx, was modified with the nucleic acid **92**, that exhibited partial complementarities to strand **91**, and was modified with *cis*-azobenzene photoisomerizable tethers. Under these conditions, the *cis*-azobenzene-modified strand **92** could not hybridize with strand **91** and the two enzymes did not communicate with each another. Photoisomerization of the *cis*-azobenzene tethers to the *trans*-azobenzene nucleic acid tethers, using visible light ($\lambda =$ 450 nm), resulted in cooperative stabilization of the duplex formed by **91** and **92** (Figure 30). The formation of the duplex **91**/**92** resulted in close proximity between GOx and HRP, thus allowing the activation of the bi-enzyme cascade. The GOx-mediated aerobic oxidation of glucose yielded gluconic acid and $H_2O_2$. The $H_2O_2$ acted as the substrate for HRP, which catalyzed the $H_2O_2$-stimulated oxidation of $ABTS^{2-}$ to the colored product $ABTS^{\bullet-}$. The close proximity between GOx and HRP generated a high local concentration of $H_2O_2$ that was fed into HRP, thus allowing the effective activation of the bi-enzyme cascade. By the UV photochemical isomerization of the *trans*-azobenzene units, to the *cis*-state the duplex, holding together the two enzymes separated, leading to the bi-enzyme cascade to be switched "OFF".

## 4. Summary and Outlook

Signal-triggered DNA switches represent a major class of important functional materials for nanobiotechnological applications. Different external triggers, such as metal ions, pH value, light or electrical stimuli were used to drive the DNA switches, and the operation of the DNA switches in solution or on surfaces was demonstrated. While substantial

progress in the development of DNA switches and their practical applications were accomplished, important challenges are still ahead of us. The introduction of additional triggering stimuli, such as other metal ions (e.g., by the incorporation of synthetic bases into the DNA, ligandosides)[87] or the use of aptamer-substrate complexes,[88] could broaden the possible applications of these molecular devices. Also, the development of additional readout signals that probe the switching systems, such as chemiluminescence resonance energy transfer (CRET),[89] surface plasmon resonance (SPR),[90] and dynamic scanning-probe microscopies, could provide novel imaging tools.[91]

The applications of DNA switches represent, however, major scientific and technological challenges, and the use of these systems for developing innovative photonic nanostructures, for "smart" nano-medicine, and for the controlled chemical synthesis may be envisaged. The switching and reconfiguration of DNA devices carrying metallic nanoparticles,[92] or fluorophore/metallic nanoparticle conjugates,[93] is anticipated to lead to interesting plasmonic phenomena, such as inter-particle plasmonic coupling or surface-enhanced fluorescence. Particularly, switchable plasmonic devices acting as antennas[94] may be envisaged. Also, exciting opportunities exist in the application of stimuli-triggered switchable DNA machines for imaging intracellular nanoenvironments and for probing the dynamics of intracellular transformations. For example, pH-value-stimulated DNA switches and the accompanying fluorescence changes and the release of nucleic acid strands may be implemented to map spatial and temporal changes in pH value in cells[95] or to silence harmful genes.[96] Furthermore, the development of switchable nanometer/micrometer-sized containers for drugs, using DNA as switchable matrices for the slow release or dose-release of the drugs is a challenging future goal. The assembly of switchable DNA hydrogels,[65] DNA-capped mesoporous nanomaterials gated by nucleic acid switches,[97] and the development of DNA switches, and the development of stimuli-responsive switchable DNA microcapsules,[98] provide interesting paths to follow. Particularly interesting would be the construction of switchable nano/micro-carriers being triggered by biomarkers. Such systems could serve as stimuli-responsive matrices for targeting cellular environments.

Finally, the triggered switchable release of substrates from stimuli-responsive containers might be applied for programmed synthesis of products by the selective and stepwise opening of the respective containers. Evidently, the area of DNA switches is a viable research area that will attract interdisciplinary research efforts of ultimate significance for materials science, the development of sensors, intracellular imaging, nano-medicine, and programmed chemical synthesis.

*Our research on DNA nanotechnology is supported by NanoSensoMach ERC Advanced Grant No. 267574 under the EC FP7/2007–2013 program.*

Received: April 24, 2014
Revised: June 25, 2014
Published online: December 17, 2014

[1] a) K. Gehring, J. L. Leroy, M. Guéron, *Nature* **1993**, *363*, 561–565; b) J. L. Leroy, M. Gueron, J. L. Mergny, C. Helene, *Nucleic Acids Res.* **1994**, *22*, 1600–1606; c) S. Nonin, J. L. Leroy, *J. Mol. Biol.* **1996**, *261*, 399–414.

[2] a) G. W. Collie, G. N. Parkinson, *Chem. Soc. Rev.* **2011**, *40*, 5867–5892; b) D. Sen, W. Gilbert, *Nature* **1988**, *334*, 364–366; c) J. T. Davis, G. P. Spada, *Chem. Soc. Rev.* **2007**, *36*, 296–313.

[3] a) Y. Miyake, H. Togashi, M. Tashiro, H. Yamaguchi, S. Oda, M. Kudo, Y. Tanaka, Y. Kondo, R. Sawa, T. Fujimoto, T. Machinami, A. Ono, *J. Am. Chem. Soc.* **2006**, *128*, 2172–2173; b) Y. Tanaka, S. Oda, H. Yamaguchi, Y. Kondo, C. Kojima, A. Ono, *J. Am. Chem. Soc.* **2007**, *129*, 244–245.

[4] A. Ono, S. Q. Cao, H. Togashi, M. Tashiro, T. Fujimoto, T. Machinami, S. Oda, Y. Miyake, I. Okamoto, Y. Tanaka, *Chem. Commun.* **2008**, 4825–4827.

[5] a) A. A. Beharry, G. A. Woolley, *Chem. Soc. Rev.* **2011**, *40*, 4422–4437; b) X. Liang, T. Mochizuki, H. Asanuma, *Small* **2009**, *5*, 1761–1768; c) X. Liang, N. Takenaka, H. Nishioka, H. Asanuma, *Chem. Asian J.* **2008**, *3*, 553–560; d) X. Liang, H. Asanuma, M. Komiyama, *J. Am. Chem. Soc.* **2002**, *124*, 1877–1883.

[6] a) S. E. Osborne, I. Matsumura, A. D. Ellington, *Curr. Opin. Chem. Biol.* **1997**, *1*, 5–9; b) R. A. Potyrailo, R. C. Conrad, A. D. Ellington, G. M. Hieftje, *Anal. Chem.* **1998**, *70*, 3419–3425; c) J. F. Lee, G. M. Stovall, A. D. Ellington, *Curr. Opin. Chem. Biol.* **2006**, *10*, 282–289; d) I. Willner, M. Zayats, *Angew. Chem. Int. Ed.* **2007**, *46*, 6408–6418; *Angew. Chem.* **2007**, *119*, 6528–6538; e) M. Famulok, G. Mayer, *Acc. Chem. Res.* **2011**, *44*, 1349–1358.

[7] a) R. R. Breaker, G. F. Joyce, *Chem. Biol.* **1994**, *1*, 223–229; b) I. Willner, B. Shlyahovsky, M. Zayats, B. Willner, *Chem. Soc. Rev.* **2008**, *37*, 1153–1165; c) M. Famulok, J. S. Hartig, G. Mayer, *Chem. Rev.* **2007**, *107*, 3715–3743; d) S. K. Silverman, *Chem. Commun.* **2008**, 3467–3485; e) G. F. Joyce, *Annu. Rev. Biochem.* **2004**, *73*, 791–836; f) G. F. Joyce, *Angew. Chem. Int. Ed.* **2007**, *46*, 6420–6436; *Angew. Chem.* **2007**, *119*, 6540–6557.

[8] a) A. H. Brivanlou, J. E. Darnell, *Science* **2002**, *295*, 813–818; b) M. C. Thomas, C. M. Chiang, *Crit. Rev. Biochem. Mol. Biol.* **2006**, *41*, 105–178; c) M. J. Moscou, A. J. Bogdanove, *Science* **2009**, *326*, 1501; d) J. Boch, H. Scholze, S. Schornack, A. Landgraf, S. Hahn, S. Kay, T. Lahaye, A. Nickstadt, U. Bonas, *Science* **2009**, *326*, 1509–1512; e) V. B. Teif, K. Rippe, *Nucleic Acids Res.* **2009**, *37*, 5641–5655.

[9] a) P. Widlak, W. T. Garrard, *J. Cell. Biochem.* **2005**, *94*, 1078–1087; b) B. L. Stoddard, *Quart. Rev. Biophys.* **2005**, *38*, 49–95; c) S. West, N. Gromak, N. J. Proudfoot, *Nature* **2004**, *432*, 522–525.

[10] a) D. Y. Zhang, E. Winfree, *J. Am. Chem. Soc.* **2009**, *131*, 17303–17314; b) D. Y. Zhang, G. Seelig, *Nat. Chem.* **2011**, *3*, 103–113.

[11] a) M. K. Beissenhirtz, I. Willner, *Org. Biomol. Chem.* **2006**, *4*, 3392–3401; b) C. Teller, I. Willner, *Curr. Opin. Biotechnol.* **2010**, *21*, 376–391; c) B. Yurke, A. J. Turberfield, A. P. Mills, Jr., F. C. Simmel, J. L. Neumann, *Nature* **2000**, *406*, 605–608; d) J. Bath, A. J. Turberfield, *Nat. Nanotechnol.* **2007**, *2*, 275–284; e) Y. Krishnan, F. C. Simmel, *Angew. Chem. Int. Ed.* **2011**, *50*, 3124–3156; *Angew. Chem.* **2011**, *123*, 3180–3215; f) F. C. Simmel, W. U. Dittmer, *Small* **2005**, *1*, 284–299; g) C. D. Mao, W. Sun, Z. Shen, N. C. Seeman, *Nature* **1999**, *397*, 144–146; h) H. Yan, X. Zhang, Z. Shen, N. C. Seeman, *Nature* **2002**, *415*, 62–65.

[12] a) I. Smirnov, R. H. Shafer, *J. Mol. Biol.* **2000**, *296*, 1–5; b) F. W. Kotch, J. C. Fettinger, J. T. Davis, *Org. Lett.* **2000**, *2*, 3277–3280; c) J. F. Chantot, W. Guschlbauer, *FEBS Lett.* **1969**, *4*, 173–176; d) W. Guschlbauer, J. F. Chantot, D. Thiele, *J. Biomol. Struct. Dyn.* **1990**, *8*, 491–511; e) N. V. Hud, P. Schultze, V. Sklenar, J. Feigon, *J. Mol. Biol.* **1999**, *285*, 233–243; f) N. V. Hud, P. Schultze, J. Feigon, *J. Am. Chem. Soc.* **1998**, *120*, 6403–6404;

  

g) J. Li, W. Tan, *Nano Lett.* **2002**, *2*, 315 – 318; h) C. M. Niemeyer, M. Adler, *Angew. Chem. Int. Ed.* **2002**, *41*, 3779 – 3783; *Angew. Chem.* **2002**, *114*, 3933 – 3937.
[13] T. Li, S. Dong, E. Wang, *J. Am. Chem. Soc.* **2010**, *132*, 13156 – 13157.
[14] a) X. Yang, T. Li, B. Li, E. Wang, *Analyst* **2010**, *135*, 71 – 75; b) T. Li, E. Wang, S. Dong, *Chem. Commun.* **2009**, 580 – 582.
[15] Y. Sannohe, M. Endo, Y. Katsuda, K. Hidaka, H. Sugiyama, *J. Am. Chem. Soc.* **2010**, *132*, 16311 – 16313.
[16] B. Ge, Y. C. Huang, D. Sen, H. Z. Yu, *Angew. Chem. Int. Ed.* **2010**, *49*, 9965 – 9967; *Angew. Chem.* **2010**, *122*, 10161 – 10163.
[17] A. E. Radi, C. K. O'Sullivan, *Chem. Commun.* **2006**, 3432 – 3434.
[18] D. Monchaud, P. Yang, L. Lacroix, M. P. Teulade-Fichou, J. L. Mergny, *Angew. Chem. Int. Ed.* **2008**, *47*, 4858 – 4861; *Angew. Chem.* **2011**, *123*, 4936 – 4939.
[19] X. Wu, J. Chen, J. X. Zhao, *Analyst* **2013**, *138*, 5281 – 5287.
[20] X. H. Yang, Y. Zhu, P. Liu, L. L. He, Q. Z. Li, Q. Wang, K. M. Wang, J. Huang, J. B. Liu, *Anal. Methods* **2012**, *4*, 895 – 897.
[21] D. Han, Y. R. Kim, J. W. Oh, T. H. Kim, R. K. Mahajan, J. S. Kim, H. Kim, *Analyst* **2009**, *134*, 1857 – 1862.
[22] X. Liu, A. Niazov-Elkan, F. Wang, I. Willner, *Nano Lett.* **2013**, *13*, 219 – 225.
[23] S. Shimron, J. Elbaz, A. Henning, I. Willner, *Chem. Commun.* **2010**, *46*, 3250 – 3252.
[24] T. Li, L. Shi, E. Wang, S. Dong, *Chem. Eur. J.* **2009**, *15*, 3347 – 3350.
[25] a) D. L. Ma, H. Z. He, K. H. Leung, H. J. Zhong, D. S. Chan, C. H. Leung, *Chem. Soc. Rev.* **2013**, *42*, 3427 – 3440; b) Y. Xiang, Y. Lu, *Inorg. Chem.* **2014**, *53*, 1925 – 1942.
[26] D. Liu, S. Balasubramanian, *Angew. Chem. Int. Ed.* **2003**, *42*, 5734 – 5736; *Angew. Chem.* **2003**, *115*, 5912 – 5914.
[27] C. Wang, Z. Huang, Y. Lin, J. Ren, X. Qu, *Adv. Mater.* **2010**, *22*, 2792 – 2798.
[28] S. Shimron, N. Magen, J. Elbaz, I. Willner, *Chem. Commun.* **2011**, *47*, 8787 – 8789.
[29] J. Elbaz, S. Shimron, I. Willner, *Chem. Commun.* **2010**, *46*, 1209 – 1211.
[30] a) P. Travascio, A. J. Bennet, D. Y. Wang, D. Sen, *Chem. Biol.* **1999**, *6*, 779 – 787; b) P. Travascio, P. K. Witting, A. G. Mauk, D. Sen, *J. Am. Chem. Soc.* **2001**, *123*, 1337 – 1348; c) V. Pavlov, Y. Xiao, R. Gill, A. Dishon, M. Kotler, I. Willner, *Anal. Chem.* **2004**, *76*, 2152 – 2156.
[31] J. Sharma, R. Chhabra, H. Yan, Y. Liu, *Chem. Commun.* **2007**, 477 – 479.
[32] a) K. Saha, S. S. Agasti, C. Kim, X. Li, V. M. Rotello, *Chem. Rev.* **2012**, *112*, 2739 – 2779; b) H. Jans, Q. Huo, *Chem. Soc. Rev.* **2012**, *41*, 2849 – 2866; c) R. A. Sperling, P. R. Gil, F. Zhang, M. Zanella, W. J. Parak, *Chem. Soc. Rev.* **2008**, *37*, 1896 – 1908.
[33] J. Elbaz, Z. G. Wang, R. Orbach, I. Willner, *Nano Lett.* **2009**, *9*, 4510 – 4514.
[34] W. Wang, Y. Yang, E. Cheng, M. Zhao, H. Meng, D. Liu, D. Zhou, *Chem. Commun.* **2009**, 824 – 826.
[35] X. J. Qi, C. H. Lu, X. Liu, S. Shimron, H. H. Yang, I. Willner, *Nano Lett.* **2013**, *13*, 4920 – 4924.
[36] a) Z. G. Wang, J. Elbaz, I. Willner, *Nano Lett.* **2011**, *11*, 304 – 309; b) C. Wang, J. Ren, X. Qu, *Chem. Commun.* **2011**, *47*, 1428 – 1430.
[37] X. Y. Gao, X. H. Li, W. M. Xiong, H. M. Huang, Z. Y. Lin, B. Qiu, G. N. Chen, *Electrochem. Commun.* **2012**, *24*, 9 – 12.
[38] X. Xu, B. Li, X. Xie, X. Li, L. Shen, Y. Shao, *Talanta* **2010**, *82*, 1122 – 1125.
[39] H. Meng, Y. Yang, Y. Chen, Y. Zhou, Y. Liu, X. Chen, H. Ma, Z. Tang, D. Liu, L. Jiang, *Chem. Commun.* **2009**, 2293 – 2295.
[40] G. Pelossof, R. Tel-Vered, S. Shimron, I. Willner, *Chem. Sci.* **2013**, *4*, 1137 – 1144.
[41] D. Liu, A. Bruckbauer, C. Abell, S. Balasubramanian, D. J. Kang, D. Klenerman, D. Zhou, *J. Am. Chem. Soc.* **2006**, *128*, 2067 – 2071.
[42] T. Liedl, M. Olapinski, F. C. Simmel, *Angew. Chem. Int. Ed.* **2006**, *45*, 5007 – 5010; *Angew. Chem.* **2006**, *118*, 5129 – 5132.
[43] T. Liedl, F. C. Simmel, *Nano Lett.* **2005**, *5*, 1894 – 1898.
[44] a) H. Asanuma, T. Takarada, T. Yoshida, D. Tamaru, X. Liang, M. Komiyama, *Angew. Chem. Int. Ed.* **2001**, *40*, 2671 – 2673; *Angew. Chem.* **2001**, *113*, 2743 – 2745; b) H. Asanuma, T. Ito, T. Yoshida, X. G. Liang, M. Komiyama, *Angew. Chem. Int. Ed.* **1999**, *38*, 2393 – 2395; *Angew. Chem.* **1999**, *111*, 2547 – 2549; c) H. Asanuma, X. G. Liang, M. Komiyama, *Tetrahedron Lett.* **2000**, *41*, 1055 – 1058.
[45] H. Asanuma, X. Liang, T. Yoshida, M. Komiyama, *ChemBioChem* **2001**, *2*, 39 – 44.
[46] H. Kang, H. Liu, J. A. Phillips, Z. Cao, Y. Kim, Y. Chen, Z. Yang, J. Li, W. Tan, *Nano Lett.* **2009**, *9*, 2690 – 2696.
[47] a) C. Dohno, S. N. Uno, K. Nakatani, *J. Am. Chem. Soc.* **2007**, *129*, 11898 – 11899; b) C. Dohno, K. Nakatani, *Chem. Soc. Rev.* **2011**, *40*, 5718 – 5729.
[48] S.-n. Uno, C. Dohno, H. Bittermann, V. L. Malinovskii, R. Häner, K. Nakatani, *Angew. Chem. Int. Ed.* **2009**, *48*, 7362 – 7365; *Angew. Chem.* **2009**, *121*, 7498 – 7501.
[49] X. Wang, J. Huang, Y. Zhou, S. Yan, X. Weng, X. Wu, M. Deng, X. Zhou, *Angew. Chem. Int. Ed.* **2010**, *49*, 5305 – 5309; *Angew. Chem.* **2010**, *122*, 5433 – 5437.
[50] Y. Yan, J. I. Chen, D. S. Ginger, *Nano Lett.* **2012**, *12*, 2530 – 2536.
[51] M. Endo, Y. Yang, Y. Suzuki, K. Hidaka, H. Sugiyama, *Angew. Chem. Int. Ed.* **2012**, *51*, 10518 – 10522; *Angew. Chem.* **2012**, *124*, 10670 – 10674.
[52] Y. Yang, M. Endo, K. Hidaka, H. Sugiyama, *J. Am. Chem. Soc.* **2012**, *134*, 20645 – 20653.
[53] Y. Hachikubo, S. Iwai, T. Q. P. Uyeda, *Biotechnol. Bioeng.* **2010**, *106*, 1 – 8.
[54] H. Nishioka, X. Liang, T. Kato, H. Asanuma, *Angew. Chem. Int. Ed.* **2012**, *51*, 1165 – 1168; *Angew. Chem.* **2012**, *124*, 1191 – 1194.
[55] X. Liang, H. Nishioka, N. Takenaka, H. Asanuma, *ChemBioChem* **2008**, *9*, 702 – 705.
[56] M. You, F. Huang, Z. Chen, R. W. Wang, W. Tan, *ACS Nano* **2012**, *6*, 7935 – 7941.
[57] D. Han, J. Huang, Z. Zhu, Q. Yuan, M. You, Y. Chen, W. Tan, *Chem. Commun.* **2011**, *47*, 4670 – 4672.
[58] M. Zhou, X. Liang, T. Mochizuki, H. Asanuma, *Angew. Chem. Int. Ed.* **2010**, *49*, 2167 – 2170; *Angew. Chem.* **2010**, *122*, 2213 – 2216.
[59] Y. Liu, D. Sen, *J. Mol. Biol.* **2004**, *341*, 887 – 892.
[60] Y. Zou, J. Chen, Z. Zhu, L. Lu, Y. Huang, Y. Song, H. Zhang, H. Kang, C. J. Yang, *Chem. Commun.* **2013**, *49*, 8716 – 8718.
[61] S. Keiper, J. S. Vyle, *Angew. Chem. Int. Ed.* **2006**, *45*, 3306 – 3309; *Angew. Chem.* **2006**, *118*, 3384 – 3387.
[62] B. Y. Won, C. Jung, K. S. Park, H. G. Park, *Electrochem. Commun.* **2013**, *27*, 100 – 103.
[63] Y. Yang, G. Liu, H. Liu, D. Li, C. Fan, D. Liu, *Nano Lett.* **2010**, *10*, 1393 – 1397.
[64] M. Frasconi, R. Tel-Vered, J. Elbaz, I. Willner, *J. Am. Chem. Soc.* **2010**, *132*, 2029 – 2036.
[65] a) J. Liu, *Soft Matter* **2011**, *7*, 6757 – 6767; b) X. Xiong, C. Wu, C. Zhou, G. Zhu, Z. Chen, W. Tan, *Macromol. Rapid Commun.* **2013**, *34*, 1271 – 1283.
[66] a) S. Nagahara, T. Matsuda, *Polym. Gels Networks* **1996**, *4*, 111 – 127; b) Y. Murakami, M. Maeda, *Biomacromolecules* **2005**, *6*, 2927 – 9292; c) S. H. Um, J. B. Lee, N. Park, S. Y. Kwon, C. C. Umbach, D. Luo, *Nat. Mater.* **2006**, *5*, 797 – 801.
[67] W. Guo, X. J. Qi, R. Orbach, C. H. Lu, L. Freage, I. Mironi-Harpaz, D. Seliktar, H. H. Yang, I. Willner, *Chem. Commun.* **2014**, *50*, 4065 – 4068.

[68] E. Cheng, Y. Xing, P. Chen, Y. Yang, Y. Sun, D. Zhou, L. Xu, Q. Fan, D. Liu, *Angew. Chem. Int. Ed.* **2009**, *48*, 7660 – 7663; *Angew. Chem.* **2009**, *121*, 7796 – 7799.
[69] H. Kang, H. Liu, X. Zhang, J. Yan, Z. Zhu, L. Peng, H. Yang, Y. Kim, W. Tan, *Langmuir* **2011**, *27*, 399 – 408.
[70] C. H. Lu, X. J. Qi, R. Orbach, H.-H. Yang, I. Mironi-Harpaz, D. Seliktar, I. Willner, *Nano Lett.* **2013**, *13*, 1298 – 1302.
[71] N. Dave, M. Y. Chan, P. J. Huang, B. D. Smith, J. Liu, *J. Am. Chem. Soc.* **2010**, *132*, 12668 – 12673.
[72] a) C. Coll, A. Bernardos, R. Martínez-Máñez, F. Sancenón, *Acc. Chem. Res.* **2013**, *46*, 339 – 349; b) M. W. Ambrogio, C. R. Thomas, Y. L. Zhao, J. I. Zink, J. F. Stoddart, *Acc. Chem. Res.* **2011**, *44*, 903 – 913; c) B. G. Trewyn, I. I. Slowing, S. Giri, H. T. Chen, V. S. Y. Lin, *Acc. Chem. Res.* **2007**, *40*, 846 – 853.
[73] a) V. Valtchev, L. Tosheva, *Chem. Rev.* **2013**, *113*, 6734 – 6760; b) P. Yang, S. Gai, J. Lin, *Chem. Soc. Rev.* **2012**, *41*, 3679 – 3698; c) J. L. Vivero-Escoto, I. I. Slowing, B. G. Trewyn, V. S. Y. Lin, *Small* **2010**, *6*, 1952 – 1967; d) M. Vallet-Regí, F. Balas, D. Arcos, *Angew. Chem. Int. Ed.* **2007**, *46*, 7548 – 7558; *Angew. Chem.* **2007**, *119*, 7692 – 7703.
[74] a) N. Liu, D. R. Dunphy, P. Atanassov, S. D. Bunge, Z. Chen, G. P. Lopez, T. J. Boyle, C. J. Brinker, *Nano Lett.* **2004**, *4*, 551 – 554; b) D. He, X. He, K. Wang, J. Cao, Y. Zhao, *Langmuir* **2012**, *28*, 4003 – 4008; c) Y. Wen, L. Xu, W. Wang, D. Wang, H. Du, X. Zhang, *Nanoscale* **2012**, *4*, 4473 – 4476.
[75] a) E. Aznar, R. Casasús, B. García-Acosta, M. D. Marcos, R. Martínez-Máñez, F. Sancenón, J. Soto, P. Amorós, *Adv. Mater.* **2007**, *19*, 2228 – 2231; b) Z. Zhang, D. Balogh, F. Wang, R. Tel-Vered, N. Levy, S. Y. Sung, R. Nechushtai, I. Willner, *J. Mater. Chem. B* **2013**, *1*, 3159 – 3166.
[76] a) R. Liu, X. Zhao, T. Wu, P. Feng, *J. Am. Chem. Soc.* **2008**, *130*, 14418 – 14419; b) Z. Luo, K. Cai, Y. Hu, L. Zhao, P. Liu, L. Duan, W. Yang, *Angew. Chem. Int. Ed.* **2011**, *50*, 640 – 643; *Angew. Chem.* **2011**, *123*, 666 – 669; c) X. Wan, D. Wang, S. Liu, *Langmuir* **2010**, *26*, 15574 – 15579.
[77] a) A. Yu, Y. Wang, E. Barlow, F. Caruso, *Adv. Mater.* **2005**, *17*, 1737 – 1741; b) C. Park, H. Kim, S. Kim, C. Kim, *J. Am. Chem. Soc.* **2009**, *131*, 16614 – 16615; c) C. Lei, Y. Shin, J. Liu, E. J. Ackerman, *J. Am. Chem. Soc.* **2002**, *124*, 11242 – 11243; d) H. Takahashi, B. Li, T. Sasaki, C. Miyazaki, T. Kajino, S. Inagaki, *Chem. Mater.* **2000**, *12*, 3301 – 3305.
[78] a) Q. Yang, S. Wang, P. Fan, L. Wang, Y. Di, K. Lin, F. S. Xiao, *Chem. Mater.* **2005**, *17*, 5999 – 6003; b) Q. Gao, Y. Xu, D. Wu, W. Shen, F. Deng, *Langmuir* **2010**, *26*, 17133 – 17138; c) H. Zheng, Y. Wang, S. Che, *J. Phys. Chem. C* **2011**, *115*, 16803 – 16813.
[79] a) X. Yang, X. Liu, Z. Liu, F. Pu, J. Ren, X. Qu, *Adv. Mater.* **2012**, *24*, 2890 – 2895; b) N. Niu, F. He, P. Ma, S. Gai, G. Yang, F. Qu, Y. Wang, J. Xu, P. Yang, *ACS Appl. Mater. Interfaces* **2014**, *6*, 3250 – 3262; c) Q. Xiao, X. Zheng, W. Bu, W. Ge, S. Zhang, F. Chen, H. Xing, Q. Ren, W. Fan, K. Zhao, Y. Hua, J. Shi, *J. Am. Chem. Soc.* **2013**, *135*, 13041 – 13048; d) J. Peng, L. Zhao, X. Zhu, Y. Sun, W. Feng, Y. Gao, L. Wang, F. Li, *Biomaterials* **2013**, *34*, 7905 – 7912; e) Y. Chen, H. Chen, J. Shi, *Adv. Mater.* **2013**, *25*, 3144 – 3176.
[80] Q. Yuan, Y. Zhang, T. Chen, D. Lu, Z. Zhao, X. Zhang, Z. Li, C. H. Yan, W. Tan, *ACS Nano* **2012**, *6*, 6337 – 6344.
[81] C. Chen, F. Pu, Z. Huang, Z. Liu, J. Ren, X. Qu, *Nucleic Acids Res.* **2011**, *39*, 1638 – 1644.
[82] D. He, X. He, K. Wang, J. Cao, Y. Zhao, *Adv. Funct. Mater.* **2012**, *22*, 4704 – 4710.
[83] H. Liu, Y. Xu, F. Li, Y. Yang, W. Wang, Y. Song, D. Liu, *Angew. Chem. Int. Ed.* **2007**, *46*, 2515 – 2517; *Angew. Chem.* **2007**, *119*, 2567 – 2569.
[84] a) Y. Tian, Z. Zhang, L. Wen, J. Ma, Y. Zhang, W. Liu, J. Zhai, L. Jiang, *Chem. Commun.* **2013**, *49*, 10679 – 10681; b) F. Xia, W. Guo, Y. Mao, X. Hou, J. Xue, H. Xia, L. Wang, Y. Song, H. Ji, Q. Ouyang, Y. Wang, L. Jiang, *J. Am. Chem. Soc.* **2008**, *130*, 8345 – 8350; c) X. Hou, W. Guo, F. Xia, F.-Q. Nie, H. Dong, Y. Tian, L. Wen, L. Wang, L. Cao, Y. Yang, *J. Am. Chem. Soc.* **2009**, *131*, 7800 – 7805.
[85] F. Wang, C. H. Lu, I. Willner, *Chem. Rev.* **2014**, *114*, 2881 – 2941.
[86] M. You, R. W. Wang, X. Zhang, Y. Chen, K. Wang, L. Peng, W. Tan, *ACS Nano* **2011**, *5*, 10090 – 10095.
[87] a) G. H. Clever, M. Shionoya, *Coord. Chem. Rev.* **2010**, *254*, 2391 – 2402; b) F. Wojciechowski, C. J. Leumann, *Chem. Soc. Rev.* **2011**, *40*, 5669 – 5679; c) G. H. Clever, C. Kaul, T. Carell, *Angew. Chem. Int. Ed.* **2007**, *46*, 6226 – 6236; *Angew. Chem.* **2007**, *119*, 6340 – 6350; d) A. Ono, H. Torigoe, Y. Tanaka, I. Okamoto, *Chem. Soc. Rev.* **2011**, *40*, 5855 – 5866; e) Y. Takezawa, M. Shionoya, *Acc. Chem. Res.* **2012**, *45*, 2066 – 2076.
[88] a) J. Elbaz, R. Tel-Vered, R. Freeman, H. B. Yildiz, I. Willner, *Angew. Chem. Int. Ed.* **2009**, *48*, 133 – 137; *Angew. Chem.* **2009**, *121*, 139 – 143; b) J. Elbaz, M. Moshe, I. Willner, *Angew. Chem. Int. Ed.* **2009**, *48*, 3834 – 3837; *Angew. Chem.* **2009**, *121*, 3892 – 3895; c) G. Pelossof, R. Tel-Vered, X. Liu, I. Willner, *Nanoscale* **2013**, *5*, 8977 – 8981.
[89] a) X. Liu, A. Niazov-Elkan, F. Wang, I. Willner, *Nano Lett.* **2013**, *13*, 219 – 225; b) X. Liu, R. Freeman, E. Golub, I. Willner, *ACS Nano* **2011**, *5*, 7648 – 7655; c) R. Freeman, X. Liu, I. Willner, *J. Am. Chem. Soc.* **2011**, *133*, 11597 – 11604; d) A. Niazov, R. Freeman, J. Girsh, I. Willner, *Sensors* **2011**, *11*, 10388 – 10397; e) R. Freeman, J. Girsh, A. F. Jou, J. A. A. Ho, T. Hug, J. Dernedde, I. Willner, *Anal. Chem.* **2012**, *84*, 6192 – 6198.
[90] a) O. A. Raitman, E. Katz, A. F. Bückmann, I. Willner, *J. Am. Chem. Soc.* **2002**, *124*, 6487 – 6496; b) O. A. Raitman, F. Patolsky, E. Katz, I. Willner, *Chem. Commun.* **2002**, 1936 – 1937; c) V. Chegel, O. Raitman, E. Katz, R. Gabai, I. Willner, *Chem. Commun.* **2001**, 883 – 884; d) O. A. Raitman, E. Katz, I. Willner, V. I. Chegel, G. V. Popova, *Angew. Chem. Int. Ed.* **2001**, *40*, 3649 – 3652; *Angew. Chem.* **2001**, *113*, 3761 – 3764.
[91] a) M. Endo, H. Sugiyama, *Acc. Chem. Res.* **2014**, *47*, 1645 – 1653; b) A. Rajendran, M. Endo, H. Sugiyama, *Chem. Rev.* **2014**, *114*, 1493 – 1520.
[92] J. Elbaz, A. Cecconello, Z. Fan, A. O. Govorov, I. Willner, *Nat. Commun.* **2013**, *4*, **2000**.
[93] a) A. Cecconello, C. H. Lu, J. Elbaz, I. Willner, *Nano Lett.* **2013**, *13*, 6275 – 6280; b) S. Shimron, A. Cecconello, C. H. Lu, I. Willner, *Nano Lett.* **2013**, *13*, 3791 – 3795.
[94] G. P. Acuna, F. M. Möller, P. Holzmeister, S. Beater, B. Lalkens, P. Tinnefeld, *Science* **2012**, *338*, 506 – 510.
[95] a) S. Surana, J. M. Bhat, S. P. Koushika, Y. Krishnan, *Nat. Commun.* **2011**, *2*, 340; b) S. Modi, M. G. Swetha, D. Goswami, G. D. Gupta, S. Mayor, Y. Krishnan, *Nat. Nanotechnol.* **2009**, *4*, 325 – 330.
[96] a) S. Modi, C. Nizak, S. Surana, S. Halder, Y. Krishnan, *Nat. Nanotechnol.* **2013**, *8*, 459 – 467; b) K. A. Afonin, M. Viard, A. N. Martins, S. J. Lockett, A. E. Maciag, E. O. Freed, E. Heldman, L. Jaeger, R. Blumenthal, B. A. Shapiro, *Nat. Nanotechnol.* **2013**, *8*, 296 – 304.
[97] a) Z. Zhang, D. Balogh, F. Wang, I. Willner, *J. Am. Chem. Soc.* **2013**, *135*, 1934 – 1940; b) Z. Zhang, D. Balogh, F. Wang, S. Y. Sung, R. Nechushtai, I. Willner, *ACS Nano* **2013**, *7*, 8455 – 8468; c) Y. Mao, C. Luo, W. Deng, G. Jin, X. Yu, Z. Zhang, Q. Ouyang, R. Chen, D. Yu, *Nucleic Acids Res.* **2004**, *32*, e144; d) Y. Mao, D. Liu, S. Wang, S. Luo, W. Wang, Y. Yang, Q. Ouyang, L. Jiang, *Nucleic Acids Res.* **2007**, *35*, e33.
[98] a) A. P. R. Johnston, E. S. Read, F. Caruso, *Nano Lett.* **2005**, *5*, 953 – 956; b) F. Cavalieri, S. L. Ng, C. Mazzuca, Z. Jia, V. Bulmus, T. P. Davis, F. Caruso, *Small* **2011**, *7*, 101 – 111; c) A. P. R. Johnston, L. Lee, Y. Wang, F. Caruso, *Small* **2009**, *5*, 1418 – 1421; d) A. P. R. Johnston, F. Caruso, *Angew. Chem. Int. Ed.* **2007**, *46*, 2677 – 2680; *Angew. Chem.* **2007**, *119*, 2731 – 2734.